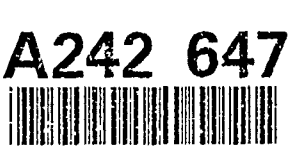

Var
(2)

WL-TR-91-2022

CATHODE SHEATH CHARGE TRANSFER EFFECTS

H. Harvey Michels
Robert H. Hobbs
United Technologies Research Center
Silver lane
East Hartford, CT 06108

July 1991

Interim Report for Period 10 June 1987 - 10 March 1991

Aero Propulsion & Power Directorate
Wright Laboratory
Air Force Systems Command
Wright-Patterson Air Force Base, Ohio 45433-6563

NOTICE

When Government drawings, specifications, or other data are used for any purpose other than in connection with a definitely Government-related procurement, the United States Government incurs no responsibility or any obligation whatsoever. The fact that the government may have formulated or in any way supplied the said drawings, specifications, or other data, is not to be regarded by implication, or otherwise in any manner construed, as licensing the holder, or any other person or corporation; or as conveying any rights or permission to manufacture, use, or sell any patented invention that may in any way be related thereto.

This report is releasable to the National Technical Information Service (NTIS). At NTIS, it will be available to the general public, including foreign nations.

This technical report has been reviewed and is approved for publication.

Alan Garscadden.
Research Physicist
Advanced Plasma Research Group
Power Components Branch
Aerospace Power Division
Aero Propulsion and Power Directorate
FOR THE COMMANDER

Lowell D. Massie
LOWELL D. MASSIE
Chief, Power Components Branch
Aerospace Power Division
Aero Propulsion and Power Directorate

Michael D. Braydich
MICHAEL D. BRAYDICH, Lt Col, USAF
Deputy Director
Aerospace Power Division
Aero Propulsion & Power Directorate

If your address has changed, if you wish to be removed from our mailing list, or if the addressee is no longer employed by your organization please notify WL/POOC-3, WPAFB, OH 45433-6563 to help us maintain a current mailing list.

Copies of this report should not be returned unless return is required by security considerations, contractual obligations, or notice on a specific document.

Unclassified
SECURITY CLASSIFICATION OF THIS PAGE

REPORT DOCUMENTATION PAGE

1a REPORT SECURITY CLASSIFICATION Unclassified	1b. RESTRICTIVE MARKINGS
2a. SECURITY CLASSIFICATION AUTHORITY	3 DISTRIBUTION / AVAILABILITY OF REPORT Approved for public release; distribution is unlimited
2b DECLASSIFICATION / DOWNGRADING SCHEDULE	
4 PERFORMING ORGANIZATION REPORT NUMBER(S) UTRC-927703	5. MONITORING ORGANIZATION REPORT NUMBER(S) WL-TR-91-2022
6a. NAME OF PERFORMING ORGANIZATION United Technologies Research Center 6b. OFFICE SYMBOL (If applicable)	7a. NAME OF MONITORING ORGANIZATION Aero Propulsion & Power Directorate Wright Laboratory AFSC
6c. ADDRESS (City, State, and ZIP Code) Silver Lane East Hartford, CT 06108	7b. ADDRESS (City, State, and ZIP Code) WL/POOC-3 WPAFB, Ohio 45433-6563
8a NAME OF FUNDING / SPONSORING ORGANIZATION 8b. OFFICE SYMBOL (If applicable)	9. PROCUREMENT INSTRUMENT IDENTIFICATION NUMBER F33615-87-C-2718
8c ADDRESS (City, State, and ZIP Code)	10 SOURCE OF FUNDING NUMBERS PROGRAM ELEMENT NO: 61102F; PROJECT NO: 2301; TASK NO.: S2; WORK UNIT ACCESSION NO: 25

11 TITLE (Include Security Classification)
CATHODE SHEATH CHARGE TRANSFER EFFECTS

12 PERSONAL AUTHOR(S)
H. H. Michels and R. H. Hobbs

13a. TYPE OF REPORT	13b TIME COVERED	14 DATE OF REPORT (Year, Month, Day)	15. PAGE COUNT
Interim	FROM 870610 TO 910310	910715	138

16 SUPPLEMENTARY NOTATION

17 COSATI CODES			18 SUBJECT TERMS (Continue on reverse if necessary and identify by block number)
FIELD	GROUP	SUB-GROUP	
20	9	4	Silane, SiH_4, silicon hydride, disilane, Si_2H_6, dissociative charge transfer. reaction rates R-matrix, SiH_4^+, SiF_n species, dissociative electron attachment
20	10	1	

19 ABSTRACT (Continue on reverse if necessary and identify by block number)

The United Technologies Research Center, under WL Contract No. F33615-87-C-2718, has carried out a theoretical research investigation of ion-molecule reactions that take place in the sheath region of low pressure discharges in silane gas mixtures. Of particular interest were the dissociative charge transfer mechanism(s) and energy dependent reaction rates of electrons, H^+, H^-, H_3^+ and several noble gas ions (He^+, Ne^+, Ar^+) in collisions with silane (SiH_4). Such reactions are an important component in the modeling of plasma-processing discharges for producing device-quality silicon films and a detailed understanding of their kinetics is required. Similar ion-molecule reactions with methane and other lower member alkanes have proven to be of importance in the analysis of hydrocarbon combustion. The results of this theoretical investigation furnish fundamental data and provide a better understanding of the role of ion collision-induced molecular decomposition.

The program for the research effort under this contract was formulated into three phases. Phase I consisted of a critical examination of available theoretical methods, including R-matrix methods, that are applicable to the prediction of

20. DISTRIBUTION / AVAILABILITY OF ABSTRACT ☒ UNCLASSIFIED/UNLIMITED ☐ SAME AS RPT ☐ DTIC USERS	21. ABSTRACT SECURITY CLASSIFICATION Unclassified
22a. NAME OF RESPONSIBLE INDIVIDUAL Alan Garscadden	22b. TELEPHONE (Include Area Code) 513-255-2923 22c. OFFICE SYMBOL POOC-3

DD FORM 1473, 84 MAR 83 APR edition may be used until exhausted. All other editions are obsolete.

SECURITY CLASSIFICATION OF THIS PAGE
Unclassified

18. Subject Terms (Continued)
SiH_n species, SiF_4.

19. Abstract (Continued)

the rates of dissociative charge transfer in ion-molecule collisions. These studies resulted in the development of an improved R-matrix code which incorporated analysis of reaction products. Specific attention was given to those methods most applicable to ion collisions with silane (SiH_4) and to those molecules where estimates of the general applicability and accuracy of the methods could be defined.

During Phase II of our research program, detailed quantum mechanical calculations of the potential energy surfaces for prototype ion-molecule reactions were carried out. The reactions that were examined included dissociative charge transfer for SiH_4 interactions with H^+, H_3^+, He^+ and Ar^+. The minimum energy reaction pathways that were obtained from these *ab initio* studies were then used as the input to our R-matrix kinetics code, wherever possible. Detailed calculations of the cross sections for dissociative charge transfer were then carried out for prototype systems.

During Phase III of this program, the focus of our studies was on negative ion dissociative charge transfer and an examination of dissociative attachment of $e + SiH_4$. A detailed study of the $H^- + SiH_4$ reaction surfaces was also carried out. In addition, a careful thermodynamic analysis of SiH_4^- and SiF_n^- anions was performed to examine the role of these species, which may have long residence times in gaseous discharges.

This investigation was carried out using, mainly, *ab initio* quantum mechanical methods. Computational programs were employed that have been developed, or adapted for use by this Center, for similar research programs that we have undertaken on the electronic structure of atoms and molecules. In addition, new computer programs were developed to expand our existing R-matrix codes for calculating reactive kinetic cross sections to include energy partitioning in the product channel. These codes provide us with the tools required to examine the energetics of a chemical reaction along the entire potential energy surface or specifically along the minimum energy reaction paths leading to all possible product channels and to analyze the rate of the reaction along the surfaces.

During the course of this research investigation, several new areas were examined at an exploratory level. These areas mainly involved the formation and reactions of negatively charged species whose chemistry and relative importance in silane plasmas is uncertain. In contrast to positive ions, which are swept to the walls by the ambipolar fields in the discharge, negative ions tend to become trapped with resultant long residence times. It has been suggested that negative ions may form clusters through a series of ion-molecule reactions similar to those for positive ion cluster growth. It is not clear whether sequential clustering reactions of negative silane ions will encounter a bottleneck at a small cluster size or whether the anion chemistry is sufficiently different that growth continues to the critical sizes needed for spontaneous formation of large silicon particulates. The results of the current investigation suggest that additional studies of the negative ion chemistry of silane molecules would represent an important area for further research.

OBJECTIVE

The objectives of this research program were: 1) to examine and expand existing computational techniques that are applicable to studies of the dissociative charge transfer kinetics of ion-molecule reactions, 2) to compute the potential energy surfaces for several prototype ion-molecule reactions which include electron, cation and anion collisions with silane and 3) to predict the reaction rates, their energy dependence and product distribution for these prototype systems. This program was directed toward improving the technical information base in support of the modeling of silane glow discharges.

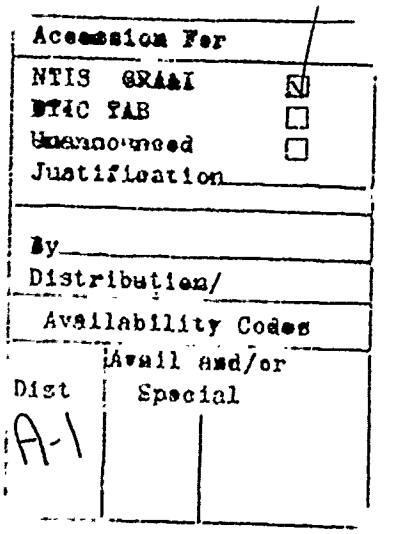

PREFACE

This report was prepared by the United Technologies Research Center, East Hartford, Connecticut, under Contract F33615-87-C-2718. The research was funded by the Wright Research and Development Center (now Wright Laboratory), Wright Patterson Air Force Base, Ohio 45433-6563.

Inclusive dates of research were 10 June 1987 through 10 March 1991. Captain James R. Shoemaker has served as Project Manager for this contract.

Very useful discussions with Dr. Alan Garscadden (WL), Captain Peter Haaland (Air Force Institute of Technology) and Professor Mark Gordon (North Dakota State University), are also acknowledged.

All aspects of the research work reported herein were aided by the skilled help of Judith B. Addison (UTRC), who assisted in the analysis of the calculated data and in the preparation of this final report.

CONTENTS

CONTENTS (Concluded)

FIGURES

TABLES

SECTION 1

INTRODUCTION

The deposition and characterization of thin films has received enormous attention owing to their importance in the fabrication of microelectronic devices and solar cells. Considerable attention has been given to silicon films deposited on quartz or other substrates and, more recently, to in situ silicon doping of compound semiconductors such as GaAs. One process for film deposition is to induce a gas phase reaction by either pyrolytic or photolytic means, the film growth being determined mainly by gas phase decomposition kinetics. Such chemical vapor deposition (CVD) processes are often slow and inefficient, particularly if laser irradiation is required to induce the decomposition reactions.

Another route toward thin film production involves the plasma enhanced deposition of silicon (Reference 1) from a gas mixture containing a silicon-bearing molecule such as silane (SiH_4), disilane (Si_2H_6) or a halogen-substituted silicon compound such as silicon tetrafluoride (SiF_4). In particular, glow discharges of silane or silane-noble gas mixtures have attracted considerable interest as a means of producing device-quality hydrogenated amorphous silicon (a-Si:H) films (Reference 2). The growth of such films depends on the complicated chemistry that is occurring in the cathode sheath region of the typical capacitively coupled rf discharge. A good deal of progress has been made over the past few years in understanding the electron energy distribution and the primary collision processes that occur in the sheath region (References 3 - 5). However, a quantitative description of all the major reactions that occur in the discharge region, including electron impact dissociation and ionization, and the chemical role of both cations and anions (formed by dissociative attachment) is required to permit reliable modeling of rf discharge sheaths. A goal of this research program was to identify the ion chemistry occurring in silane discharges, and to predict both the kinetic reaction rates and product distributions. Emphasis was placed on the development of sound theoretical methods to predict the collisional energy dependence of the reaction rates and to examine the role of dissociative charge transfer in silane ion-molecule reactions.

Several qualitative pictures of both ion and neutral fragment production in silane discharges have been developed. Haller (Reference 6) has analyzed the current status of ion species of the type, $Si_\ell H_m^+$, using mass spectrometric techniques. Secondary ion-silane reactions to form disilane ions were proposed to explain the observed ion currents. A separate model was proposed by Turban, et al (Reference 7) in which primary silane ions are formed by low-energy electron impact dissociation, followed by secondary ion-molecule reactions. Chapman and Gallagher (Reference 5), however, have criticized the applicability of this model to cathode sheath conditions where it is believed that high energy electron processes (10-100 eV) govern the overall reaction

kinetics. Their interpretation of the discharge ion chemistry is that electron impact dissociation of silane occurs as a primary process forming SiH_n^+ (n=0,3), with n=2 or 3 heavily favored over more highly stripped silane. Neutral SiH_n radical production as a primary process must also be considered. Based on the known rate of H atom abstraction from silane and the direct electron impact dissociation reaction, SiH_3 radicals are believed to predominate in the discharge region. SiH_2^+, and more highly stripped silane cations, are probably driven to SiH_3 by fast reactions of the type $SiH_n^+ + SiH_4 \rightarrow SiH_{n+1} + SiH_3^+$.

The largest uncertainties, at present, in the chemistry of the discharge sheath region, are with the secondary ion-molecule reactions occurring in pure silane-noble gas mixtures. The possible silane ion-molecule reactions are well known (Reference 8) but in most cases, the rate coefficients are known experimentally only in the low-energy region (< 1 eV) or have been estimated using the Langevin-Gioumousis-Stevenson formula for the collision cross sections. This simple model predicts that the ion-molecule reaction rate coefficients are independent of collision energy. Dissociative charge transfer rates for collisions between SiH_n^+ ions and silane are mainly unknown at present since knowledge of the detailed mechanism of the ion-molecule collision is required t o determine branching into the dissociation channels. The somewhat simpler reactions between silane and H^+, H_3^+ or the noble gas ions, which are more amenable to theoretical analysis, are also mainly unknown at present in a mechanistic sense. In addition, a preliminary analysis of the role of silicon hydride anions, SiH_n^-, has recently been reported (Reference 4). This study suggested that electron dissociative attachment to silane may exhibit a large cross section, particularly if the silane molecule is vibrationally or rotationally excited. The role of anion chemistry in describing the kinetic processes in the sheath region is uncertain at present. As an example, Garscadden (Reference 9) and Haaland (Reference 10) have dismissed the possible role of silane anions in plasma assisted CVD devices. A significant production rate for SiH_n^- would greatly influence our understanding of the overall chemistry since fast mutual neutralization reactions between cations and anions could occur.

The intent of this technical program was to address these uncertainties in the chemistry of silane ion-molecule reactions through a theoretical analysis of the governing reaction rates. Since dissociative reactions, with or without accompanying charge transfer may occur, our approach was based on detailed quantum mechanical studies of the reaction surfaces to yield all possible reaction product channels. Subsequent to this analysis of the reaction energetics, cross sections for the various ion-molecule processes were calculated within a quantum framework. During the course of this research investigation, several new areas were examined at an exploratory level. These areas mainly involved the formation and reactions of negatively charged species whose chemistry and relative importance in silane plasmas is uncertain. In contrast to positive ions, which are swept to the walls by the ambipolar fields in the discharge, negative ions tend to become trapped with resultant long residence times. Garscadden (Reference 1) has suggested that negative ions may

form clusters through a series of ion-molecule reactions similar to that discussed by Mandich, Reents and Jarrold (Reference 11) and Raghavachari (Reference 12), for positive ion cluster growth. It is not clear whether sequential clustering reactions of negative silane ions will encounter a bottleneck at a small cluster size or whether the anion chemistry is sufficiently different that growth continues to the critical sizes needed for spontaneous formation of large silicon particulates. Additional research effort in silane negative ion chemistry is recommended.

The general composition of this report is as follows. In Section 2, we present a description of the mathematical methods which were employed in this research. Included in Section 2 are sub-sections which deal with the construction of electronic wavefunctions, the calculations of expectation properties, the calculation of electronic wavefunctions using *ab initio* methods, a description of the development of R-matrix codes and a description of several electronic structure codes that were utilized during the course of this research program. The calculated results and pertinent discussion are presented in Section 3. Based on these present studies, we have identified several areas for further technical work. Recommendations are also presented in Section 3 and a concluding summary of this program is given in Section 4. A list of all technical presentations and publications that have resulted from this research program are given in Appendix A. Abstracts of the pertinent published papers, reports and technical talks are collected in Appendix B. Appendix C contains a preprint of a paper to be submitted for publication.

SECTION 2

MATHEMATICAL BACKGROUND

Central to these theoretical studies are the actual quantum-mechanical calculations which must be carried out for the atomic and molecular species. In particular, the methodology for computing the minimum energy reaction pathways and testing for vibrational stability must be carefully analyzed. For added clarity, various aspects of these calculations are discussed below.

Much evidence on diatomic and polyatomic systems indicates the inadequacy of minimum basis sets for constructing quantitatively correct molecular wavefunctions (References 13 and 14). This means inner-shell and valence-shell orbitals of quantum numbers appropriate to the atoms (ls, 2s, 2p, for C, N, O; etc.). The main deficiency of the minimum basis set is its inability to properly describe polarization and the change of orbital shape for systems which exhibit large charge transfer effects. Values of the screening parameters for each orbital can either be set from atomic studies or optimized in the molecule, the latter approach is indicated for studies of higher precision. When high chemical accuracy is required, as for detailed studies of the ground or a particular excited state of a system, a more extended basis must be used. Double-zeta plus polarization functions or optimized MO's are usually required as a minimum representation for reliable calculated results of chemical accuracy.

The chosen basis sets give good results only when used in a maximally flexible manner. This implies the construction of perturbation expansions or the use of CI wavefunctions with all kinds of possible orbital occupancies, so that the correlation of electrons into overall states can adjust to an optimum form at each geometrical conformation and for each state. Except when well-defined pairings exist, as for closed shell and exchange dominated systems, a single-configuration study (even of Hartree-Fock quality) will be inadequate.

Proper electronic states for systems composed of light atoms should possess definite eigenvalues of the spin operator S^2 as well as an appropriate geometrical symmetry. The geometrical symmetry can be controlled by the assignment of orbitals to each configuration, but the spin state must be obtained by a constructive or projective technique. Formulas have been developed (Reference 15) for projected construction of spin states from orthogonal orbitals, and programs implementing these formulas have been in routine use at UTRC for several years. One of the least widely appreciated aspects of the spin-projection problem is that the same set of occupied spatial orbitals can sometimes be coupled to give more than one overall state of a given spin quantum number. It is necessary to include in calculations all such spin couplings, as the optimum coupling will continuously change with changes in the molecular conformation. This is especially important in describing degenerate or near-degenerate excited electronic states.

In the sections below, we describe the several mathematical approaches that are applicable to calculation of the electronic structure of molecules, to the calculation of potential energy surfaces for chemically reacting systems, and to the subsequent calculation of radiation and collisional processes. Since several different approaches are indicated, we describe their expected areas of applicability.

2.1 Method of *Ab Initio* Calculation

2.1.1 Born-Oppenheimer Separation

For a system of n electrons and N nuclei, and considering only electrostatic interactions between the particles, we have for the total Hamiltonian

$$\mathfrak{H} = \mathfrak{H}_{el} - \sum \frac{\hbar^2}{2m_\alpha}\nabla_\alpha^2 + \frac{\hbar^2}{2M_T}\left[\sum_{\beta=1}^{N}\sum_{\alpha=1}^{N}\nabla_\alpha\cdot\nabla_\beta + 2\sum_{\alpha=1}^{N}\sum_{i=1}^{n}\nabla_\alpha\cdot\nabla_i + \sum_{\substack{i=1\\ i\neq j}}^{n}\sum_{j=1}^{n}\nabla_i\cdot\nabla_j\right] \quad (1)$$

where

$$\mathfrak{H}_{el} = -\frac{\hbar^2}{2m_e}\sum_{i=1}^{n}\nabla_i^2 + V^{el}(\vec{r}_n, \vec{R}_N) \quad (2)$$

and where m_e, m_α, M_T, are the masses of the electron, atom and combined system mass, respectively. Now since the ratios m_e/m_α, and m_e/M_T are both small, $(2\cdot 10^{-6} - 5\cdot 10^{-4})$ we can effect a separation of the electronic and nuclear coordinates treating the total wavefunction as a product of a nuclear and an electronic part. We have

$$\psi(\vec{r}_n, \vec{R}_N) = \sum_k \chi_k(\vec{R}_N)\psi_k(\vec{r}_n, \vec{R}_N) \quad (3)$$

where $\psi_k(\vec{r}_n, \vec{R}_N)$ is an electronic wavefunction parametric in the nuclear coordinates as given in Equation (3) and $\chi_k(\vec{R}_N)$ are nuclear motion wavefunctions which satisfy (neglecting terms of the order of m_e/m_α)

$$\left[-\sum_{\alpha=1}^{N}\frac{\hbar^2}{2m_\alpha}\nabla_\alpha^2+\frac{\hbar^2}{2M_T}\sum_{\alpha=1}^{N}\sum_{\beta=1}^{N}\nabla_\alpha\cdot\nabla_\beta+V^{el}(\vec{r}_n,\vec{R}_N)\right]\chi_k=i\hbar\frac{\partial\chi_k}{\partial t} \tag{4}$$

The cross term in $\nabla_\alpha \ \nabla_\beta$ can be eliminated by a proper change of variables and Equation (4) then reduces to a 3N–3 dimensional Schrödinger equation.

For most systems, where the velocity of motion of the nuclei is slow relative to the electron velocity, this decoupling of electron and nuclear motion is valid and is referred to as the adiabatic approximation. Equation (3) thus defines an electronic eigenstate $\psi_k(\vec{r}_n,\vec{R}_N)$, parametric in the nuclear coordinates, and a corresponding eigenvalue $E_k(\vec{R}_N)$ which is taken to represent the potential energy curve or surface corresponding to state k.

2.1.2 Variational Methods

By an *ab initio* method is meant one that starts from a zero–order Hamiltonian which is exact except for relativistic and magnetic effects, and which involves the evaluation of electronic energies and other relevant quantities for wavefunctions which are properly antisymmetrized in the coordinates of all the electrons. For a system containing n electrons and M nuclei, the zero–order Hamiltonian depends parametrically on the nuclear positions and is of the form

$$\mathfrak{H}=-\frac{1}{2}\sum_{i=1}^{N}\nabla_i^2-\sum_{i=1}^{n}\sum_{j=1}^{M}\frac{z_j}{\left|\vec{r}_i-\vec{R}_j\right|}+\sum_{1\le i<j}^{M}\frac{z_iz_j}{\left|\vec{R}_i-\vec{R}_j\right|}+\sum_{1\le i<j}\frac{1}{\left|\vec{r}_i-\vec{r}_j\right|} \tag{5}$$

where Z_i and $\vec{R}_i$ are the charge and position of nucleus i, $\vec{r}_j$ is the position of electron j, and ∇_j^2 is the Laplacian operator for electron j. All quantities are in atomic units, i.e. lengths in bohrs, energies in hartrees (1 hartree = 2 Rydbergs). The many–electron wavefunction consists of one, or a linear combination, $\psi=\sum_\mu c_\mu\psi_\mu$, of terms of the form

$$\Psi_\mu(R)=\mathcal{A}\mathcal{O}_s\prod_{i=1}^{n}\phi_{\mu i}(\vec{r}_i,R)\theta_{\mu M} \tag{6}$$

where each $\phi_{\mu i}$ is a spatial orbital, $\mathcal{A}$ is the antisymmetrizing operator, $\mathcal{O}_s$ is the spin–projection operator for spin quantum number S, and $\theta_{\mu m}$ is a product of α and β one–electron spin

functions of magnetic quantum number M_s. No requirement is imposed as to the double occupancy of the spatial orbital, so linear combinations of the form given by Equation (6) can describe a completely general wavefunction. The spatial orbitals $\phi_{\mu i}$ may be whatever basis orbitals have been introduced, arbitrary linear combinations thereof, or specific linear combinations determined pursuant to the particular calculational method in use.

The spatial orbitals $\phi_{\mu i}$, the spin functions $\theta_{\mu m}$ and the coefficients of different ψ_μ, if a linear combination of ψ_μ is used, may be explicitly determined by invoking the variational principle. Various specific methods are described below for determining wavefunctions. However, we should first observe that the adequacy of an *ab initio* calculation, or for that matter any energy calculation, will depend crucially upon the extent to which the wavefunction can be qualitatively appropriate. Some of the considerations surrounding the choice of a wavefunction are the following:

(i) Necessity that the wavefunction possess sufficient flexibility to be able to describe dissociation to the correct atomic and molecular fragments as various internuclear separations are increased;

(ii) Maintenance of equivalent quality of calculation for nuclear geometries differing in the nature or number of chemical bonds;

(iii) Ability to describe degenerate or near-degenerate electronic states when they are pertinent;

(iv) Ability to describe different electronic states to equivalent accuracy when their interrelation (e.g., crossing) is relevant, in particular, ability to describe ionic-valence state mixing;

(v) Ability to represent changes in the coupling of electron spins as bonds are broken or reformed.

The foregoing considerations indicate that it will often be necessary to consider wavefunctions with more than a minimum number of singly-occupied spatial orbitals, and that there will be many potential curves or surfaces for which a wavefunction consisting of a single ψ_μ cannot suffice. It will then be necessary to allow mixing of ψ_μ with different degrees of orbital spatial occupancy so as to obtain smooth transitions from the occupancies characteristic of separated atoms or molecules (or ions) to those characteristic of a compound system or a different fragmentation.

Another implication of the considerations surrounding the choice of a wavefunction is related to the treatment of electron spin. Not only is it necessary to require that the wavefunction

be an eigenfunction of S^2 and S_z but it is also necessary to take account of the fact that under many conditions, there will be more than one spin eigenfunction of given S and m_s. The different spin eigenfunctions correspond to different couplings among the individual spins. Since reactive processes involve the breaking and forming of electron-pair bonds, they must necessarily be accompanied by reorganizations of the spin coupling. A failure to take account of this will lead to qualitatively inappropriate wavefunctions.

In Hartree-Fock calculations $\psi(R)$ is restricted to a single ψ_μ which is assumed to consist as nearly as possible of doubly-occupied orbitals. The orbitals $\phi_{\mu i}$ are then selected to be the linear combinations of basis orbitals best satisfying the variational principle. Writing $\phi_{\mu i} = \sum_\nu a_{\nu i}\chi_\nu$, the $a_{\nu i}$ are determined by solving the matrix Hartree-Fock equation

$$\sum_\nu F_{\lambda\nu}a_{\nu i} = \epsilon_i \sum_\nu S_{\lambda\nu}a_{\nu i} \text{ (each } \lambda) \tag{7}$$

where ϵ_i is the orbital energy of $\phi_{\mu i}$.

The Fock operator $F_{\lambda\nu}$ has been thoroughly discussed in the literature (Reference 16) and depends upon one- and two-electron molecular integrals and upon the $a_{\nu i}$. This makes Equation (7) nonlinear and it is therefore solved iteratively. UTRC has developed programs for solving Equation (7) for both closed and open-shell systems, using basis sets consisting of either Slater-type or Gaussian-type atomic orbitals. Examples of their use are in the literature (Reference 17).

In configuration interaction calculations, the overall wavefunction has more than one term, ψ_μ, and the c_μ are determined by invoking the variational principle to obtain the secular equation

$$\sum_\nu (H_{\mu\nu} - wS_{\mu\nu})c_\nu = 0 \qquad \text{(each } \mu) \tag{8}$$

where

$$H_{\mu\nu} = \int \Psi_\mu^*(R)\mathfrak{H}(R)\Psi_\nu(R)d\tau \qquad S_{\mu\nu} = \int \Psi_\mu^*(R)\Psi_\nu(R)d\tau \tag{9}$$

Equation (8) is solved by matrix diagonalization using either a modified Givens method (Reference 18) or a method due to Shavitt (Reference 19) or Raffenetti (Reference 20).

The matrix elements $H_{\mu\nu}$ and $S_{\mu\nu}$ may be reduced by appropriate operator algebra to the forms

$$H_{\mu\nu} = \sum_P \epsilon_P \langle \theta_M | O_s P | \theta_M \rangle \langle \prod_{i=1}^{n} \Psi_{\mu i}(\vec{r}_i, \vec{R}_N) | \mathcal{H}(\vec{R}_N) P | \prod_{i=1}^{n} \Psi_{\nu i}(\vec{r}_i, \vec{R}_N) \rangle \qquad (10)$$

$$S_{\mu\nu} = \sum_P \epsilon_P \langle \theta_M | O_s P | \theta_M \rangle \langle \prod_{i=1}^{n} \Psi_{\mu i}(\vec{r}_i, \vec{R}_N) | P | \prod_{i=1}^{n} \Psi_{\nu i}(\vec{r}_i, \vec{R}_N) \rangle \qquad (11)$$

where P is a permutation and ϵ_P its parity. The sum is over all permutations. $\langle \theta_m | O_s P | \theta_m \rangle$ is a "Sanibel coefficient" and the remaining factors are spatial integrals which can be factored into one- and two-electron integrals. If the $\phi_{\mu i}$ are orthonormal, Equations (10) and (11) become more tractable and the $H_{\mu\nu}$ and $S_{\mu\nu}$ may be evaluated by explicit methods given in the literature (Reference 15). Computer programs have been developed for carrying out this procedure, and they have been used for problems containing up to 106 total electrons, 10 unpaired electrons, and several thousand configurations.

The CI studies described above can be carried out for any orthonormal set of $\phi_{\mu i}$ for which the molecular integrals can be calculated. Programs developed by UTRC make specific provision for the choice of the $\phi_{\mu i}$ as Slater-type atomic orbitals, as Gaussian-type orbitals, as symmetry molecular orbitals, as Hartree-Fock orbitals, or as more arbitrary combinations of atomic orbitals.

The one- and two-electron integrals needed for the above described method of calculation are evaluated for STO's by methods developed by this Center (Reference 21). For Gaussian orbitals, either the Carnegie-Mellon integral package (Reference 22) or the integral routines incorporated in the HONDO or GAMESS programs (Reference 23) can be employed.

2.1.3 Configuration Selection

Using a double-zeta plus polarization basis set of one-electron functions, a typical system can easily have of the order of 10^6 configurations in full CI (that resulting from all possible orbital occupancies). It is therefore essential to identify and use the configurations describing the significant part of the wavefunction. There are several ways to accomplish this objective. First,

one may screen atomic-orbital occupancies to eliminate configurations with excessive formal charge. Alternatively, in a molecular-orbital framework, one may eliminate configurations with excessive numbers of anti-bonding orbitals. A third possibility is to carry out an initial screening of configurations, rejecting those whose diagonal energies and interaction matrix elements do not satisfy energy significance criteria.

Another common method of classifying configurations is to examine the total number of orbitals in the wavefunction that differ from the SCF reference wavefunction. We write the CI wavefunction as

$$\psi_{CI} = C_o\psi_o + \sum_i C_i\phi_i^S + \sum_j C_j\phi_j^D + \ldots \tag{12}$$

where a single excitation function, ϕ_i^S differs from the SCF reference ψ_o by one orbital and the double excitation function ϕ_j^D by two, and so on. The CI coefficients, C_i, are then determined variationally to yield the lowest possible total energy. In the limit of a complete basis set ($N\rightarrow\infty$), and where all possible substitutions are included in ψ_{CI}, the variational energy approaches the correct nonrelativistic Born Oppenheimer result. Errors arise from a truncation of the functions used to determine the SCF reference wavefunction and from the truncation of the excitation functions series in ψ_{CI}. The reference wavefunction ψ_o will typically be the same for a CI or Many Body Perturbation Theory (MBPT) calculation, however, for a molecule even as small as water, ψ_{CI} becomes a function of a very large number of basis functions. Additionally, the reference state itself may be multi-dimensional in order to describe systems such as diradicals or systems with orbital degeneracy. Because of this, one must truncate the expansion and eliminate unimportant configurations. In general one can show that

$$\langle\psi_o|\mathcal{H}|\phi^T\rangle = \langle\psi_o|\mathcal{H}|\phi^Q\rangle = 0 \tag{13}$$

In words, the matrix elements between the reference wavefunction and triple and quadruple excitations is zero. Thus to first order, only single and double excitations contribute. Because of this, many CI calculations attempt to include all single and double excitations in the expressions for ψ_{CI}. To go beyond this, generally more than one reference wavefunction is used. Programs to handle configurations on all the above criteria are available at UTRC.

Other, potentially more elegant methods of configuration choice involve formal approaches based on natural orbital (Reference 24) or multiconfiguration SCF (Reference 25) concepts. To implement the natural-orbital approach, an initial limited CI wavefunction is transformed to natural orbital form, and the resulting natural orbitals are used to form a new CI. The desired result is a concentration of the bulk of the CI wavefunction into a smaller number of significant terms. The multiconfiguration SCF approach is more cumbersome, but in principle more effective. It yields the optimum orbital choice for a preselected set of configurations. This approach works well when a small number of dominant configurations can be readily identified. The method is described briefly below.

2.1.4 Multiconfiguration – Self Consistent Field Method (MC-SCF)

The Hartree-Fock self consistent field method has been proven to be a powerful tool for the calculation and understanding of many ground state properties of molecules in the vicinity of their equilibrium structure. However, in most cases the one configuration Hartree-Fock approximation is not adequate to properly describe the dissociation of molecular bonds. Also, many excited states cannot be represented by a single configuration wave function. In order to calculate properties for such states, or to investigate the formation of molecular bonds, one often needs multiconfiguration wave functions for which both the linear coefficients, C_i of the configuration expansion

$$\psi = \sum_i C_i \psi_i \tag{14}$$

as well as the set of orthonormal molecular orbitals $\{\phi_j\}$, from which the configurations ψ_i are constructed, are optimized according to the variational principle. As is well known, this "MC-SCF" problem presents many more difficulties than the simple one configuration Hartree-Fock case and much work has been devoted to obtaining convergent solutions during the last decade.

The difficulties mainly arise from the fact that for general MC-SCF wave functions the energy is not invariant with respect to rotations between occupied orbitals. Hence, instead of a relatively simple pseudo-eigenvalue equation in the one determinant case, the set of coupled Fock equations

$$\sum_j F_{ij} |\phi_j\rangle = \sum_j \epsilon_{ij} |\phi_j\rangle, \tag{15}$$

with the hermiticity conditions

$$\epsilon_{ij} = \epsilon_{ji}^{*} \tag{16}$$

has to be solved. ϵ_{ij} are Lagrange multipliers which account for the orthonormality constraints imposed on the orbitals. The Fock operators F_{ij} depend on the orbitals $\{\phi_i\}$ and the set of CI coefficients $\{C_i\}$. In analogy to the one determinant case many attempts have been made to solve these equations iteratively by keeping the Fock operators fixed in each iteration step. Then the Lagrange multipliers can be expressed by coupling operators constructed such that the Fock equations are transformed into pseudo-eigenvalue equations yielding the improved orbitals. These are used in a second step to determine new CI coefficients by diagonalizing the CI matrix $\langle\psi_i|\mathcal{H}|\psi_j\rangle$. The convergence of these algorithms, however, has often been found to be poor.

A second group of MC-SCF methods is based on the generalized Brillouin theorem. In these methods, the orbital changes are derived from the coefficients of a CI expansion consisting of the MC-SCF wavefunction and all one-electron singly excited configurations. A computer program (ALIS) implementing this method has been developed by Ruedenberg, et al. (Reference 26). A somewhat more elegant program (GAMESS) which also incorporates analytical gradients is also available (Reference 23). More recently, various methods have been proposed which are based on direct minimization of the energy, avoiding the Fock operators altogether. Such methods are now being studied in our laboratory and will be incorporated into our existing computer programs if they prove to be highly efficient.

2.1.5 Many-Body Perturbation Theory (MBPT)

In MBPT we again begin with the SCF wavefunction (ψ_o) as our reference and attempt to account for E_c, the correlation energy. The concept of excitation functions described in the above section on CI calculations carries over to MBPT calculations. In MBPT one can write the wavefunction, ψ_p, as

$$\psi_p = e^{T}|\phi_o\rangle \tag{17}$$

where T is an excitation operator defined as

$$T = T_S + T_D + T_T + T_Q... \tag{18}$$

where S, D, T, and Q refer to single, double, triple, and quadruple substitutions respectively. One can write T_n, in general, where n refers to the number of excitations as

$$T_n = \frac{1}{n!} \sum_{\substack{ijk... \\ abc...}} t_{ijk...}^{abc...} \chi_a^+ \chi_b^+ \chi_c^+ ... \chi_i \chi_j \chi_k \tag{19}$$

where a,b,c,... are excited orbitals and i,j,k,... are orbitals occupied in ϕ_o. The total energy is now given by

$$E_{MBPT} = \langle \phi_o | \mathcal{H} e^T | \phi_o \rangle \tag{20}$$

To evaluate E_{MBPT}, the $t_{i...}^{a...}$ from above must be determined. An equivalent expression that makes the perturbation expansion clearer is

$$E_{MBPT} = \sum_{k=0}^{\infty} \langle \phi_o | \mathcal{H} [(E_o - \mathcal{H}_o)^{-1} \mathcal{H}]^k | \phi_o \rangle \tag{21}$$

where the sum is over only so–called linked diagrams, $\mathcal{H}_o$ has eigenfunctions ϕ_o, and the expansion is of orders in the perturbation, $V = (\mathcal{H} - \mathcal{H}_o)$. The $k = 0$ term gives the reference energy and for $k > 0$ correlation corrections are included. In practice the MBPT total energy is calculated by truncating the T operator expansion and projecting $\mathcal{H} e^{T_o} | \phi_o \rangle$ onto the appropriate n-space. This leads to a set of nonlinear coupled equations for the $t_{i...}^{a...}$ coefficients which correspond to the CI expansion coefficients. The equations are solved iteratively and E_{MBPT} evaluated. In practice T_4 is an upper limit that corresponds to quadruple substitutions. The series is an oscillatory convergent sum, which in practice has proven to be at least as accurate as E_{CI} with single and double excitations included.

The best possible method to use would be a full CI (all possible configurations) with a complete basis set. However, since the number of configurations is proportional to $\{n\}^r$, where n

is the number of basis functions and ℓ is the level of excitation, it would be prohibitive to even include all single and double excitations. This truncation causes the loss of size consistency, which implies that the energy calculated for A and B as a molecular system, but dimensionally far apart, is the sum of the energy calculated for A and B separately. In a size extensive calculation the energy is proportional to the size of the system. These properties are very important if one wishes to compute correct relative energies on a potential energy surface, a necessary criteria for defining the reactive pathways of interest in this research program. MBPT, on the other hand, is guaranteed to have the correct size-dependence because the expansions contain only the so-called linked diagrams. In addition, because of the computational efficiency of MBPT, calculations can be performed up to fourth order in the perturbation expansion and include single, double, triple, and quadruple excitations in the calculation of the correlation energy. Such calculations are usually performed with at least a split valence plus polarization basis set. For the light element compounds which exhibit ionic bonding, the inclusion of diffuse basis functions and possibly higher polarization d or f-functions may be required for a more quantitative treatment.

2.2 *Ab Initio* Gaussian Wavefunction Electronic Structure Codes

Owing to the complexity of evaluating multicenter electron repulsion integrals over Slater-type (exponential) orbitals, various groups have adopted a computational approach to electronic structure calculations based on gaussian orbitals. A highly developed series of programs, named GAUSSIAN 8.X (X = 2, 6, 8), is available from Carnegie-Mellon University (Reference 22). A second series of programs has evolved from the original version of Dupuis and King's (Reference 27) HONDO code. This code has been further developed by separate groups as GAMESS (Reference 23), CADPAC (References 28) and HONDO 7 (Reference 29). Finally a new code named COLUMBUS (Reference 30 and 31) has been developed by the Ohio State/Argonne/Battelle group. UTRC has been designated as a beta test site for this new development. A brief description of the features of these codes follows.

2.2.1 GAUSSIAN 88

GAUSSIAN 88 is a connected system of programs for performing *ab initio* molecular orbital (MO) calculations. It represents further development of the GAUSSIAN 70/76/80/82/86 systems already published. The contributors to this program include: M. J. Frisch, J. S. Binkley, H. B. Schlegel, K. Raghavachari, C. F. Melius, R. L. Martin, J. J. P. Stewart, F. W. Bobrowicz, C. M. Rohlfing, L. R. Kahn, D. J. Defrees, R. Seeger, R. A. Whiteside, D. J. Fox, E. M. Fleuder, and J. A. Pople. GAUSSIAN 8X was originally implemented on the chemistry department DEC VAX 11/780 computer at Carnegie-Mellon University. Since then this program has been installed on a number of different computers.

GAUSSIAN 88 was designed with a transparent input data stream, making this program very user friendly. All of the standard input is free-format and mnemonic. Reasonable defaults

for input data have been provided, and the output is intended to be self-explanatory. Mechanisms are available for the sophisticated user to override defaults or interface their own code to the GAUSSIAN system. In this respect, we intend to utilize GAUSSIAN 88 as a fundamental framework for several applications. Options are being incorporated into this code to provide capabilities beyond Hartree-Fock and various perturbation theory options.

The capabilities of the GAUSSIAN 88 system include:

a) Calculation of one- and two-electron integrals over s, p, d, and f contracted gaussian functions. The basis functions can either be cartesian gaussians or pure angular momentum functions and a variety of basis sets are stored in the program and can be requested by name.

b) Self-consistent field calculations for restricted closed-shell (RHF), unrestricted open-shell (UHF), and open-shell restricted (ROHF) Hartree-Fock wavefunctions as well as those types of multiconfigurational wavefunctions that fall within the Generalized Valence Bond-Perfect Pairing (GVB-PP) formalism.

c) Evaluation of various one-electron properties of the Hartree-Fock wavefunction, including Mulliken population analysis, multipole moments, and electrostatic fields.

d) Automated geometry optimization to either minima or saddle points, and analytical or numerical differentiation to produce force constants, polarizabilities, and dipole derivatives. This feature can be used to develop minimum energy reaction paths along a complicated many dimensional potential energy surface.

e) Correlation energy calculations using Møller-Plesset perturbation theory carried to second, third, or fourth order.

f) Correlation energy calculations using configuration interaction (CI) with either all double excitations (CID) or all single and double excitations (CISD).

g) Correlation energy calculations using coupled cluster theory with double substitutions (CCD).

h) Correlation energy calculations using quadratic convergence SCF (QCSCF). This is a new highly efficient size-consistent method recently developed by Pople.

i) Analytic computation of the nuclear coordinate gradient of the RHF, UHF, ROHF, GVB-PP, MP2, CID and RCISD energies.

j) Computation of force constants (nuclear coordinate second derivatives), polarizabilities, hyperpolarizabilities, dipole derivatives, and polarizability derivatives either analytically or numerically.

k) Harmonic vibrational analysis.

l) Determination of intensities for vibrational transitions at the HF, MP2, and CI levels.

m) Testing the SCF wavefunctions for stability under release of constraints.

n) Correlated electron densities and properties.

o) Minimum–energy pathway following from products to reactants through a transition state–intrinsic reaction coordinate finder.

2.2.2 GAMESS

A wide range of quantum chemical computations are possible using GAMESS (Reference 23), a refinement by M. Schmidt and S. Elbert of the original HONDO code (Reference 27).

The capabilities of this code include:

a) Calculations of RHF/UHF/ROHF/GVB–SCF molecular wavefunctions.

b) Calculations of multiconfiguration SCF (MCSCF) wavefunctions.

c) Calculations of CI wavefunctions using the unitary group method.

d) Optimization of molecular geometries using an energy gradient in terms of Cartesian or internal coordinates.

e) Searches for potential energy surface saddle points.

f) Tracing the intrinsic reaction path from a saddle point to reactants or products.

g) Computation of normal modes and vibrational frequencies.

h) Calculation of the following properties:

1. dipole, quadrupole, and octupole moments
2. electrostatic potentials
3. electric field and electric field gradients
4. electron density and spin density
5. Mulliken and Löwdin population analysis
6. localized orbitals by the Boys method
7. virial theorem and energy components.

GAMESS is a synthesis, with many major modifications, of several programs. A large part of the program is from HONDO. For pure sp basis sets, the HONDO symmetry and supermatrix procedure has been adapted from GAUSSIAN 76 and GRADSCF integrals, both for the SCF and gradient parts. The GVB section is a heavily modified version of GVBONE. A Boys localization algorithm is implemented from a heavily modified version of Streitweiser's QCPE program.

The CI module is based on Brooks and Schaefer's unitary group program which was modified to run within GAMESS, using a Davidson eigenvector method written by S. T. Elbert. The MCSCF module is a Newton-Raphson procedure, developed at NRCC, based on the unitary group CI package. The intrinsic reaction coordinate pathfinder was written at North Dakota State University.

2.2.3 CADPAC

The Cambridge Analytic Derivatives Package (CADPAC) (Reference 28) is a group of programs which has been under development at Cambridge University, UK. It originated as a version of Dupuis and King's HONDO program. From its initial state as an SCF gradient package for closed-shell and UHF wavefunctions, this program has been extensively modified with many of the old features being enhanced and many new features being added. The input data is now in free format with a 'keyword' system, to make the program easier to use. The integral routines use essentially the same methods as those in HONDO, being based on the Rys polynomial method, but have been extended to cover f-functions. These routines have also been vectorized to take advantage of the much greater availability of supercomputers such as the Cray in recent years. The SCF programs are by now a blend of techniques, but still contain a few features from the initial HONDO program, particularly in the way symmetry is handled. There have been many modifications to improve efficiency and the addition of level-shifting and damping techniques and the implementation of the DIIS method to aid convergence. A high-spin open-shell SCF program, and a completely general open-shell SCF program have also been included.

The gradient routines have been considerably altered from those in the original HONDO, the method having been changed to one which is more efficient and easier to extend to higher order derivatives. These routines also work for f-functions. The original program's capabilities for the calculation of force-constants by numerical differentiation of gradients and for the optimization of geometries remain essentially intact. However there is now a choice of two optimization algorithms with the inclusion of Schlegel's method.

In addition to the above modifications a range of extra facilities were developed. These included a more powerful method of calculating one-electron properties and analyzing molecular charge distributions, and various 'post-SCF' stages, beginning with a 4-index transformation.

These new sections include Mϕller-Plesset perturbation theory for total energies and molecular properties, and coupled Hartree-Fock calculations of molecular polarizabilities. The polarizability routines can calculate dynamic properties at real or imaginary frequencies, and obtain dispersion coefficients. It is also possible to use CHF theory to obtain the perturbations due to nuclear displacements. These can be used to obtain, analytically, all the dipole and quadrupole moment derivatives of a molecule. They also form part of the most important addition to the package, the section which calculates analytic second derivatives of the energy. This is a powerful technique whose speed and accuracy represents a considerable improvement over numerical differentiation.

The capabilities of the latest CADPAC code (Version 4) include

a) the evaluation of one- and two-electron integrals over contracted cartesian gaussian basis functions of type s, p, d, or f.

b) SCF calculations for closed shell, open-shell, UHF and generalized open-shell techniques.

c) calculation of one-electron properties for these types of wavefunction, including a distributed multipole analysis.

d) calculation of the gradients of the SCF energy.

e) use of the gradients for automatic geometry optimization, and for the calculation of force constants by numerical differentiation. There is a choice of two optimization algorithms.

f) transformation of the integrals from the atomic orbital to the molecular orbital basis.

g) Mϕller-Plesset perturbation theory calculations to third order in the energy and second order in the one-electron properties.

h) coupled Hartree-Fock calculations of polarizabilities, including frequency dependence, and magnetizabilities.

i) coupled Hartree-Fock calculations of the perturbation due to nuclear displacements.

j) calculation of the dipole and quadrupole moment derivatives.

k) calculation of the second derivatives (force constants) of the energy by analytic methods.

l) analytic calculations of polarizability derivatives.

m) calculation of infrared and Raman intensities, and the study of vibrational circular dichroism.

n) calculation of MP2 gradients, dipole moment derivatives, polarizabilitites and force constants using analytic algorithms.

o) spin-projected UHF MP2 energies

2.2.4 HONDO

The HONDO program, (Reference 27) originally developed by Dupuis and King at NRCC has recently been refined and updated by M. Dupuis at IBM-Kingston (Reference 29).

The following features are available in the present version (HONDO 7) of the program:

a) Single configuration self-consistent-field wavefunctions (closed shell RHF, spin unrestricted UHF, restricted open shell ROHF), generalized valence bond GVB and general multiconfiguration self-consistent-field MCSCF wavefunctions, and configuration interaction CI wavefunctions can be calculated.

b) The electron correlation correction to the energy of closed shell RHF wavefunctions can be calculated by means of Mϕller-Plesset (MP) perturbation theory applied to second-, third-, and fourth-order (with or without the effects of triple excitations).

c) The effective core potential approximation can be used.

d) Optimization of molecular geometries using the gradient of the energy with respect to nuclear coordinates is possible with all but the CI and MP wavefunctions. Optimization can be carried out in the cartesian space or in the internal coordinate space with the possibility of freezing some cartesian or internal coordinates.

e) The force constant matrix in the cartesian space, and the vibrational spectrum, including infrared and Raman intensities, can be calculated with all but the CI and MP wavefunctions.

f) Calculation of the dipole moment and polarizability derivatives with respect to the nuclear coordinates is possible, for use with a previously calculated force constant matrix. The force constant matrix can be transformed to the internal coordinate basis.

g) Transition state structures can be determined with all but the CI and MP wavefunctions by taking advantage of the energy gradients.

h) The 'Intrinsic Reaction Coordinate' (IRC) pathway can be determined with all but the CI and MP wavefunctions by taking advantage of the energy gradients.

i) Molecular energies for several points on a potential energy surface can be calculated in a single run.

j) Non-gradient optimization of basis function exponents is possible. The source code can be modified to carry out optimization of other non-linear parameters, for example, contraction coefficients and geometrical parameters.

k) The following electronic properties can be extracted from the wavefunction:

1. Dipole moment
2. Quadrupole moment
3. Mulliken population, bond order and valency analyses
4. Spin density maps
5. Electron density maps
6. Electrostatic potential maps
7. Localized orbitals via Boys' method
8. Static dipole polarizability
9. Static first and second hyperpolarizabilities.

l) The potential due to finite point charges for a classical representation of an environment, or a uniform electric field can be incorporated into the one-electron Hamiltonian.

2.2.5 COLUMBUS

The COLUMBUS code (Reference 30 and 31) is a continuing development based on a joint project at Ohio State University (I. Shavitt), University of Karlsruhe (R. Ahlrichs), and Argonne National Laboratory (R. Shepard). The unique features of this code are the incorporation of relativistic or non-relativistic core potentials to permit analysis of heavy atom molecular systems and the inclusion of a sophisticated CI package based on the unitary group approach of Shavitt (Reference 32). The basic programs included in the COLUMBUS code are as follows.

1. AO Integrals
   This is R. Pitzer's version of the integral package from HONDO with partial vectorization of auxiliary integral routines. This package can handle up to g-functions.

2. Integral Transformation
   The transformation algorithm is written over all the orbitals which constitute a shell, using contraction coefficients defined over the primitive basis functions. Limited vectorization is possible over the innermost loops for dyadic operations.

3. SCF Gradients
   These routines are based on the HONDO version but include checks on integral symmetry to avoid operations over zero or near zero elements. At this time, only a first derivative analysis has been included.

4. SCF Energy
   The SCF routines are typical of those found in the molecular structure codes. They incorporate level shifting, damping and the incorporation of Pulay's DIIS convergence acceleration procedure.

5. MCSCF Analysis
   The MCSCF package is due to R. Shepard and incorporates extensive vectorization. The output vectors can be taken directly from this package and transferred to the CI program.

6. Multireference Direct CI
   This set of routines is based on the graphical representation of the unitary group approach (GUGA) for constructing a CI wavefunction. This code differs from conventional CI in that a matrix representation of the hamiltonian is not explicitly computed. The unitary group approach can be much more efficient in most applications since ~80% of the hamiltonian matrix elements are usually zero but must still be included. This leads to the storage and diagonalization problems associated with large, sparse matrices. However, little work has been done on analysis of excited states with the same molecular symmetry as the ground state. An approach that looks promising is to define an approximate vector corresponding to the excited state wavefunction and to iteratively improve upon this solution using the direct CI contraction. The uncertainties in the procedure are applications to situations where degeneracies or near-degeneracies arise. Further studies of this case are in progress.

2.3 Spin-Projected Unrestricted Hartree-Fock Method

The unrestricted Hartree-Fock (UHF) method developed by Pople and Nesbet (References 33 and 34) yields the best single-determinant approximation to the exact wavefunction for an atomic or molecular system. Such a wavefunction incorporates correlation by allowing orbitals of different spin to adjust to spatially different forms, thus breaking the symmetry restrictions of the conventional (RHF) method (References 35 and 36). It is necessary, however, to project from such a wavefunction, a properly antisymmetrized spin and angular momentum state in order to define eigenstates and eigenenergies corresponding to observable spectroscopic states.

Let $|\alpha\rangle$, $|\beta\rangle$ refer to the doubly-occupied molecular orbitals (MO's), ϕ_α, ϕ_β. Let $|\gamma\rangle, |\delta\rangle, |\tau\rangle$ refer to the singly occupied MO's. We assume that all MO's have been subjected to a

transformation to orthogonal form. Let $C_{\gamma\delta}$ be the coefficient associated with the permutation $\gamma \longleftrightarrow \delta$ (this permutation is (-1) times the overlap of the permuted spin eigenfunction with the original spin eigenfunction), and adopt the convention $C_{\gamma\gamma} = -1$. Then the expectation value of the nonrelativistic Hamiltonian

$$\mathcal{H} = \sum_i U(i) + \sum_{i<j} V(i,j) \tag{22}$$

is given by

$$\begin{aligned}\langle \mathcal{H} \rangle = {} & 2\sum_{\alpha}\langle \alpha|U|\alpha\rangle + \sum_{\gamma}\langle \gamma|U|\gamma\rangle + 2\sum_{\alpha\beta}\langle \alpha\beta|V|\alpha\beta\rangle \\ & - \sum_{\alpha\beta}\langle \alpha\beta|V|\beta\alpha\rangle + 2\sum_{\alpha\gamma}\langle \alpha\gamma|V|\alpha\gamma\rangle - \sum_{\alpha\gamma}\langle \alpha\gamma|V|\gamma\alpha\rangle \\ & - \frac{1}{2}\sum_{\gamma\delta}\langle \gamma\delta|V|\gamma\delta\rangle + \frac{1}{2}\sum_{\gamma\delta} C_{\gamma\delta}\langle \gamma\delta|V|\delta\gamma\rangle\end{aligned} \tag{23}$$

where i, j refer to electron numbers, α, β.. γ, δ etc., refer to MO's and the sums run over all α, β....

The equations for determining the optimum MO's can be derived from the following variational form

$$\delta\left[\langle \mathcal{H} \rangle - 2\sum_{\alpha\beta}\epsilon_{\alpha\beta}\langle \alpha|\beta\rangle - \sum_{\alpha\beta}\left(\epsilon_{\gamma\alpha}\langle \alpha|\gamma\rangle + \epsilon_{\alpha\gamma}\langle \gamma|\alpha\rangle\right) - \sum_{\gamma\delta}\epsilon_{\gamma\delta}\langle \gamma|\delta\rangle\right] = 0 \tag{24}$$

These equations are

$$\left(U + 2J_c - K_c + J_o - \frac{1}{2}K_o\right)|\alpha\rangle = \sum_\beta \epsilon_{\beta\gamma}|\beta\rangle + \frac{1}{2}\sum_\delta \epsilon_{\delta\alpha}|\delta\rangle \tag{25}$$

$$\left(U + 2J_c - K_c + J_o\right)|\gamma\rangle + \sum_\delta C_{\gamma\delta}|\langle\delta|V|\gamma\rangle\delta\rangle = \sum_\beta \epsilon_{\beta\gamma}|\beta\rangle + \sum_\delta \epsilon_{\delta\gamma}|\delta\rangle \tag{26}$$

where

$$|\langle\delta|V|\gamma\rangle\delta\rangle = \int d\vec{r}'\,\phi_\delta^*(\vec{r})V(\vec{r},\vec{r}')\phi_\gamma(\vec{r})\phi_\delta(\vec{r})$$

$$\langle W|V|W'\rangle = \int d\vec{r}'\,W^+(\vec{r})V(\vec{r},\vec{r}')W'(\vec{r}') \tag{27}$$

$$J_c = \sum_\beta \langle\beta|V|\beta\rangle \qquad J_o = \sum_\delta \langle\delta|V|\delta\rangle$$

$$K_c|W = \sum_\beta |\langle\beta|V|W\rangle\beta\rangle \qquad K_o|W = \sum_\delta |\langle\delta|V|W\rangle\delta\rangle$$

Left-multiplying Equation (25) by $\langle\gamma|$ and Equation (26) by $\langle\alpha|$, these equations can be combined to yield

$$\epsilon_{\gamma\alpha} = \sum_\delta (2C_{\gamma\delta} + 1)\langle\gamma\delta|V|\delta\alpha\rangle \tag{28}$$

Noting that

$$\sum_\gamma C_{\gamma\tau}\langle\delta\tau|V|\tau\gamma\rangle = \sum_\tau C_{\delta\tau}\langle\delta\tau|V|\tau\gamma\rangle, \tag{29}$$

Equations (25) and (26) can be recast as follows. From Equation (25),

$$\frac{1}{2}\sum_{\delta}\epsilon_{\delta\alpha}|\delta\rangle = \frac{1}{2}M|\alpha\rangle$$

with (30)

$$M = \sum_{\delta\tau}(2C_{\delta\tau} + 1)|\delta\rangle\langle\tau\langle\delta|V|\tau\rangle|$$

From Equation (26),

$$\sum_{\beta}\epsilon_{\beta\gamma}|\beta\rangle = \sum_{\beta\tau}(2C_{\gamma\tau} + 1)|\beta\rangle\langle\beta\tau|V|\delta\gamma\rangle = \sigma_c M^{\dagger}|\gamma\rangle \quad (31)$$

with

$$\sigma_c = \sum_{\beta}|\beta\rangle\langle\beta|; \quad \sigma_o = \sum_{\delta}|\delta\rangle\langle\delta| \quad (32)$$

Using Equations (31) and (32) in (25) and (26), we find

$$\left(U + 2J_c - K_c + J_o - \frac{1}{2}K_o - \frac{1}{2}M\right)|\alpha\rangle = \sum_{\beta}\epsilon_{\beta\alpha}|\beta\rangle \quad (33)$$

$$\left(U + 2J_c - K_c + J_o - \frac{1}{2}K_o + \frac{1}{2}M^{\dagger} - \sigma_c M^{\dagger}\right)|\gamma\rangle = \sum_{\delta}\epsilon_{\delta\gamma}|\delta\rangle \quad (34)$$

Finally, Equations (33) and (34) can be rearranged to yield the same Hermitian operator on the left-hand side with the resulting definition of the one-electron eigenenergies for the closed and open-shell eigenstates:

$$\epsilon_\alpha' = \left\langle \alpha \middle| U + 2J_c - K_c + J_o - \frac{1}{2}K_o \middle| \alpha \right\rangle \tag{35}$$

$$\epsilon_\gamma' = \left\langle \gamma \middle| U + 2J_c - K_c + J_o - \frac{1}{2}K_o + \frac{1}{2}M^\dagger \middle| \gamma \right\rangle \tag{36}$$

Equations (35) and (36) represent the correct one-electron energy expressions for the spin-projected eigenstate.

This formalism has been developed to extend the conventional HF method to include split-shell correlation and proper spin and symmetry projections. It is being incorporated into a computer program using gaussian-type orbitals (GTO's) as the elementary basis functions. A crucial feature of this method is that dissociation always follows the lowest energy pathway thereby permitting a proper description of bond formation and breakage. In contrast, RHF or MC-SCF methods often exhibit improper dissociation character or exhibit size inconsistencies owing to correlation energy changes in going from molecular geometries to separated atom-molecule or atom-atom dimensions.

2.4 Dissociative Recombination Calculations

The theory of the capture of an electron by a positive molecular ion has been developed for both direct attachment processes (Reference 37), and for several possible indirect processes which involve the formation of an intermediate excited Rydberg state belonging to the molecular ion core configuration (References 38-40). Let ψ_f ($\underset{\sim}{r}$, R, ϵ) represent the continuum wavefunction describing the free electron with energy ϵ plus the n-1 electron bound system of the molecular ion. Let ψ_d ($\underset{\sim}{r}$, R) represent the wavefunction for an eigenstate of the neutral molecule which can be written, in the Born-Oppenheimer approximation, as the product of an electronic and nuclear wavefunction in the form

$$\psi_d(\vec{r}, R) = \psi_d^{el}(\vec{r}, R)\xi_d(R) \tag{37}$$

The cross section for electron capture in dissociative-recombination is determined by the asymptotic form of the nuclear wavefunction $\xi_d(R)$. Let the incident flux of electrons per unit area be

$$\frac{k^2}{2\pi^2\hbar}\delta\epsilon \tag{38}$$

where $\delta\epsilon$ is a measure of the energy spread of the incoming beam and k is the wave number associated with the incoming electron. The outgoing flux of atoms is given by

$$\frac{\hbar K\delta\epsilon}{\mu}|\xi_d(R)|^2 \tag{39}$$

where $\frac{\hbar K}{\mu}$ is the relative velocity of the separating neutral atoms. Equations (37) and (39) yield for the cross section

$$\sigma(\epsilon,\Omega) = \lim_{R\to\infty}\frac{2\pi^2\hbar^2 K}{\mu k^2}|\xi_d(R)|^2 \tag{40}$$

Equation (40) must finally be averaged over all rotational orientations as

$$\sigma(\epsilon) = \frac{1}{4\pi}\int\sigma(\epsilon,\Omega)d\Omega \tag{41}$$

Assuming that the total cross section can be written as the product of a resonant capture cross section and a survival factor, in the form

$$\sigma(\epsilon) = \sigma_{cap}(\epsilon)S(\epsilon) \tag{42}$$

we have

$$\sigma_{cap}(\epsilon) = \frac{\pi^2\hbar^2}{2m\epsilon}\left(\frac{\omega_o}{\omega_+}\right)\left\langle \psi_f\,(\vec{r}, R, \epsilon)\middle| V(R,\epsilon)\middle|\psi_d(\vec{r}, R)\right\rangle^2 \tag{43}$$

where the factor ω_o/ω_+ is the ratio of the electronic degeneracies of the neutral and ionic states, respectively. The capture width, $\Gamma_c\,(R,\epsilon)$, is determined by integrating over the coordinates of the electronic wavefunctions

$$\Gamma_c(R,\epsilon) = 2\pi\ \left\langle \psi_+^{el}(\vec{r}, R)\ f\ (\epsilon, \vec{r}, R)\middle|\mathfrak{H}_{el} - \epsilon\middle|\psi_{AB}^{el}(\vec{r}, R)\right\rangle^2 \tag{44}$$

Thus, the capture cross section can be written as

$$\sigma_{cap}(\epsilon) = \frac{\pi^2\hbar^2}{2m\epsilon}\ \left(\frac{\omega_o}{\omega_+}\right)\frac{1}{\sqrt{2\pi}}\ \left\langle \xi_+(R)\middle|\Gamma_c^{1/2}(R,\epsilon)\middle|\xi_o(R)\right\rangle^2 \tag{45}$$

or equivalently

$$\sigma(\epsilon) = \frac{\pi^2\hbar^2}{2m\epsilon}\left(\frac{\omega_o}{\omega_+}\right)\ \left\langle \xi_+(R)\psi_+^{el}(R)\psi_f(\vec{r}, R, \epsilon)\middle| V(R,\epsilon)\middle|\psi_d(\vec{r}, R)\xi_o(R)\right\rangle^2 \tag{46}$$

The nuclear wavefunction, ξ_o, is energy normalized so that asymptotically

$$\xi_o \sim \left(\frac{2\mu}{\hbar^2}x\frac{1}{\pi k}\right)^{1/2}\sin(kr + \eta) \tag{47}$$

Equation (46) can be cast into the computational form

$$\sigma(\epsilon, V)cm^3/\sec = \frac{1.38188 \times 10^{-16}}{\epsilon(a.u.)}\left(\frac{\omega_o}{\omega_+}\right) \left\langle \xi^v_+(R)\right| \frac{\Gamma_c^{1/2}(R,\epsilon)}{\sqrt{2\pi}} \left|\xi_o(R)\right\rangle^2 \tag{48}$$

where the electron energy ϵ and the capture width Γ_c are in atomic units.

Assuming a Maxwellian temperature distribution for the electrons, the rate coefficient can be written as

$$\alpha_v(T_e) = \frac{2}{\sqrt{\pi}} \frac{1}{(kT_e)^{3/2}} \int_o^\infty \sigma(\epsilon, v) * v_{el} * e^{-\epsilon/kT_e} \epsilon^{1/2} d\epsilon \tag{49}$$

or equivalently

$$\alpha_v(T_e) = \frac{2\sqrt{2}}{\sqrt{\pi m}(kT_e)^{3/2}} \int_o^\infty \sigma(\epsilon, v) \epsilon e^{-\epsilon/kT_e} d\epsilon \tag{50}$$

The capture width Γ_c can be calculated by examining the high members of the Rydberg series of neutral states which have the structure of a ground state molecular ion coupled to an electron in diffuse hydrogenic orbitals of large effective principal quantum numbers. A direct calculation of the capture width involves the knowledge of the continuum wavefunction for the electron as a function of the interparticle coordinates. This approach is computationally very difficult and at the present stage of development would probably lead to errors of at least the same magnitude as an extrapolation procedure of the corresponding neutral Rydberg states.

2.4.1 Indirect Models

An indirect model for calculating electron-molecular ion recombination coefficients can also be formulated. Here we postulate the formation of a collision complex (AB^* for purposes of illustrating this for a diatomic system) during the collision and its subsequent decay to form A^*, B^{**}, or $AB^+ + e$ (References 38–40). The approaches differ by the nature of the (AB^*) complex. The high-energy approximation assumes that all of the energy of the incident electron goes into exciting one of the electrons in the AB^+ core, resulting in the capture of the incident electron into a doubly excited state of AB. This mechanism is unlikely to be applicable to AB^+ recombination at thermal energies because of the energy required to promote an electron out of the AB^+ core. A

second approach is more applicable to thermal energy collisions, since it requires that the electron-molecular ion collision results in a vibrationally excited molecular ion which captures an electron in the Coulomb field of AB^+. This collision complex is equivalent to a vibrationally or rotationally excited Rydberg state of AB. Experimental evidence for the existence of such states and their autoionization has been independently obtained from photoionization spectra of AB, within a few electron volts of the threshold (Reference 41). With this model, the prediction of the atomic products of the recombination reaction reduces to calculating the Rydberg states of AB that are most likely to be populated during the initial recombination, and also those atomic states to which they subsequently decay.

As contrasted with the direct recombination process which is governed by the configuration interaction strength, the nonadiabatic coupling of the electron and nuclear motion is the dominant mechanism in both stages of the indirect recombination process. In the first stage, it is the vibrational (or rotational) excitation of the AB^+ core which results in the initial capture of the incident electron. The subsequent decay of the collision complex is due to a transition to a repulsive molecular state which crosses the Rydberg state. It is then the nonadiabatic coupling of the electronic and nuclear motion which results in the transition between these two molecular states. Actually, it is the same term in the Hamiltonian for the entire molecular system that causes the key transition in both stages of the recombination process. This becomes obvious in the quantum mechanical formulation of the problem. A possible competing process for the decay of the AB^* complex is the radiative transition to lower-lying states of the molecule. The importance of this effect can be estimated from calculations of the band transition probabilities.

Implicit in this model of dissociative-recombination processes is the existence of three excited electronic states of AB. Since this recombination process is envisioned as occurring in two stages, we are concerned with only two of these states at a time. The state common to both stages of the recombination process is the highly excited Rydberg state (AB^*), which is bound with respect to dissociation to AB^+ and a free electron. For the calculation of the initial rate of recombination, a wavefunction for a continuum Rydberg state is needed. This wavefunction has the asymptotic behavior of a free electron moving in the field of AB^+.

To determine the transition rates in the two stages of the recombination process, it is necessary to identify the terms in the Hamiltonian that are responsible for the transition. The Hamiltonian for the complete molecular system with respect to the center of mass is

$$\mathcal{H} = \mathcal{H}_0 - \frac{\hbar^2}{2\mu}\nabla_R^2 - \frac{\hbar^2}{2M}\sum_i\sum_j \nabla_i\cdot\nabla_j \qquad (51)$$

where R is the vector joining nucleus B, $\mathcal{H}_0$ is the Hamiltonian for the system when the nuclei are held fixed, μ is the reduced mass of the two nuclei, M is the sum of the nuclear masses, and the summations extend over all of the electrons. Since all of the electronic eigenfunctions under discussion are implicitly dependent on the internuclear separation $|\vec{R}|$, it is the term $\mathcal{H} = -(\hbar^2/2\mu)\nabla^2_{\vec{R}}$ which plays a dominant role in coupling the electronic and nuclear motion giving rise to the appropriate transition (References 42–45). This becomes more obvious when we write the total wavefunction for the collision complex, AB*, as

$$\psi_c{}^* = \chi_c(\vec{r}_e, |\vec{R}|)F_c(\vec{R}) \tag{52}$$

where $X_c(\vec{r}_e, |\vec{R}|)$ is the electronic wavefunction for the appropriate Rydberg state of AB at internuclear separation $|\vec{R}|$ and $F_c(\vec{R})$ is the wavefunction associated with the vibration and rotation of the nuclei. In a similar manner, the total wavefunction associated with the repulsive state is

$$\psi_r = \chi_r(\vec{r}_e, |\vec{R}|)F_r(\vec{R}) \tag{53}$$

where $F_r(\vec{R})$ is the wavefunction for the neutral atomic products as they separate. With the use of Fermi's golden rule, the transition rate for the decay of the collision can be obtained by evaluating the matrix elements:

$$\tau^{-1} = \frac{2\pi}{\hbar}|\langle \psi_c|\mathcal{H}'|\psi_r \rangle|^2 \tag{54}$$

The initial rate of recombination into the highly excited Rydberg states can be calculated in a similar manner.

2.5 Dissociative Attachment and Vibrational Excitation Calculations

A model that has been quite successful in explaining the dissociative attachment (DA) and vibrational excitation (VE) of diatomic molecules is the resonance model in which the projectile electron is temporarily trapped by the target molecule. The molecular anion (or the resonant

state) thus formed has a finite lifetime and it can either autodetach leading to VE of the molecule or, if the lifetime is sufficiently large, it can lead to DA forming a neutral atom and an atomic anion.

A few points of this model are the following: first, the dissociative electron attachment and the vibrational excitation of the molecule are two possible decay channels, apart from electronic excitation etc., resulting from a particular resonance state. Thus a calculation of the cross section for the dissociative electron attachment to a molecule will provide resonant contributions, of that particular resonant state, to the cross sections for vibrational excitation of the molecule and vice versa. Second, in explaining vibrational excitation by this resonance model, it is implicitly assumed that the transition from the resonant state $V^-(R)$ to the neutral state $V_0(R)$ after autodetachment is a Franck-Condon transition, that is, an instantaneous transition with no change in nuclear velocities or positions. This is a so-called local complex potential model. This is true only if the energy of the projectile electron is much greater than the vibrational spacing. At very low impact energies or if the vibrational spacing of the molecule is relatively large, a description of the DA and VE processes using a non-local complex potential for the resonant state is essential since the neutral molecule, for its vibrational excitation, can accept only quanta of vibrational energy. Third, in the cases of some molecules it might be possible, for certain electron energies, to form more than one intermediate resonant state. Alternatively, the resonant anion state may decay into more than one electronic state of the neutral molecule. In such cases, the total width $\Gamma(R)$ is the sum of various partial widths - each partial width corresponding to a certain transition between the resonant anion state (or states) and the neutral molecular state (or states).

2.5.1 Dissociative Attachment

The theory of the capture of an electron through the process of dissociative attachment (DA) to a molecule parallels that developed above for the dissociative recombination process. The process of dissociative attachment to a neutral molecule, XY, can be written as

$$e + XY \rightarrow \begin{bmatrix} X + Y^- \\ X^- + Y \end{bmatrix} \tag{55}$$

where X, Y are the dissociation fragments. The cross section for dissociative attachment is obtained by comparing the flux of the incoming electrons per unit area to the outgoing

ion-neutral pair flux defined by the asymptotic continuum wavefunction. We find, for energy normalized asymptotic functions,

$$\sigma_{DA} = \frac{2\pi^2\hbar^2 K}{\mu k_i^2} \lim_{R\to\infty} |\xi_j(R)| \tag{56}$$

where k_i is the wave number associated with the incoming electron and $\frac{\hbar K}{\mu}$ is the relative velocity of the asymptotic ion-neutral pair. The partial wave, $\xi_j(R)$ satisfies the radial equation:

$$\begin{aligned}\left(-\frac{1}{2\mu}\frac{d^2}{dr^2} + \frac{J(J+1)}{2\mu r^2} + V^-(R) - E\right)\xi_j(R) \\ = -\sum_V V_{VJE}(R)\xi_{VJ}(R)\left[\delta_{VV_i} - i\pi\int dR'\zeta^*_{VJ}(R')V^*(R')\zeta_{VJ}(R')\right]\end{aligned} \tag{57}$$

Here:

$$V_{VJE}(R) = \left\langle \psi_{VJE}(R)\middle|\mathfrak{H}_{el} - E\middle|\phi_D(R)\right\rangle \tag{58}$$

$\psi_{VJE}(R)$ is the wavefunction of the neutral molecule in vibrational state V in the presence of the scattering electron. $\phi_D(R)$ is the wavefunction of the anion at short internuclear separations as described, for example, by a stabilization calculation. If the electron energy is large or the vibrational spacing is small, one can replace E - E_V by the local classical electron energy (in a.u.):

$$V^-(R) - V_o(R) = \frac{k_o^2(R)}{2} \tag{59}$$

Then using the closure property:

$$\sum_{V,J} \xi^{*}_{VJ}(R)\xi_{VJ}(R') = \delta(R - R') \tag{60}$$

Equation (57) reduces to a local width model:

$$\left(-\frac{1}{2\mu}\frac{d^2}{dr^2} + \frac{J(J+1)}{2\mu r^2} + V^{-}(R) = \frac{i}{2}\Gamma(R) - E\right)\xi_J(R) = \xi_{V_i J}(R)[\Gamma_o(R)/2\pi k_o(R)]^{1/2} \tag{61}$$

where $\xi_{V_i J}(R)$ is the wavefunction of the initial rovibrational state of the target molecule. The resonant wavefunction $\xi_J(R)$ can be obtained by numerical integration of Equation (61) using, for example, the Numerov technique.

2.5.2 Vibrational Excitation

Vibrational excitation of a molecule can be written schematically as

$$e(k_i) + XY(V_i) \rightarrow e(k_f) + XY(V_f) \tag{62}$$

When the electron is far from the molecular target, we have $V[e + XY(V_i)] = 0$. The initial wavefunction can then be written as

$$\psi_i = A(k_i)e^{-i\vec{k}_i\cdot\vec{r}}\,\psi^{el}_{XY}\,\chi_{V_i} \tag{63}$$

where $A(k_i)$ is the initial plane wave amplitude. ψ^{el}_{XY} is just the electronic wavefunction of the unperturbed target. In a similar fashion, we can write for the asymptotic wavefunction after vibrational excitation

$$\psi_f = A(k_f)e^{-i\vec{k}_f\cdot\vec{r}}\psi_{XY}^{el}\,\chi_{V_f} \tag{64}$$

Conservation of energy requires

$$E(V_i) + \frac{k_i^2}{2} = E(V_f) + \frac{k_f^2}{2} \tag{65}$$

Finally the cross section for vibrational excitation can be written as

$$\sigma_{V_i\rightarrow V_f} = \frac{k_f}{k_i}\int dk_f' |T_{if}|^2 \tag{66}$$

where the transition matrix element from the initial to the final excitation state is obtained from

$$T_{if} = \frac{4\pi^2}{[k_i k_f]^{1/2}}\int d\vec{r}\psi_f^* V_{e+XY}\,\psi_i \tag{67}$$

Equation (67) can be further decomposed into resonant and nonresonant contributions and a partial wave expansion corresponding to the outgoing plane wave.

A computer program for calculating dissociative attachment cross sections has been developed based on the local width model. This model is generally valid when the electron collision energy is large relative to the vibrational and rotational spacings of the neutral target. For the problem of interest in this research, the dissociative attachment of electrons to silane, the local width approximation should be valid for collision energies greater than ~1.0 eV. This is approximately five times the vibrational quantum of the fundamental mode in silane. An upper limit is determined by the convergence properties of the outgoing plane wave representation of the dissociation species, X^- + Y or X + Y^-. In practice, this upper limit is 10 to 20 eV, depending on the extent of the long-range potential. For dissociative attachment at lower collision energies, the non-local width model described by Bardsley (Reference 46) must be employed. In either method, the calculation of the complex part of the interaction potential (capture width) is the most difficult aspect of the theoretical analysis.

2.6 Discussion of Charge Transfer Calculations

Low-to-intermediate energy ($\lesssim$ 100eV) ion-atom and ion-molecule charge transfer reactions play an important role in many physical processes. Until recently, comparatively little effort has been devoted to theoretical studies of the appropriate cross sections. In the past, both theoreticians and experimental physicists have found it easier to study high-energy ($\gtrsim$ 1 keV) collisions. At these energies, the two colliding particles preserve their identities, and it is possible to treat the interaction between them as a perturbation. There is no guarantee that this procedure, known as the Born approximation, will always converge to the correct result (Reference 47). As the energy of the colliding particles decreases, it is necessary to take account of the distortion these particles undergo during the collision. The method of perturbed stationary states was developed for calculating charge transfer and electronic excitation cross sections in relatively slow collisions between heavy particles (Reference 48). The method has been presented in both wave and impact parameter formalisms. In the first of these, the entire system is treated quantum-mechanically, while in the latter the nuclei are assumed to behave as classical particles, traveling along straight line trajectories, and the time-dependent Schrödinger equation is solved to calculate the probability of various types of electronic transitions (References 49-51). Forcing the particles to travel along straight lines limits the validity of the impact parameter method to collisions of several hundred electron-volts or greater (Reference 52). The wave formulation of the method of perturbed stationary states appears to be one practical method of calculating thermal energy charge-exchange cross sections. A semi-classical close-coupling method (Reference 53), based on an averaging scaling procedure, also offers utility for low to intermediate collision energies.

Approximate quantal treatments of reactive charge transfer at intermediate energies fall generally into three basic categories:

(a) Born approximation ignoring distortion

(b) Distorted wave Born approximations (adiabatic perturbations)

(c) Quantal impulse approximation

(a) In the Born approximation, distortion of the target by the projectile ion is ignored and the reactive and product wavefunctions are replaced by their asymptotic forms. Since no explicit mechanism for either charge transfer or dissociation is possible within this end-state approximation, the method is not particularly useful for ion-molecule collisions at low collision energies. The qualitative behavior of the Born approximation does, however, indicate that the cross sections should decrease very rapidly with increasing collision energy.

(b) The distorted wave Born approximation is based on the exact solution for the reactive cross section in terms of the T-matrix elements:

$$T_{\beta\alpha} = \langle \chi_\beta | V_\beta' | \chi_\sigma \rangle \tag{68}$$

where χ_β is a solution of the Schrödinger equation using incoming boundary conditions and χ_α is the solution of the complete Hamiltonian for the outgoing reaction channel, including all possible internal product states. V_β' is the reaction perturbation potential which includes distortion, polarization, etc. In the distorted wave Born approximation, χ_β and χ_α are replaced by simpler approximations, usually corresponding to a single internal state only. Choi and Tang (References 54 and 55) have discussed the numerical problems associated with evaluating matrix elements arising from this approximation and several applications to reactive collisions have been reported (References 56 and 57).

A still simpler approximation is available by reducing the matrix elements given by Equation (68) to a product of an electronic matrix element coupling the reactant and product states and a Franck-Condon overlap of the corresponding nuclear wavefunctions:

$$T_{\beta\alpha} = M_{el} \langle \chi_\beta | \chi_\alpha \rangle \tag{69}$$

This so-called overlap or Franck-Condon model was introduced by Halavee and Shapiro (Reference 58) and has been described in detail by Schatz and Ross (Reference 59).

(c) In the impulse approximation, the operator of the T-matrix element given by Equation (68) is replaced by an approximation which describes the elastic scattering corresponding to a collision between the projectile ion and the final free particle of the target molecule. This approximation is equivalent to the assumption that the collisions between the particles are sudden so that the collision time is much shorter than the vibrational period of the target molecule. Henglein, et al. (Reference 60) have argued that for ion-molecule collisions of several eV, this model, also called the spectator stripping mechanism, should be valid. Bates, et al. (Reference 61) have described a classical treatment of this impulse approximation.

In the following section, a very powerful method for solving the reactive coupled-channel collision problem is described. This approach is often referred to as the R-matrix or reactance

matrix propagation method. It generally yields a fast, efficient solution and automatically produces unitarity in the S-matrices. By freezing open channels or including the effects of closed channels, several levels of approximation are possible within the same computational framework.

2.7 R-Matrix Propagator Solution for Charge Exchange Reactions

The theory of heavy particle charge exchange is complicated by the fact that, in general, no simple natural coordinate system exists for which a uniform description of reactant and product states can be written. Considering the reaction:

$$\begin{aligned} H^+ + SiH_4 \left[{}^1T_D \right] &\rightarrow SiH_3^+ \left[{}^1A_1 \right] + H_2 \left[{}^1\Sigma_g^+ \right] \\ &\rightarrow SiH_3^+ \left[{}^1A_1 \right] + 2H \left[{}^2S \right] \end{aligned} \tag{70}$$

the internal coordinates describing SiH_4 cannot be uniformly mass-scaled to represent SiH_3^+ formed as a product. A natural coordinate system for such a collision has been described by Marcus (Reference 62), but this yields very complicated forms for the kinetic energy operator and presents many computational difficulties.

Recently, Stechel, et al. (Reference 63) have described an approach in which two separate nonorthogonal frameworks are employed to describe reactant and product states. The total scattering wavefunction is written as:

$$\psi = \psi^{\alpha}(R, \varrho_{\alpha}) + \psi^{\gamma}(R, \varrho_{\gamma}) \tag{71}$$

where α and γ represent reactant and product states, respectively. Expanding each as a linear combination of wavefunctions of the type:

$$\psi^i = \sum_j f_j^i (R)\, \phi_j^i (\varrho_i) \tag{72}$$

they show that a unique connection between reactant and product states can be achieved, provided the basis functions, $\{\phi^i(\varrho_i)\}$ are taken to be nonorthogonal, i.e., $S^{\alpha\gamma} = < \phi^{\alpha} | \phi^{\gamma} > \neq 0$.

We note that Equation (72), in molecular language, is a product wavefunction of the valance-bond type. We also note that an SCF or MCSCF framework for Equation (72) may not be appropriate for treating the collisional aspects of the reactant channel due to the orthogonality constraints that must be imposed on such wavefunctions. The use of non-orthogonal basis functions is simplified through the application of projection algebra techniques for the construction of wavefunctions of overall symmetry. Efficient computer codes for implementing such techniques has been developed in this Research Center over the past years and can be utilized in constructing the proper asymptotic reactant and product state channels.

The solution of the reactive charge exchange problem, including the product dissociation channels, can be accomplished using a direct Numerov integration of the Schrödinger equations arising from the basis representation of Equation (72). Alternatively, the R-matrix propagator method, originally formulated by Diestler (Reference 64), can be employed. This approach relates the known asymptotic solution in the reactant channel to that in the product channel through a series of recursive steps. Defining the normal derivative to the surface R = constant by $\nabla_n\psi(R,\varrho)$, we seek a propagator operator of the form:

$$\psi(R,\varrho) = \vec{R}\nabla_n\psi(R,\varrho) \tag{73}$$

The explicit matrix representation of this operator can be written as:

$$\psi\left[R_i - \frac{h_i}{2},\varrho\right] = -\vec{r}_1^{\,i}\nabla_n\psi\left[R_i - \frac{h_i}{2},\varrho\right] + \vec{r}_2^{\,i}\nabla_n\psi\left[R_i + \frac{h_i}{2},\varrho\right] \tag{74}$$

$$\psi\left[R_i + \frac{h_i}{2},\varrho\right] = -\vec{r}_3^{\,i}\nabla_n\psi\left[R_i - \frac{h_i}{2},\varrho\right] + \vec{r}_4^{\,i}\nabla_n\psi\left[R_i + \frac{h_i}{2},\varrho\right] \tag{75}$$

Stechel, et al. (Reference 63), have given explicit expressions for constructing the components of this operator, both in the asymptotic and overlap regions of the interaction. The initial boundary condition in the reactant channel is $\vec{R}^i = 1/\lambda_i$, where λ_i is the eigenvalue of the reactant target (in this case, SiH_4). The accuracy in developing the final R-matrix depends on the chosen step size, h_i, which is taken as an adjustable parameter that can be optimized during the course of the propagator solution.

We have recently implemented this R-propagator analysis at UTRC, using a modified version of the code developed by Stechel, et al. (Reference 63). One application has been the low-energy collisional de-excitation reaction:

$$N^*\left[^2D\right] + O\left[^3P\right] \rightarrow N\left[^4S\right] + O\left[^3P\right] \tag{76}$$

which occurs along a curve-crossing $^2\Sigma^+ - ^2\Sigma^+$ potential surface. The results of this study have been reported (Reference 65). A similar study of the kinetics of the charge transfer reaction, $O^+ + N_2 \rightarrow NO^+ + N$, has been carried out (Reference 66).

In summary, we have found that a description of the energetics of charge transfer reactions in a valence-bond framework, coupled with an analysis of the kinetics of these collisions using a non-orthogonal basis for reactant and product channels, within the R-propagator method of solution, represents an optimum analysis for the low to intermediate-energy kinetics.

2.8 Collisionally Induced Transitions

Consider the charge transfer process:

$$A^+ + B \rightarrow C^+ + D \tag{77}$$

where A^+ is a charged atomic or molecular ion reactively scattered by a target gas B to yield products, $C^+ + D$. If the reactant and product channels can be separately decoupled, it is often possible to treat Equation (77) as a pseudo-curve crossing problem. For near-adiabatic collisions, this type of system can be handled using a semi-classical approach, directly solving the second order differential equations which couple the adiabatic levels, possibly of different angular momentum.

The adiabatic states $\psi_1(\vec{r}, R)$ and $\psi_2(\vec{r}, R)$ are eigenstates of the non-relativistic Hamiltonian, $\mathfrak{H}$, for a fixed internuclear separation, R. We have

$$\mathcal{H}\phi_i(\vec{r}, R) = \epsilon_i\phi_i(\vec{r}, R); \quad i = 1,2 \tag{78}$$

In the two-state approximation we have, using impact parameter formulation,

$$\begin{aligned}\psi = {} & c_1(t)\phi_1(\vec{r}, R)\, e^{-\frac{i}{\hbar}\int_0^t \epsilon_1 d\tau} \\ & + c_2(t)\phi_2(\vec{r}, R)\, e^{-\frac{i}{\hbar}\int_0^t \epsilon_2 d\tau}\end{aligned} \tag{79}$$

where $R = R(t)$ and is defined by the collision trajectory.

We now require the inner product of ψ and ϕ_1 to vanish over the electronic coordinates.

$$\left\langle \phi_1 \left| \mathcal{H} - i\hbar\frac{\partial}{\partial t} \right| \psi \right\rangle = 0 \tag{80a}$$

$$\left\langle \phi_2 \left| \mathcal{H} - i\hbar\frac{\partial}{\partial t} \right| \psi \right\rangle = 0 \tag{80b}$$

Combining Equations (78), (79), and (80), we have

$$\left[\frac{\partial c_1}{\partial t} + c_1 < \phi_1 | \frac{\partial \phi_1}{\partial t} > \right] e^{-\frac{i}{\hbar}\int_o^t \epsilon_1 d\tau} + c_2 < \phi_1 | \frac{\partial \phi_2}{\partial t} > e^{-\frac{i}{\hbar}\int_o^t \epsilon_2 d\tau} \tag{81a}$$

$$\left[\frac{\partial c_2}{\partial t} + c_2 < \phi_2 | \frac{\partial \phi_2}{\partial t} > \right] e^{-\frac{i}{\hbar}\int_o^t \epsilon_2 d\tau} + c_1 < \phi_2 | \frac{\partial \phi_1}{\partial t} > e^{-\frac{i}{\hbar}\int_o^t \epsilon_1 d\tau} \tag{81b}$$

Converting from differentiation with respect to time, to velocity and angular momentum, we have

$$\frac{\partial \phi_i}{\partial t} = \frac{\partial R}{\partial t}\frac{\partial \phi_i}{\partial R} + \frac{i}{\hbar}\frac{\partial V_\theta}{\partial t} L_T \phi_i; \frac{\partial V_\theta}{dt} L_T \phi_i \tag{82}$$

where V_θ is the angular velocity of the internuclear axis and L_T is the angular momentum coupling operator. The first term on the right hand side of Equation (82) leads to the well known Landau-Zener (Reference 67) solution for states of identical molecular symmetry. For such cases the second term in Equation (82) vanishes.

For the systems under study here, where the second term on the right hand side of Equation (82) contributes in Equation (81), we are led to the following coupled equations:

$$\frac{\partial c_1}{\partial t} + \frac{i}{\hbar}\frac{\partial V_\theta}{\partial t} c_2 < \phi_1 | L_T | \phi_2 > e^{-\frac{i}{\hbar}\int_o^t (\epsilon_2 - \epsilon_1) d\tau} = 0 \tag{83a}$$

$$\frac{\partial c_2}{\partial t} + \frac{i}{\hbar}\frac{\partial V_\theta}{\partial t} c_1 < \phi_2 | L_T | \phi_1 > e^{-\frac{i}{\hbar}\int_o^t (\epsilon_1 - \epsilon_2) d\tau} = 0 \tag{83b}$$

Assuming a linear dependence of ϵ on R near the crossing point of the collision, we have

$$\epsilon_2 - \epsilon_1 = b\hbar(R - R_x) = \alpha t \tag{84}$$

$$\alpha = \frac{V_R}{\hbar} \frac{d(\epsilon_2 - \epsilon_1)}{dR}\Big|_{R_x} \tag{85}$$

Assuming also that $< \phi_1 | L_T | \phi_2 > = < L_T >$ is essentially constant over the dominant region of the collision, we have

$$\frac{\partial c_1}{\partial t} + \frac{iw < L_T >}{\hbar} c_2 e^{-\frac{i}{\hbar}\int_o^t (\epsilon_2 - \epsilon_1) d\tau} = 0 \tag{86a}$$

$$\frac{\partial c_2}{\partial t} + \frac{iw < L_T >}{\hbar} c_1 e^{-\frac{i}{\hbar}\int_o^t (\epsilon_1 - \epsilon_2) d\tau} = 0 \tag{86b}$$

Equations (86a) and (86b) have been solved numerically by Russek (Reference 68) for the case of curve-crossing states with $\Delta\Lambda = \pm 1$. For small values of angular velocity, Russek shows that Equation (86) reduces to a standard Landau-Zener form. For large velocities, the general solution of Equation (86) must be employed.

When more than one product channel is possible, a matrix of coupled equations of the type given by Equation (83) arises and a multi-surface mechanism is required for a complete description of such systems. Often a single reaction channel dominates and electron or H transfer

occurs with nearly unit probability along a single reaction surface. For such systems where a curve crossing is evident, the harpoon (Reference 69) or spectator stripping model (Reference 70) is often useful. This leads to the simplest reaction cross section, $\sigma = \pi R^2$, where R is the effective separation for a crossing on the reaction path. In a next higher order approximation, the reaction cross section is given by

$$\sigma = 2\pi \int_o^R P_{ij}(b) b db \tag{87}$$

where P_{ij} is the single crossing transition probability (≤ 1.0) which can often be approximated by the Landau - Zener formula. An extension of this simplified treatment to include internal vibrational states has been given by Bauer, et al. (Reference 71).

2.9 Classical Ion-Molecule Collisions: The Langevin-Gioumousis-Stevenson Reaction Rate

In the simplest development of ion-molecule kinetics, it is often assumed that the reaction will occur at the first collision between the reactant pair, provided that there is at least one exothermic reaction channel available. Simple ion-molecule reaction rates have therefore been equated with ion-molecule collision rates. Experimentally, many ion-molecule reactions do occur at every collision between the ion-molecule pair, but there are many exceptions to this simple case. It is now established that in many cases, ion-molecule collisions may be unreactive even if an exothermic channel is available (Reference 72). Competing reaction channels or the presence of barriers in the reaction path (ex: $O^+ + N_2$) may also cause a drastic reduction in the collisional reaction rate (References 73 and 74).

An elementary treatment of ion-molecule reaction kinetics can be developed from a classical description of the scattering cross section. For scattering by a spherical potential, the reaction cross section can be written as

$$\sigma(E) = 2\pi \int_o^\infty P(b, E) b db \tag{88}$$

where b is the classical impact parameter and P(b, E) is the probability that the reaction will occur for a given energy, E, and impact parameter, b. For ion-molecule reactions, a model can be constructed based on the assumption that for values of the impact parameter less than a critical orbiting parameter, b_0, the reaction probability can be taken as unity. This critical orbiting impact

parameter, b_0, is defined so that ion orbits for which $b < b_0$, spiral in close to the target and orbits for which $b > b_0$ come no closer than $b_0/\sqrt{2}$. For the simplest possible case of a spherical molecule with isotopic polarizability and with no permanent moment, interacting with a point charge, the interaction potential takes the form

$$V(R) = \frac{e^2\alpha}{2R^4} \tag{89}$$

In this case the orbiting parameter, b_0, is found to be

$$b_o = \left[\frac{4e^2\alpha}{\mu v^2}\right]^{1/4} \tag{90}$$

where μ is the reduced mass of the colliding pair and v is their initial relative velocity. Using b_0 as an upper integration limit in Equation (88), we find for the reaction cross section:

$$\sigma(v) = \pi b_o^2 = \frac{2\pi}{v}\left[\frac{e^2\alpha}{\mu}\right]^{1/2} \tag{91}$$

Equation (91) has been restated by Gioumousis and Stevenson (Reference 75) in terms of the energy, E, of the primary ion of mass, m, as

$$\sigma(E) = \pi\left[\frac{2e^2\alpha m}{\mu E}\right]^{1/2} \tag{92}$$

which shows an inverse square root behavior of the reaction cross section with collision energy. Assuming a Maxwellian distribution function, f(v), for both the ions and neutral molecules, the rate coefficient corresponding to the cross section given by Equation (91) becomes

$$k = \int_o^\infty f(v)\sigma v dv = 2\pi\left[\frac{e^2\alpha}{\mu}\right]^{1/2} cm^3/sec \tag{93}$$

Equation (93) is the well-known Langevin formula (Reference 76) for the reaction rate, valid for close encounters and typically of the order of 10^{-9} cm^3/sec. The validity of Equation (93) is

strengthened for systems where the polarizability of the molecule is large and the reduced mass is small, so that few collisions occur outside of the orbiting radius. The Langevin rate, which is predicted to be independent of the collision energy, is thus most valid for collisions with small target gases such as $He^+ + H_2$. For large target molecules and ion-molecule systems with many internal degrees of freedom, including target dissociation, the Langevin rate will predictably be too large. This simple model also is incapable of predicting the product distribution of an ion-molecule reaction. It should be noted that, in this regard, the Langevin formula is formally invalid since the requirement of unitary in the scattering matrix (principle of detailed balancing) is violated for this classical treatment.

SECTION 3

DISCUSSION OF RESULTS

The main focus of our current studies was on understanding the role that positive ion-molecule dissociative charge transfer reactions play in the discharge chemistry pertinent to deposition of amorphous silicon thin films. A preliminary analysis of the production of negative silane ions by dissociative attachment and negative ion-molecule dissociative charge transfer reactions was also undertaken. A summary of our results from these investigations follows.

3.1 Dissociative Charge Transfer

3.1.1 Thermochemistry of SiH_n Species

The first part of our study of positive ion silane reactions was concerned with an examination of the electronic structure, predicted equilibrium geometries and thermochemistry of both neutral and ionic silane species. After some computer experimentation with basis sets and the appropriate level of theory, it was decided that a globally accurate analysis of the reaction surfaces could be accomplished using the MP2/6-31++G** level of theory (References 22 and 77). At this level, a split valence description of the valence electrons is employed, augmented by d-orbital polarization functions on Si and p-orbital polarization functions on H. In addition, diffuse sp shells are added to give a more balanced treatment to negative ions. This choice of basis was also employed by Curtiss and Pople (Reference 78) in earlier work on SiH_n species. The Møller-Plesset (MP2) level of theory is not really adequate for an accurate thermodynamic analysis but was a compromise choice since large regions of the reaction surfaces (multiple geometries) needed to be examined. In Table 1, we give the calculated geometry and electronic energy for species of the silane/hydrogen system at the MP2/6-31++G** level of theory. These calculated data were combined in isodesmic reaction groups to estimate heats of formation. Our resultant enthalpies at 0 K are given in Table 2 where we have also included the known thermochemistry of non-silane species. This table is the basis of our energetic analysis for the ion-molecule reactions in the silane/hydrogen system.

3.1.2 $H^+ + SiH_4$

Our next task involved the generation of the potential energy surface for the ion-molecule reaction:

$$H^+ + SiH_4 \rightarrow H_2 + SiH_3^+ \qquad (94)$$

Table 1. Calculated Energies of the Silane/Hydrogen System

MP2/6-31++G** Level of Theory

Species	State	Point Group	R(Si-H)	Angle	E(MP2)
SiH_4	$^1A_1$	T_d	1.4719		– 291.353112
SiH_3	$^2A_1$	C_{3v}	1.4723	107.67	– 290.711666
SiH_2	$^1A_1$	C_{2v}	1.5079	92.55	– 290.097098
SiH_2	$^3B_1$	C_{2v}	1.4699	118.27	– 290.074758
SiH	$^2\Pi$	$C_{\infty v}$	1.5144		– 289.483907
SiH_4^+	(not bound as T_d or C_{3v} structure, weakly bound in C_s)				
SiH_3^+	$^1A_1'$	D_{3h}	1.4550		– 290.426400
SiH_3^+	$^3E''$	D_{3h}	1.5349		– 290.228128
SiH_2^+	$^2A_1$	C_{2v}	1.4684	119.97	–289.206614
SiH^+	$^1\Sigma^+$	$C_{\infty v}$	1.4945		– 289.206614
SiH_3^-	$^1A_1$	C_{3v}	1.5281	120.72	– 290.740824
SiH_2^-	$^2B_1$	C_{2v}	1.5353	93.09	– 290.124127
SiH^-	$^3\Sigma^-$	$C_{\infty v}$	1.5441		– 289.517930

Energies are in hartrees (1 h = 27.21161 eV), geometries are in Angstroms and degrees.

Table 2. Enthalpies for Silane/ Hydrogen/Noble Gas Species

Species	$\Delta H°f_0$ (kcal/mol)	$\Delta H°f_0$ (eV)	I_p(eV)
SiH_4 [$^1A_1$]	10.5	0.455	11.00
SiH_3 [$^2A_1$]	47.6	2.064	8.01
SiH_2 [$^1A_1$]	65.5	2.845	9.15
SiH_2 [$^3B_1$]	86.6	3.755	8.24
SiH [$^2\Pi$]	89.6	3.885	7.91
Si [^3P]	106.6	4.623	8.151
SiH_4^+ [$^2A'$]	264.2	11.457	
SiH_3^+ [$^1A'$]	232.4	10.078	
SiH_2^+ [$^2A_1$]	276.6	11.995	
SiH^+ [$^1\Sigma^+$]	272.0	11.795	
Si^+ [^2P]	294.5	12.771	
H_2 [$^1\Sigma_g^+$]	0.0	0.0	15.426
H [^2S]	51.63	2.239	13.598
H_3^+ [$^1A'$]	265.82	11.527	
H_2^+ [$^2\Sigma_g^+$]	355.73	15.426	
H^+ -	365.72	15.838	
Ar [^1S]	0.0	0.0	15.759
Ar^+ [^2P]	363.41	15.759	
He [^1S]	0.0	0.0	24.587
He^+ [^2S]	566.99	24.587	
ArH^+ [$^1\Sigma^+$]	270.73	11.740	
HeH^+ [$^1\Sigma^+$]	322.68	13.993	

over a wide range of internuclear geometries. This surface was first examined at the HF/6-31G* level of theory and subsequently at the correlated MP2/6-31G* level. The most interesting feature of the global surface for this reaction is the abstraction of an H^- along the H^+–H–SiH_3 bond axis. In Figure 1 we show this region of the reaction surface, plotting the energy of the reactants as a function of the expanding H–SiH_3 bond, with the H^+–SiH_3 distance as a parameter. The Si–H bond angles and the three Si-H bonds not involved in the H^+ attack were optimized for each fixed H^+–H–SiH_3 geometry. Basically, this region of the surface illustrates the energy change as the H^- is stripped from SiH_4 and attaches to the colliding H^+. At the Hartree Fock (HF) level, Figure 1 indicates that the H^- transfer is endothermic (transfer does not occur) until the H^+–SiH_3 distance of closest approach, b , is less than approximately 4.5 Å. For collisions with $b \leq 4.5$ Å, the probability of the H^- abstraction reaction (94) is unity since the surface is uniformly attractive.

The $H^+ + SiH_4$ reaction surface was also calculated globally at the MP2/6-31G* level of theory. This surface, which is shown in Figure 2, was chosen as our prototype surface for analyzing the validity of R-matrix calculations. The surface shown in Figure 2 is an extension and refinement of the HF surface shown in Figure 1. The kinetics of the ion-molecule reaction given by Equation (94) were computed using the minimum energy reaction path along the global surface given in Figure 2. The intrinsic reaction path hamiltonian method, as described by Diestler (Reference 64) was utilized for most of our kinetic studies of positive ion-molecule reactions.

In order to study this same reaction without imposing high collisional symmetry, we have calculated the $H^+ + SiH_4$ reaction in C_s symmetry where only a reflection plane for the SiH_5^+ complex is imposed. The calculated results are shown in Figure 3. Here the strength of the H^- abstraction reaction is clearly illustrated. In reaction sequence c), we already see the proton attraction causing a rotation of the silane molecule to yield a shorter H-H^+ bond distance. By sequence f), the H^- abstraction has occurred and the resulting SiH_3^+ ion is collapsing to a trigonal form. No constraints at all were placed on bond lengths or bond angles in this reaction sequence. At the reaction sequence illustrated in f), a large electron density has suddenly built up around the reactant ion. This resembles the harpooning type of reaction that occurs in ionic-covalent curve-crossing situations but the analogy should not be taken too literally since only a single reaction surface is involved in this $H^+ + SiH_4$ collision. This reaction is dramatically portrayed in Figure 4 which illustrates the electric potential contour plots for this same sequence of geometries. Both the rotation of the SiH_4 molecule in sequence c) and d), and the H^- abstraction by sequence f) are identifiable in these contour plots. The rapid concentration of contours about the reactant H^+ ion illustrates the electron charge buildup. We find no evidence of a direct reaction pathway leading to SiH_2^+ formation in C_s symmetry.

The potential energy reaction surfaces for the various product channels of the reaction, H^+ +

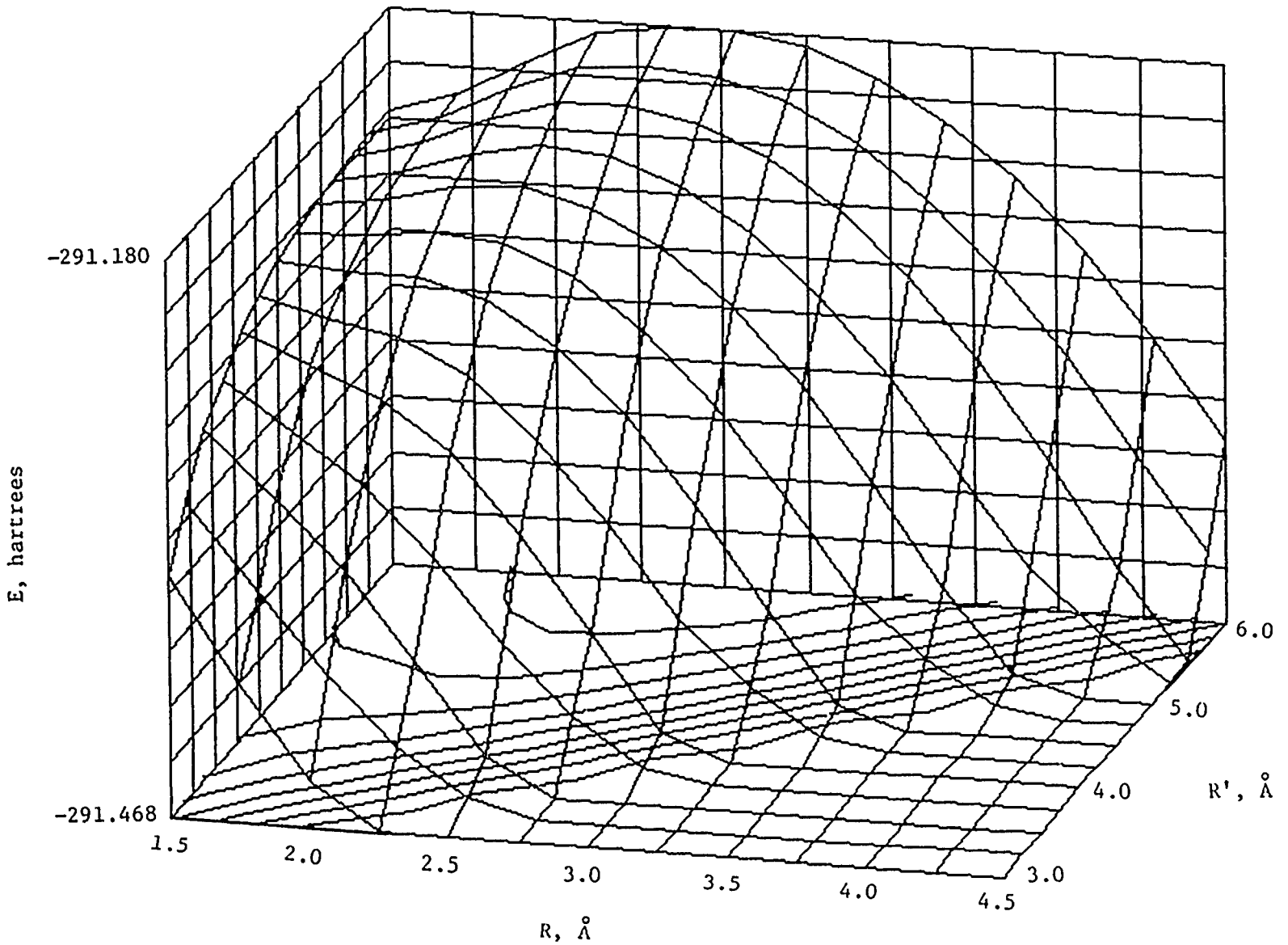

Figure 1. Global Potential Energy Surface for $H^+ + SiH_4$ Along the Bond Axis.

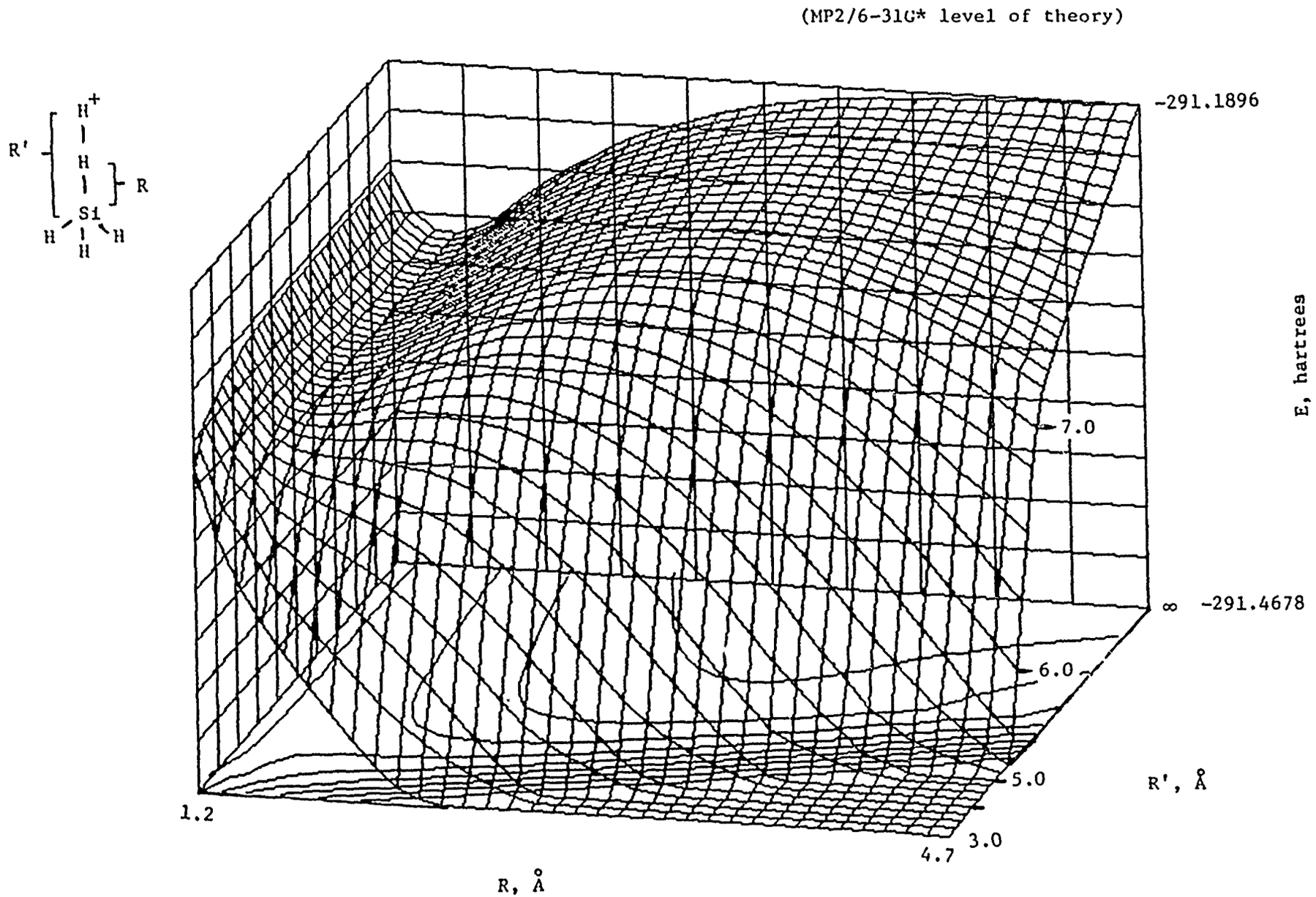

Figure 2. Global Potential Energy Surface for $H^+ + SiH_4$.

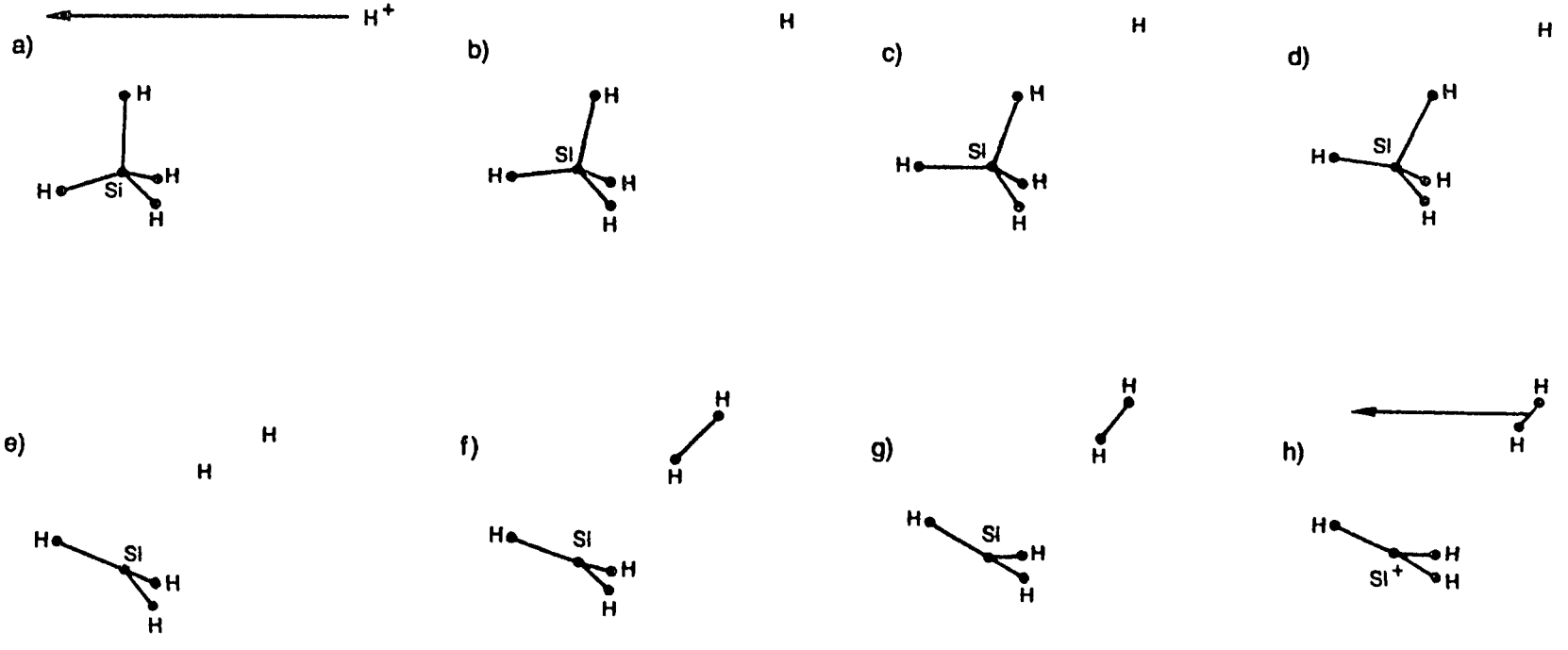

Figure 3. Reaction Sequence for $H^+ + SiH_4 \rightarrow H_2 + SiH_3^+$.

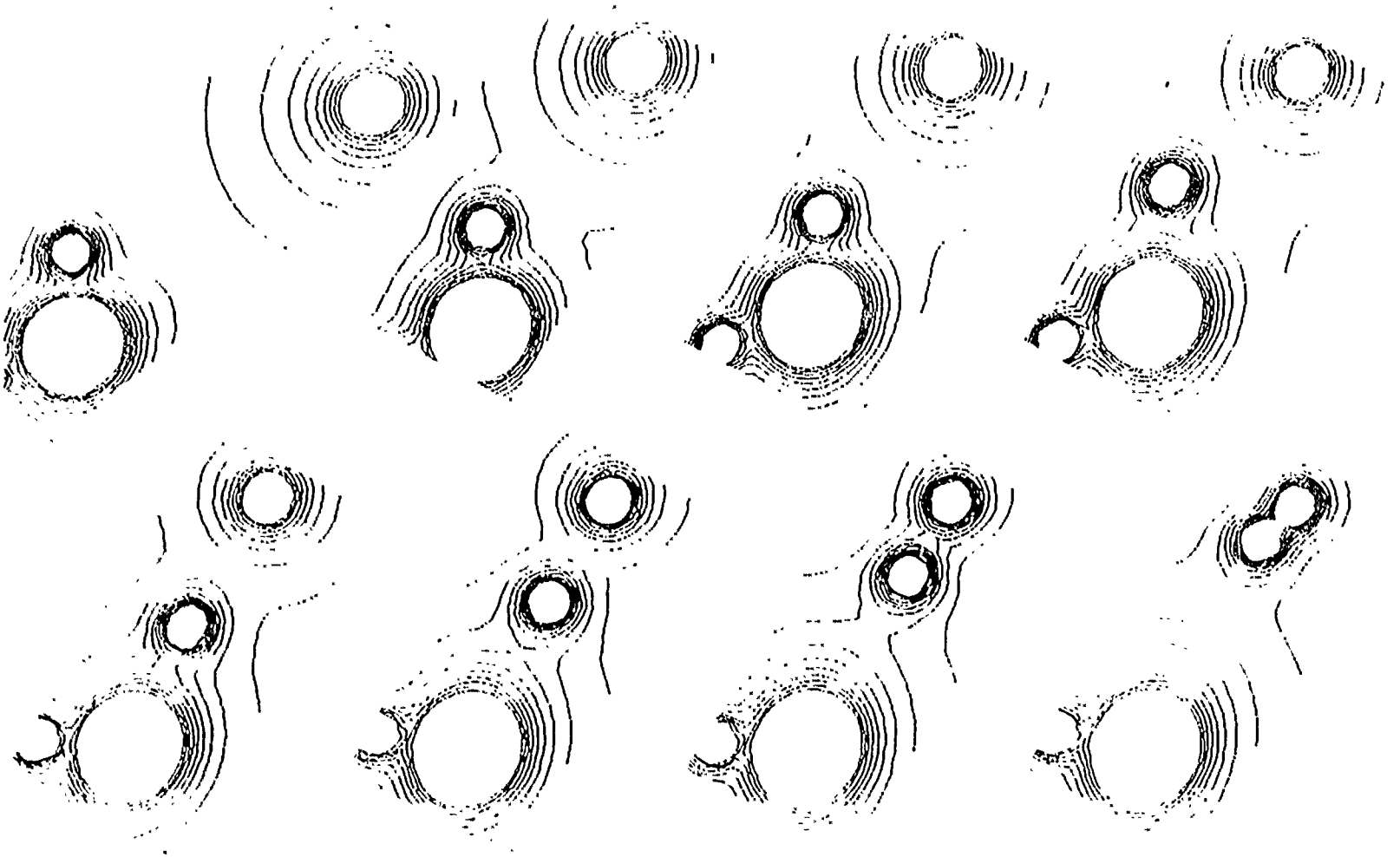

Figure 4. Electric Potential ($H^+ + SiH_4 \rightarrow H_2 + SiH_3^+$).

SiH_4, were next examined using correlated wavefunctions. The calculations were carried out at the MP2 level of theory using a Gaussian 6-31++G** basis, which includes both polarization functions and diffuse functions on silane and hydrogen atoms. The product channels $SiH^+ + H_2$ and SiH_3^+ are shown in Figure 5 at the MP2 level. We find a potential energy ridge of ~ 6.8 eV separating these product channels, similar to a 6.0 eV barrier found at the HF level of theory. SiH^+ is thus not an important product for collision energies less than ~ 2.3 eV [6.8 eV (barrier) - 4.5 eV (exothermicity)]. The dissociation channel, $SiH_2^+ \rightarrow Si^+ + H_2$, is shown in the contour plot given in Figure 6. An activation barrier of 2.3 eV is found at the MP2 level of theory, similar to a 3.0 eV barrier found at the SCF level. In agreement with the SCF results, the MP2 minimum energy reaction path is for a perpendicular approach of H_2 to Si^+. The contours are somewhat smoother at the MP2 level with the plateau of the reaction surface at $R_{HH} = 1.6$ Å, $R_{Si\text{-}H_2} = 1.35$ Å. Minimum energy reaction paths for the addition of H to Si^+, SiH^+ and SiH_2^+ are shown in Figure 7. There are no apparent activation barriers for the addition (or elimination) of H atoms to silane ions.

The diabatic potential energy surfaces describing both the reactant and product channels for reaction (1) were next calculated. The long range attractive potential for the reactant channel was fit to an ion-induced dipole form, $V(R) = -\alpha/2R^4$. The polarizability of silane was taken to be 4.62 $Å^3$, in agreement with Haaland's (Reference 10) recommendation. The long range form for the product channel was scaled to the asymptotic value calculated for a H_2–SiH_3^+ separation of 5.5 bohrs. The correct long range form should be :

$$V(R) = -\frac{e^2}{R^4}\frac{(\alpha_{\parallel} - \alpha_{\perp})}{3} P_2(\cos\theta) - \frac{e^2}{2R^4}\frac{(\alpha_{\parallel} + \alpha_{\perp})}{3} \qquad (95)$$

where $\alpha_{\parallel}$ and $\alpha_{\perp}$ are, respectively, the parallel and perpendicular components of the polarizability tensor for the H_2 molecule. The averaging of the anisotropy of the polarizability mainly affects the elastic cross section for $H_2 + SiH_3^+$ collisions and has little effect on the reactant channel. The resultant diabatic curves are shown in Figure 8 where H_{ij} is the coupling element connecting reactant to product channels. For comparison, the calculated global adiabatic surface for this reaction is shown in Figure 2. Diagonalization of the diabatic potentials shown in Figure 8 leads to the minimum energy pathway representing the valley on the global adiabatic surface.

Reactive scattering cross sections were calculated for the reaction, $H^+ + SiH_4 \rightarrow H_2 + SiH_3^+$, using the R-matrix method. The input diabatic interaction potentials illustrated in Figure 8 were employed. Our calculated cross sections, as a function of center-of-mass collision energy, are given in Table 3 and illustrated in Figure 9. We find that the calculated cross sections generally follow the Langevin rate energy dependence, but are 10-40% higher in absolute value, for collision energies $\geq$ 0.1 eV. This suggests that the effective reactive collisional diameter is underestimated

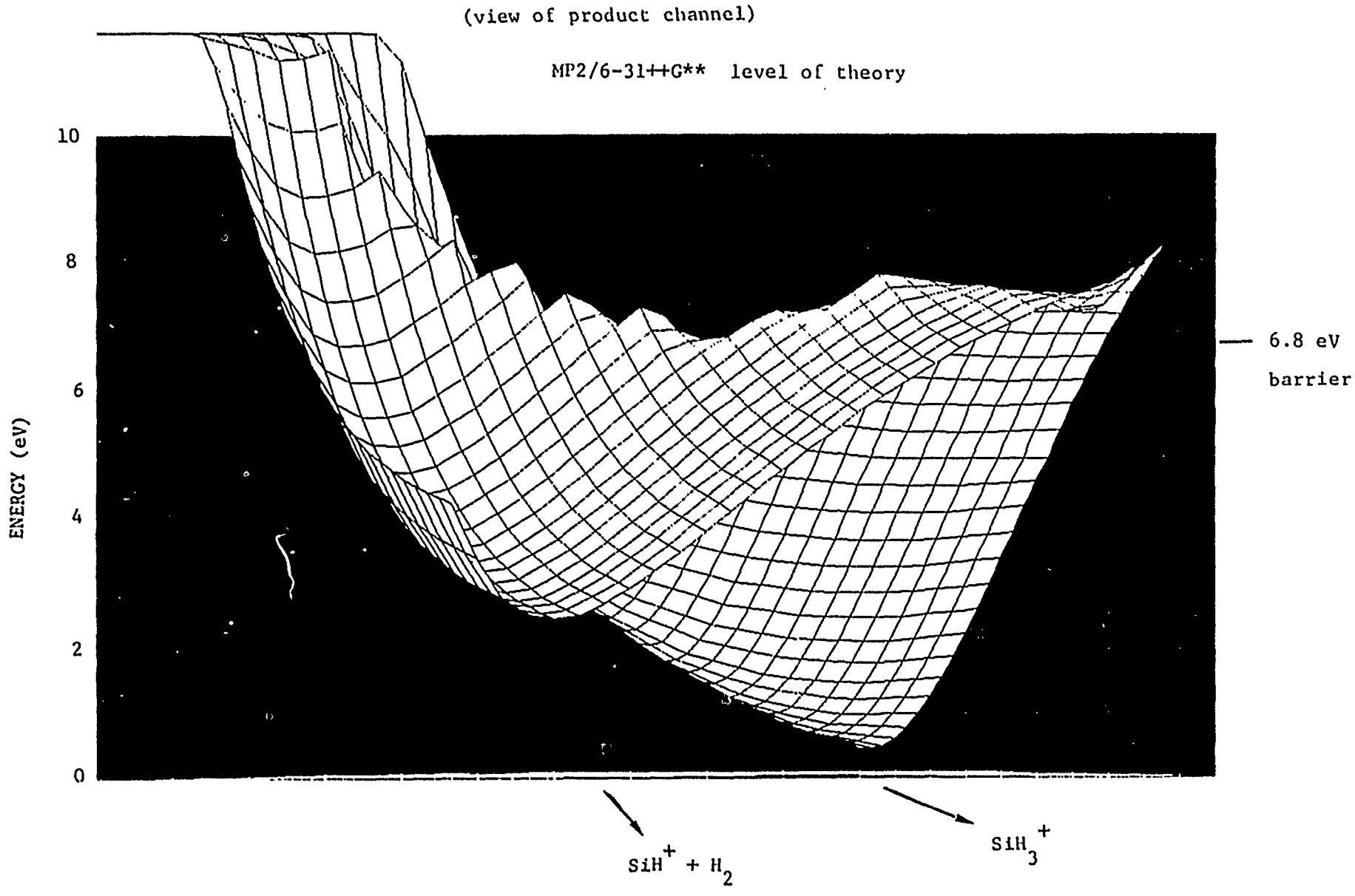

Figure 5. Potential Energy Surface for $SiH_3^+ \rightarrow SiH^+ + H_2$.

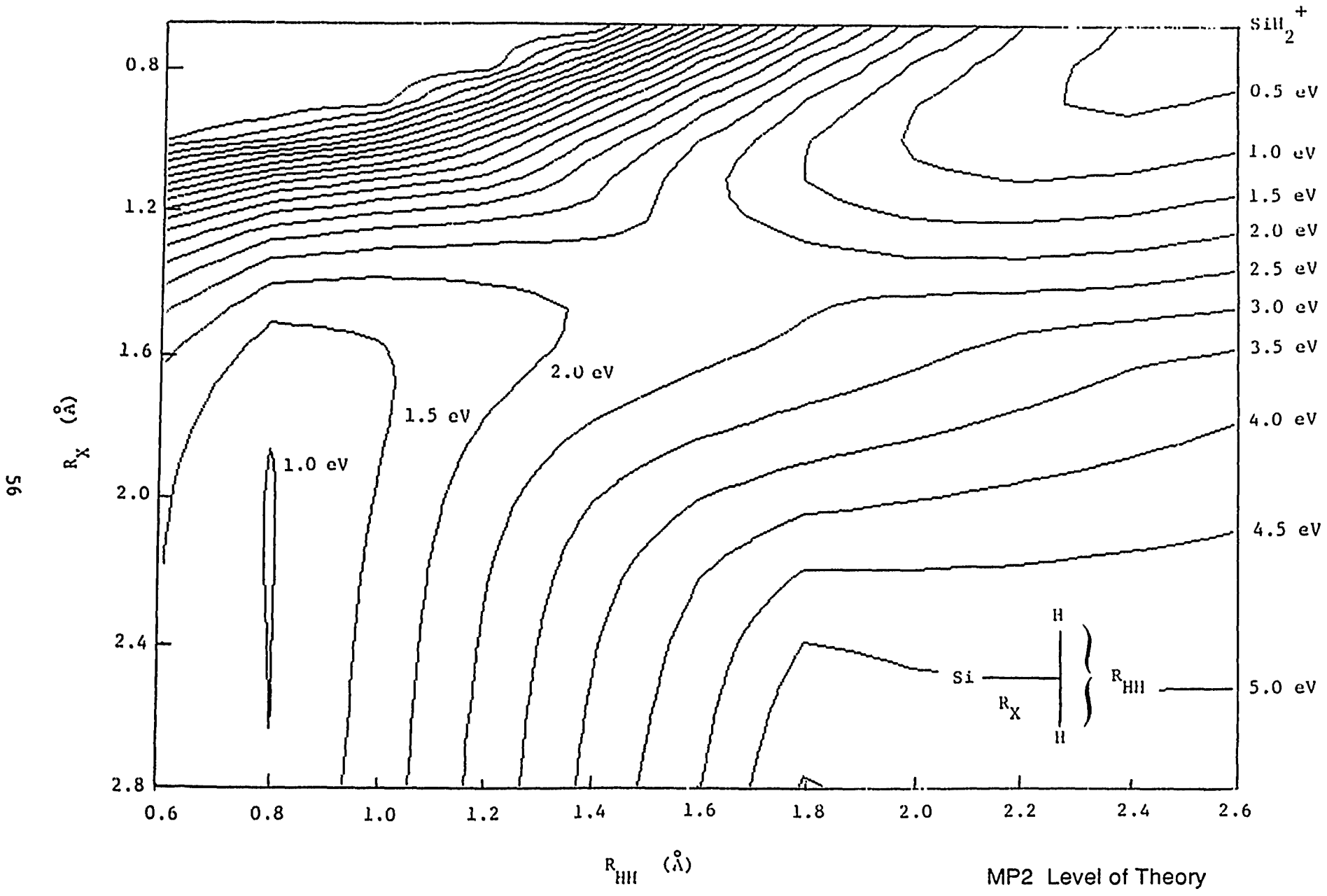

Figure 6. Contour Plot for $Si^+ + H_2$.

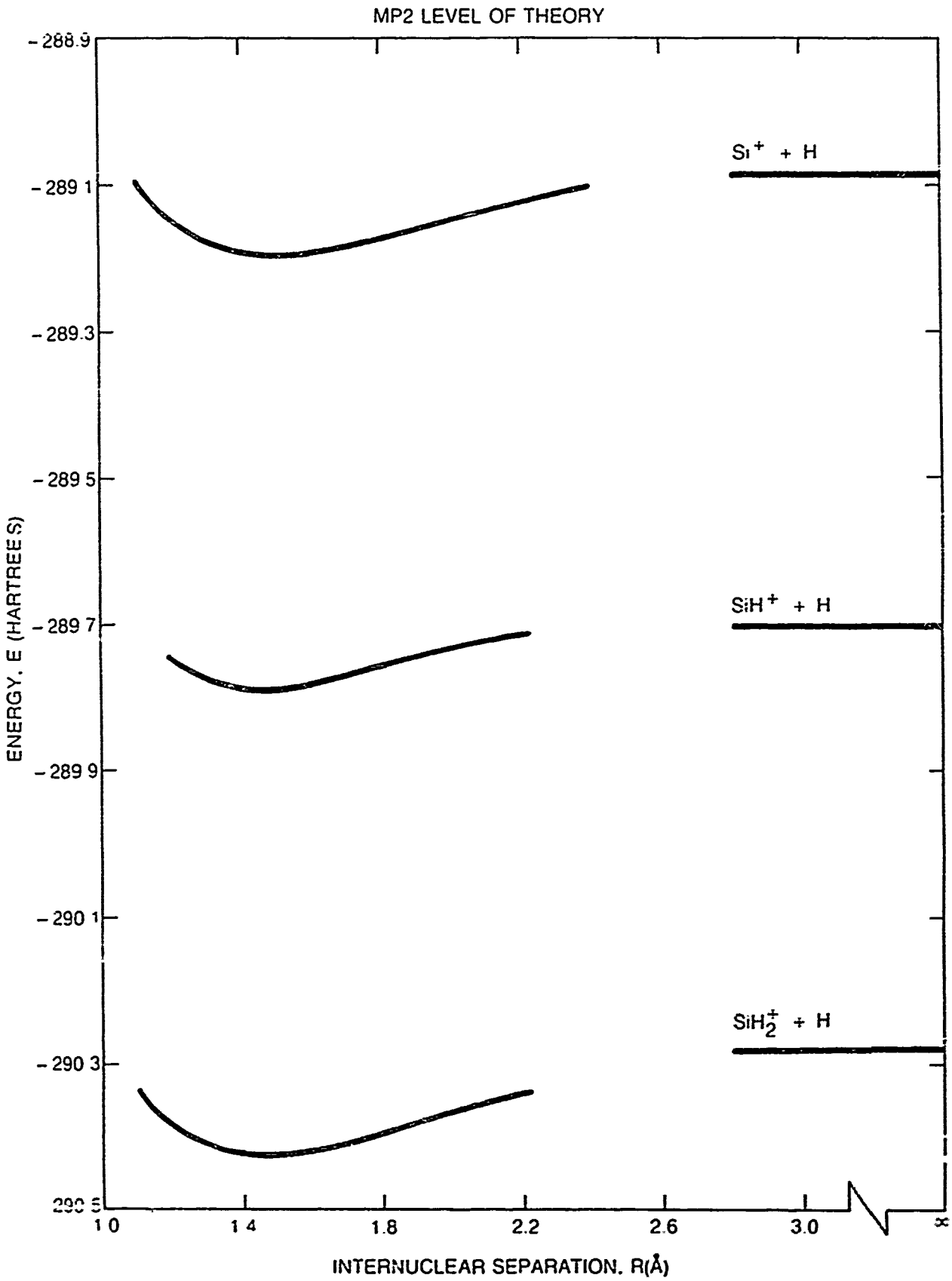

Figure 7. Minimum Energy Reaction Coordinates for $SiH_n^+ + H$ (n=0,1,2).

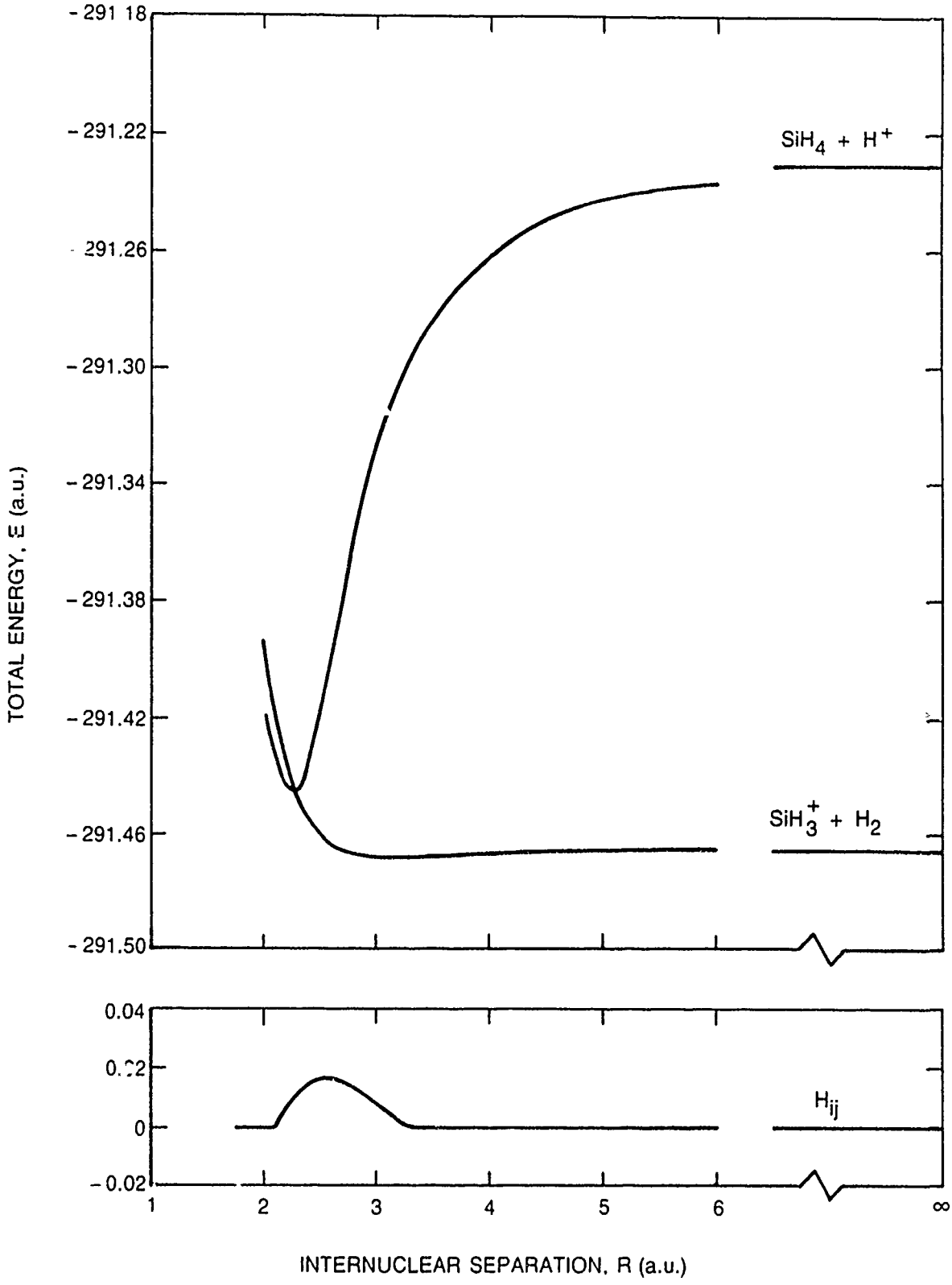

Figure 8. Diabatic Potential Energy Curves for the Reaction: $SiH_4 + H^+ \rightarrow SiH_3^+ + H_2$.

Table 3. Calculated Reaction Cross Section

$$SiH_4 + H^+ \rightarrow H_2 + SiH_3^+$$

Energy (eV)	Energy (hartrees)	Jmax	Sigma ($Å^2$)
0.01	0.00037	70	384.7
0.03	0.0011	90	274.5
0.10	0.0037	150	182.2
0.30	0.011	210	108.5
1.00	0.037	330	59.8
3.00	0.11	530	29.0
10.00	0.37	890	13.4
30.00	1.1	1230	8.2
100.00	3.7	2270	5.4

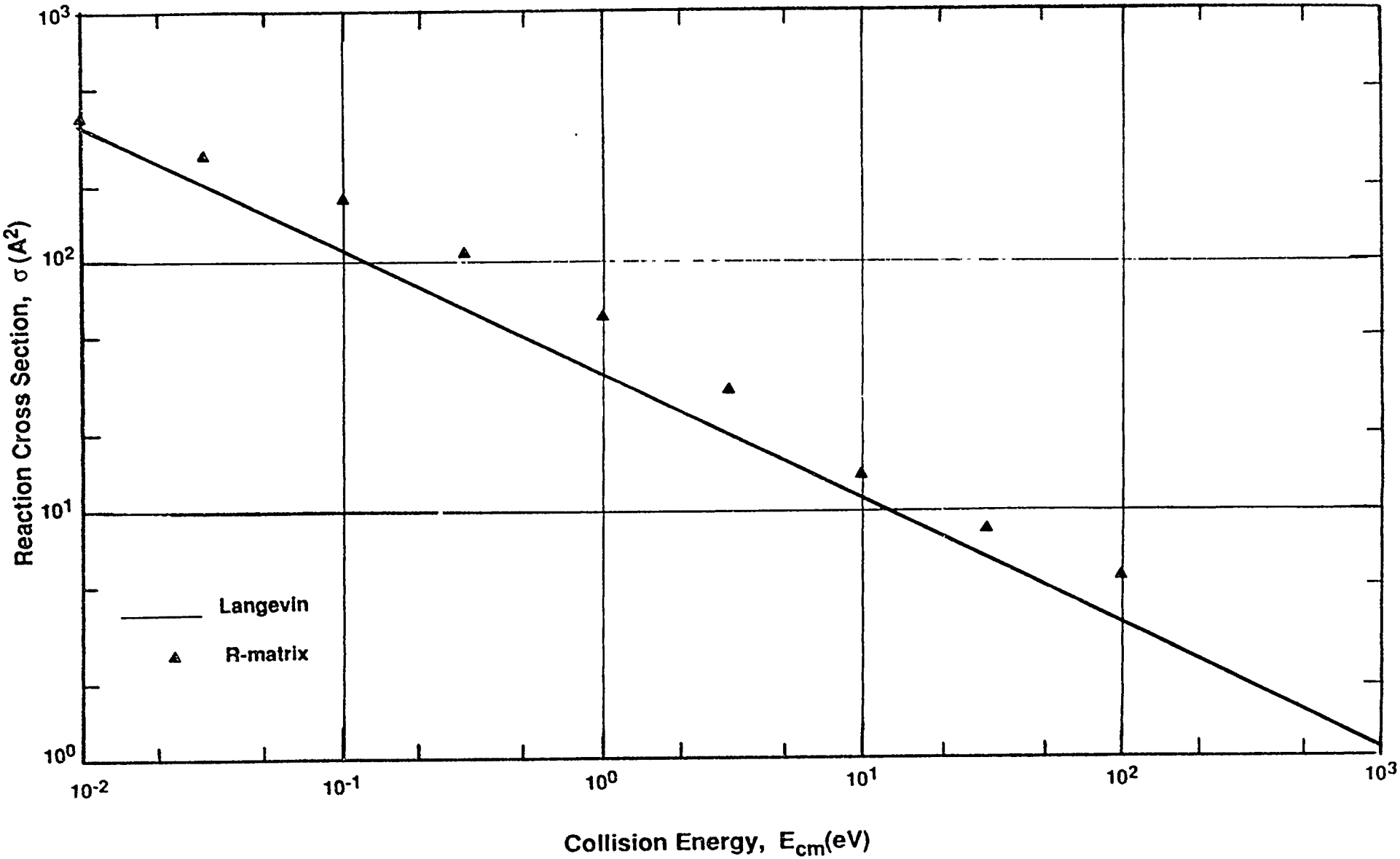

Figure 9. Calculated Cross Section for: $H^+ + SiH_4 \rightarrow H_2 + SiH_3^+$.

by the Langevin model. Further studies of this point, including sensitivity of the R-matrix results to the calculated input potentials, are suggested as possible extensions of the present investigation.

3.1.3 SiH_4^+ Structure

As an addendum to our studies of the $H^+ + SiH_4$ reaction surfaces, a study of the stability of SiH_4^+ was carried out. Haaland and Rahbee (Reference 79) report negative evidence for the silane cation using Fourier transform mass spectrometry. Recently, Pople and Curtiss (Reference 80) have reported that SiH_4^+ is stable as a donor-acceptor-complex of H_2 with SiH_2^+ (Cs structure) at the HF/6-31G* level of theory. Previous theoretical studies have indicated no stability for SiH_4^+ as a T_d or C_{3v} structure. The C_s structure reported by Pople and Curtiss should appear at 11.22 eV which is in excellent agreement with the result of 11.0 eV reported by Berkowitz, Greene and Cho (Reference 81). In order to gain more insight into this C_s structure for SiH_4^+, a structure optimization calculation was carried out at the MP2/6-31++G** level of theory. We find an optimized structure very similar to that reported by Pople and Curtiss as indicated below.

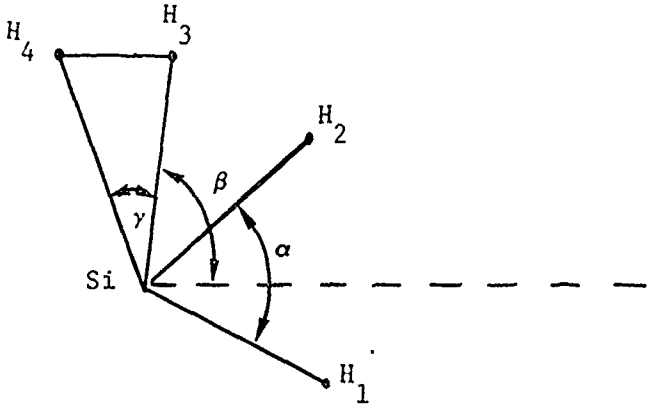

$R(Si\text{-}H_{1,2}) = 1.459$ Å
$R(Si\text{-}H_3) = 1.859$ Å
$R(Si\text{-}H_4) = 1.819$ Å
$\alpha = 120.9°$
$\beta = 89.3°$
$\gamma = 24.1°$

E = – 290.9592 8775 hartrees

We find that this C_s structure has slightly more stability (shorter Si-H_2 bonds) at the MP2 correlated level of theory relative to the Hartree Fock study. Our calculated thermodynamics for this ion are:

$$SiH_4 \rightarrow SiH_4^+ + e \qquad I_p = 10.7 \text{ eV} \qquad (96)$$

$$SiH_4^+ \rightarrow SiH_2^+ + H_2 \qquad \Delta H = +\ 10.8 \text{ kcal/mol} \qquad (97)$$

These calculated data are in excellent agreement with the experiments of Berkowitz, et al. (Reference 10) and the recent study by Börlin, Heins and Jungen (Reference 82).

3.1.4 Thermochemistry of SiF_n Species

The chemical reactions involving SiF_n and SiF_n^+ species are computationally more difficult to analyze than the corresponding hydride systems owing to their more complex electronic structure. After some experimentation with basis sets, it was decided to restrict our studies to the use of the 6-31G* split-valence shell + polarization basis set at the MP2 level of theory. Although absolute thermochemistry is not well described at this level, recent studies reported by Weber and Armentrout (Reference 83) and older data on SiF_n species reported in JANAF (Reference 84) could be used to calibrate our data, which should be accurate for isodesmic processes. In Table 4, we give the calculated geometry and electronic energy for species of the silane/fluorine system at the MP2/6-31G* level of theory. These calculated data were combined in isodesmic reaction groups and combined with best estimate experimental values, where available, to predict a consistent set of heats of formation. Our resultant enthalpies at 0 K are given in Table 5. This table is the basis for our energetic analysis for ion-molecule reactions in the silane/fluorine system.

3.1.5 Positive Ion-Molecule Reactions

The thermochemical values for the SiH_n and SiF_n systems given in Tables 2 and 5, respectively, can be employed to construct the energetics of the product channels for silane ion-molecule reactions. These data are collected in Table 6 which illustrates the exothermic character for most of the reaction channels. The following reactions were examined:

$$H^+ + SiH_4 \qquad (98)$$
$$H_3^+ + SiH_4 \qquad (99)$$
$$Ar^+ + SiH_4 \qquad (100)$$
$$He^+ + CH_4 \qquad (101)$$
$$H_3^+ + SiF_4 \qquad (102)$$

Table 4. Calculated Energies of the Silane/Fluorine System

MP2/6-31G* Level of Theory

Species	State	Point Group	R(Si-H)	Angle	E(MP2)
SiF_4	$^1A_1$	T_d	1.5810	109.472	– 687.740660
SiF_3	$^2A_1$	C_{3v}	1.5993	110.777	– 587.983952
SiF_2	$^1A_1$	C_{2v}	1.6160	100.894	– 488.321054
SiF_2	$^3B_1$	C_{2v}	1.6174	115.923	– 488.206088
SiF	$^2\Pi$	$C_{\infty v}$	1.6272		– 388.585225
SiF_4^+	(not bound as T_d or C_{3v} structure, weakly bound in C_s)				
SiF_3^+	$^1A_1'$	D_{3h}	1.5410		–587.664495
SiF_2^+	$^2A_1$	C_{2v}	1.5557	119.850	– 487.946747
SiF^+	$^1\Sigma^+$	$C_{\infty v}$	1.5592		– 388.353729
SiF^+	$a^3\Pi$	$C_{\infty v}$	1.5775		– 388.166157

Energies are in hartrees (1h = 27.21161 eV), geometries are in Angstroms and degrees.

Table 5. Enthalpies For Silane/Fluorine/Noble Gas Species

Species	ΔH_f^o (kcal/mol)	ΔH_f^o (eV)	I_p(eV)
SiF_4 [$^1A_1$]	– 384.96	– 16.68	[15.7]
SiF_3 [$^2A_1$]	– 239.	– 10.4	[9.3]
SiF_2 [$^1A_1$]	– 139.	– 6.0	[10.7]
SiF_2 [$^3B_1$]			
SiF [$^2\Pi$]	– 13.	– 0.6	7.54
Si [^3P]	106.6	4.62	8.15
Si_2 [$^3\Sigma_g^-$]	140.320	6.08	
SiF_4^+ [$^2A'$]	[– 24]	[– 1.0]	
SiF_3^+ [$^1A'$]	[– 26.2]	[– 1.1]	
SiF_2^+ [$^2A_1$]	109.0	4.73	
SiF^+ [$^1\Sigma^+$]	170.4	7.39	
Si^+ [^2P]	294.5	12.77	
F_2 [$^1\Sigma_g^+$]	0.0	0.0	15.43
HF [$^1\Sigma^+$]	– 65.13	– 2.82	16.06
F [^2P]	18.47	0.80	17.43
F_2^+	361.7	15.68	
HF^+ [$^2\Sigma^+$]	305.2	13.23	
F^+ [^3P]	420.25	18.22	
Ar [^1S]	0.0	0.0	15.76
Ar^+ [^2P]	363.41	15.76	
He [^1S]	0.0	0.0	24.59
He^+ [^2S]	566.99	24.59	

[ ] Uncertain

Table 6. Product Channels for Silane Ion-Molecule Reactions

						ΔH (kcal/mol)
1)	H^+	+ SiH_4	→			0.0
				H_2 +	SiH_3^+	−143.8
				$2H_2$ +	SiH^+	−103.7
				H +	SiH_4^+	−60.4
				H_2 + H +	SiH_2^+	−48.0
				2H +	SiH_3^+	−40.5
				$2H_2$ + H +	Si^+	−30.1
				H_2 + 2H +	SiH^+	−0.44
2)	H_3^+	+ SiH_4	→			0.0
				$2H_2$ +	SiH_3^+	−43.9
				$3H_2$ +	SiH^+	−3.8
3)	He^+	+ CH_4	→			0.0
				He +	CH_4^+	−276.0
				He + H +	CH_3^+	−236.9
				He + H_2 +	CH_2^+	−219.7
				He + $2H_2$ +	C^+	−121.4
				He + 2H +	CH_2^+	−116.4
				He + H_2 + H +	CH^+	−112.4
				He + H_2 + 2H +	C^+	−18.1
				He + 3H +	CH^+	−9.1
4)	H_3^+	+ SiF_4	→			0.0
				HF + H_2 +	SiF_3^+	+27.5
5)	H^+	+ SiF_4	→			0.0
				HF +	SiF_3^+	−72.4
6)	He^+	+ SiH_4	→			0.0
				He +	SiH_4^+	−313.0
				He + H_2 +	SiH_2^+	−300.9
				He + H +	SiH_3^+	−293.5
				He + $2H_2$ +	Si^+	−283.0
				He + H2 + H +	SiH^+	−253.4
				He + 2H +	SiH_2^+	−197.6
				He + H_2 + 2H +	Si^+	−179.7
				He + 3H +	SiH^+	−150.1
				He + 4H +	Si^+	−76.5
7)	Ar^+	+ SiH_4	→			0.0
				Ar +	SiH_4^+	−141.5
				Ar + H_2 +	SiH_2^+	−97.3
				Ar + H +	SiH_3^+	−89.9
				Ar + $2H_2$ +	Si^+	−79.4
				Ar + H_2 + H +	SiH^+	−49.8

In Figure 9 we illustrated the dissociative charge transfer cross section for reaction (98) calculated as a single product channel problem. Other possible product channels are listed in Table 6. Our previous studies of the potential energy surfaces for silane ions indicated an activation barrier of 6.8 eV for the decomposition of SiH_3^+ to $SiH^+ + H_2$. In addition, we find a barrier of 2.3 eV for the decomposition of SiH_2^+ to $Si^+ + H_2$. There appeared to be no barrier for hydrogen atom extraction from either SiH_3^+ or SiH_2^+. These data were incorporated into our R-matrix code for calculation of the reaction cross sections. The multi-channel data for reaction (98) are shown in Figure 10, along with the Langevin rate for this reactant pair. We find that product channels (2), (5) and (6) all exhibit greatly reduced cross sections for low energy collisions. This effect is primarily due to the barriers in the product channel for these three branching routes. Note that at higher energies (> 10 eV), all of the cross sections appear to be large and approach the Langevin limit. There is some scatter at these higher energies which we believe is due to numerical instability in describing the high frequency oscillatory behavior of the outgoing wave packet.

For the $H_3^+ + SiH_4$ system, an unexpected sensitivity of the calculated charge transfer cross sections to the collision energy was found. The potential energy along the minimum reaction path for $H_3^+ + SiH_4 \rightarrow 2H_2 + SiH_3^+$ is shown in Figure 11. Our calculated cross sections for this reaction are displayed in Figure 12 where we see both quantum structure and a sharp falloff in the cross section for $E_{coll} < 2$ eV. The quantum structure is not unexpected and was also found to some degree in our earlier studies of the prototype $H^+ + SiH_4 \rightarrow H_2 + SiH_3^+$ reaction. Several tests were carried out, however, to better understand the falloff in the calculated cross section at low collision energies. Since the energy defect for $H_3^+ + SiH_4 \rightarrow 2H_2 + SiH_3^+$ is small (ΔE = - 43.9 kcal/mol), we suspected that there was a phase cancellation in the reaction product channel. Close inspection of the potential curves shown in Figure 11 indicated a strong dependence of the product channel to the repulsive nature of $V_f(R)$ near the asymptotic region of $V_i(R)$. This dependence is clearly illustrated in Figure 13 which shows that this falloff in the calculated reaction cross sections is not found if $V_f(R)$ is shifted downward by ~ 5 kcal/mol. The $H^+ + SiH_4$ reaction is also shown in Figure 13 for comparison. We believe that this sensitivity of our calculated cross sections to the repulsive interaction potential is peculiar to the $H_3^+ + SiH_4$ system which exhibits a small energy defect. More studies are required to further test this hypothesis.

The $Ar^+ + SiH_4$ ion-molecule reaction (100) is especially interesting since several experimental groups (Refs. 85-87) have reported that this reaction is inefficient at low collisional energies. The long-range interaction potentials correlating with the several possible product channels are shown in Figure 14. We have examined the interaction potential as a function of SiH_4 orientation. For collision along the SiH bond, reaction occurs as a charge transfer event at large (~ 10 Å) $Ar^+ - SiH_4$ separations. For collisions along the H-Ar-H bisector the SiH_4 target is distorted to C_s symmetry with an energy barrier of ~ 53 kcal/mol, relative to its equilibrium geometry. This orientation results in a very small reaction rate for low energy (< 1 eV) collisions, in agreement

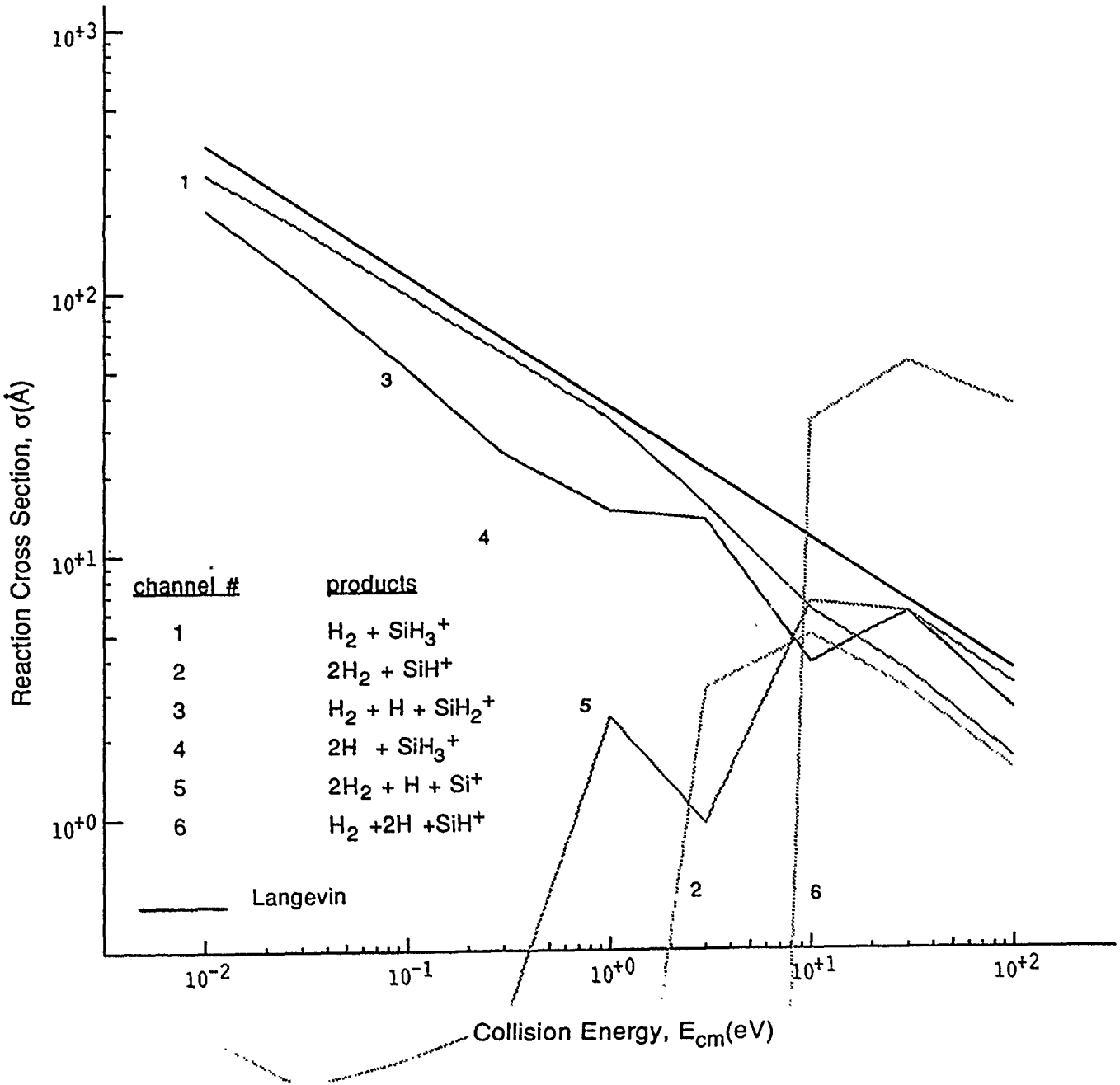

Figure 10. Calculated Cross Sections for: $H^+ + SiH_4 \rightarrow$ products.

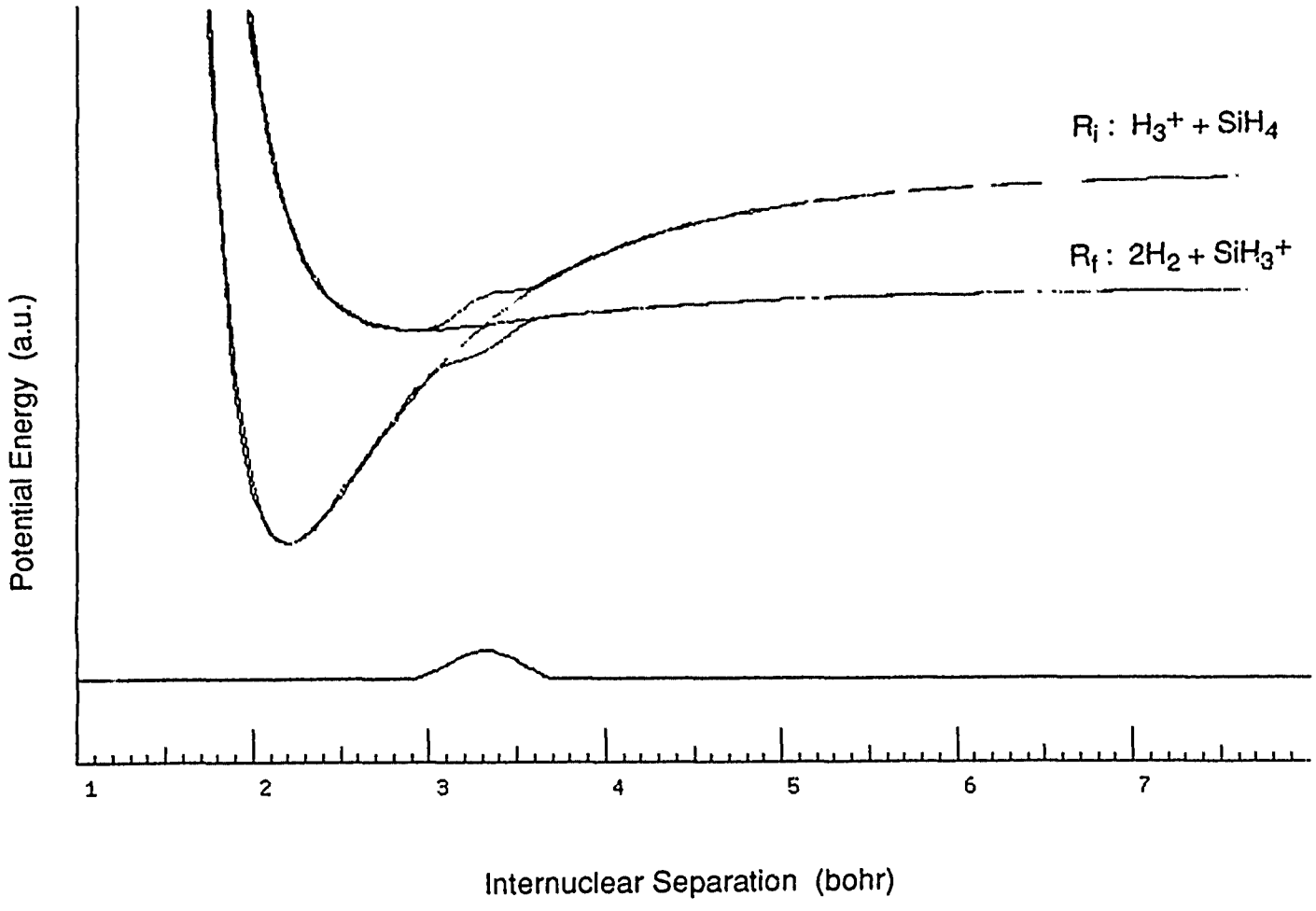

Figure 11. Potential Energy Along the Intrinsic Reaction Path for $H_3^+ + SiH_4 \rightarrow 2H_2 + SiH_3^+$.

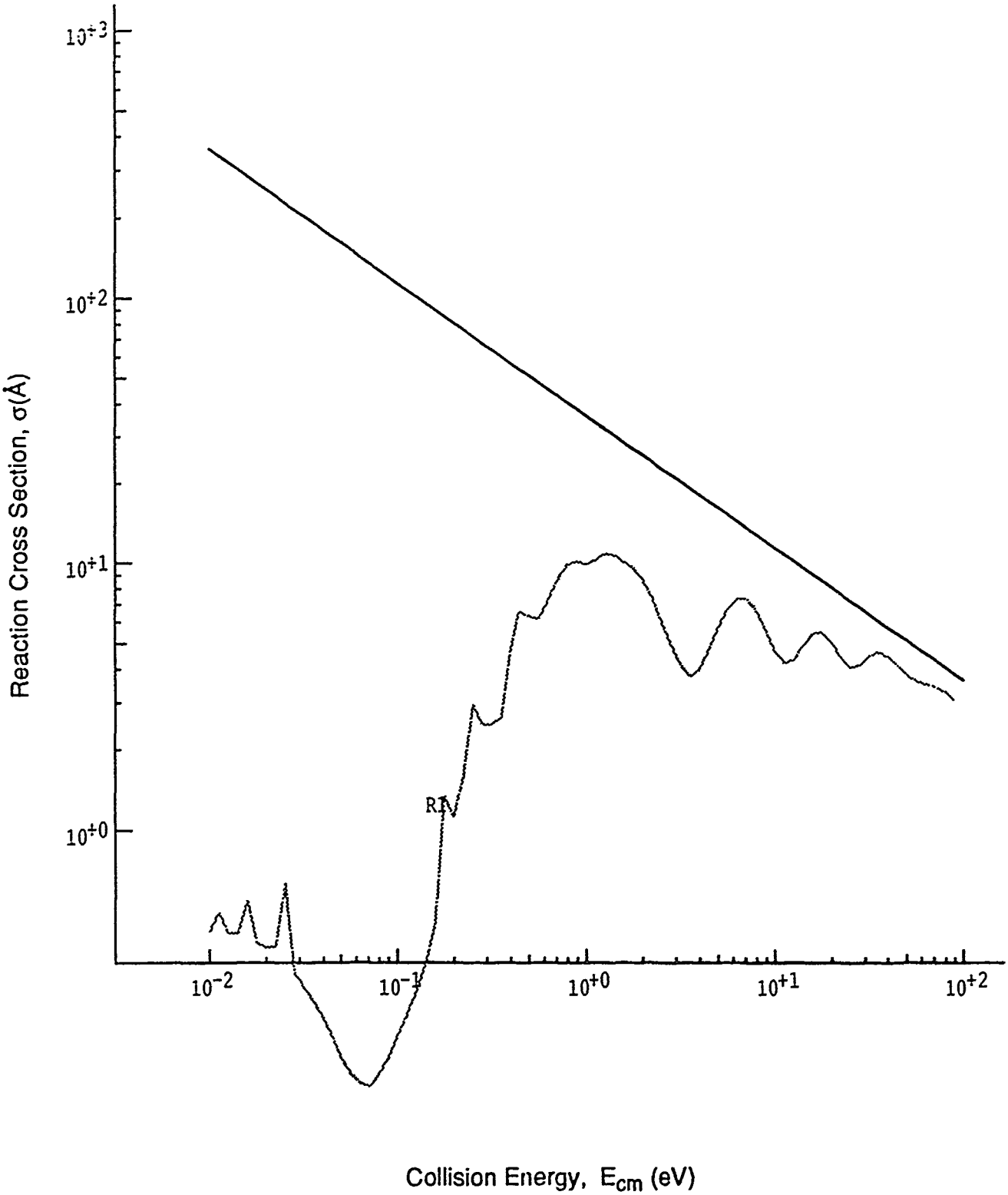

Figure 12. Calculated Cross Sections for $H_3^+ + SiH_4 \rightarrow 2H_2 + SiH_3^+$.

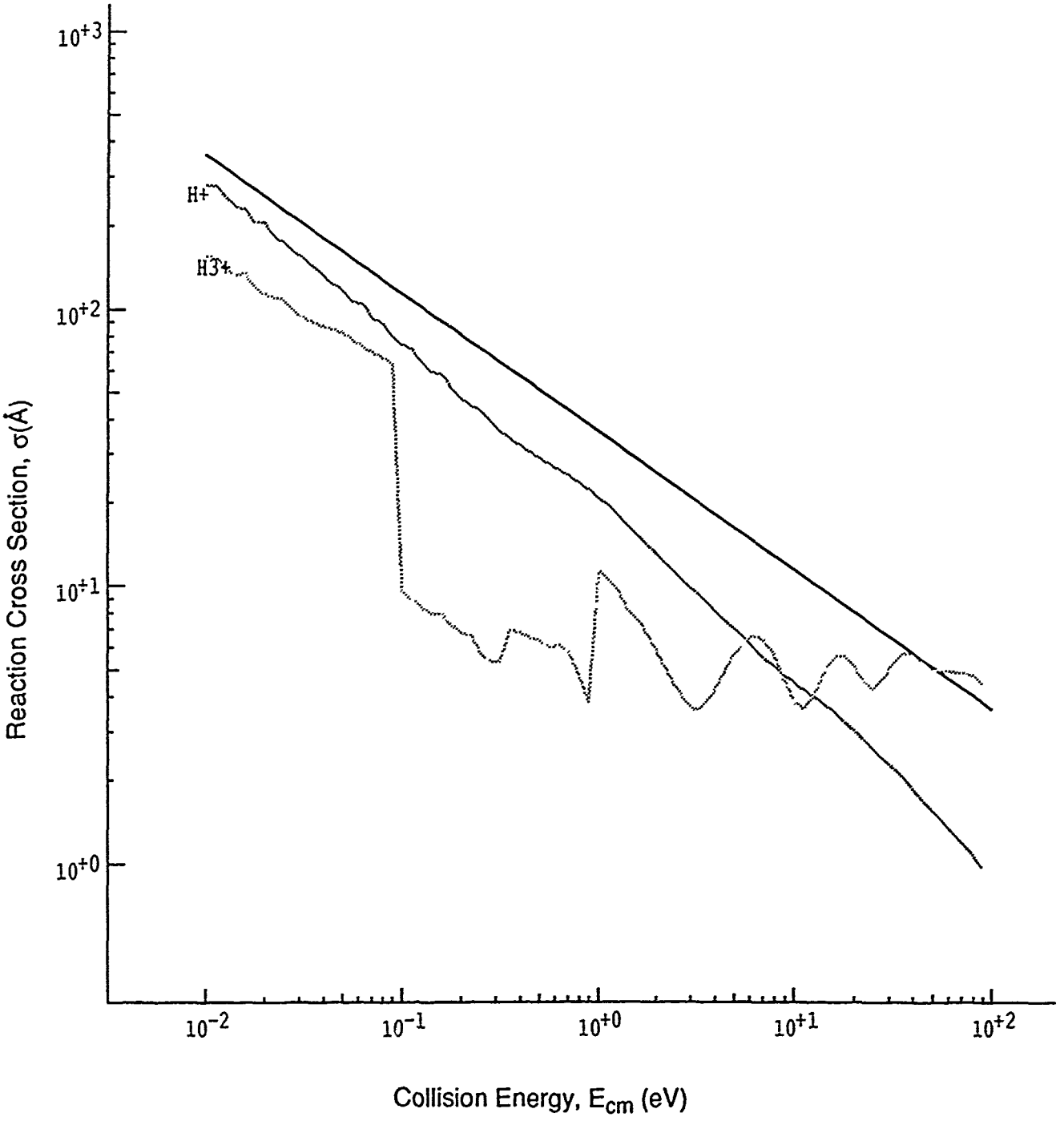

Figure 13. Calculated Cross Sections for $H_3^+ + SiH_4 \rightarrow 2H_2 + SiH_3^+$ [$V_f(R)$ shifted].

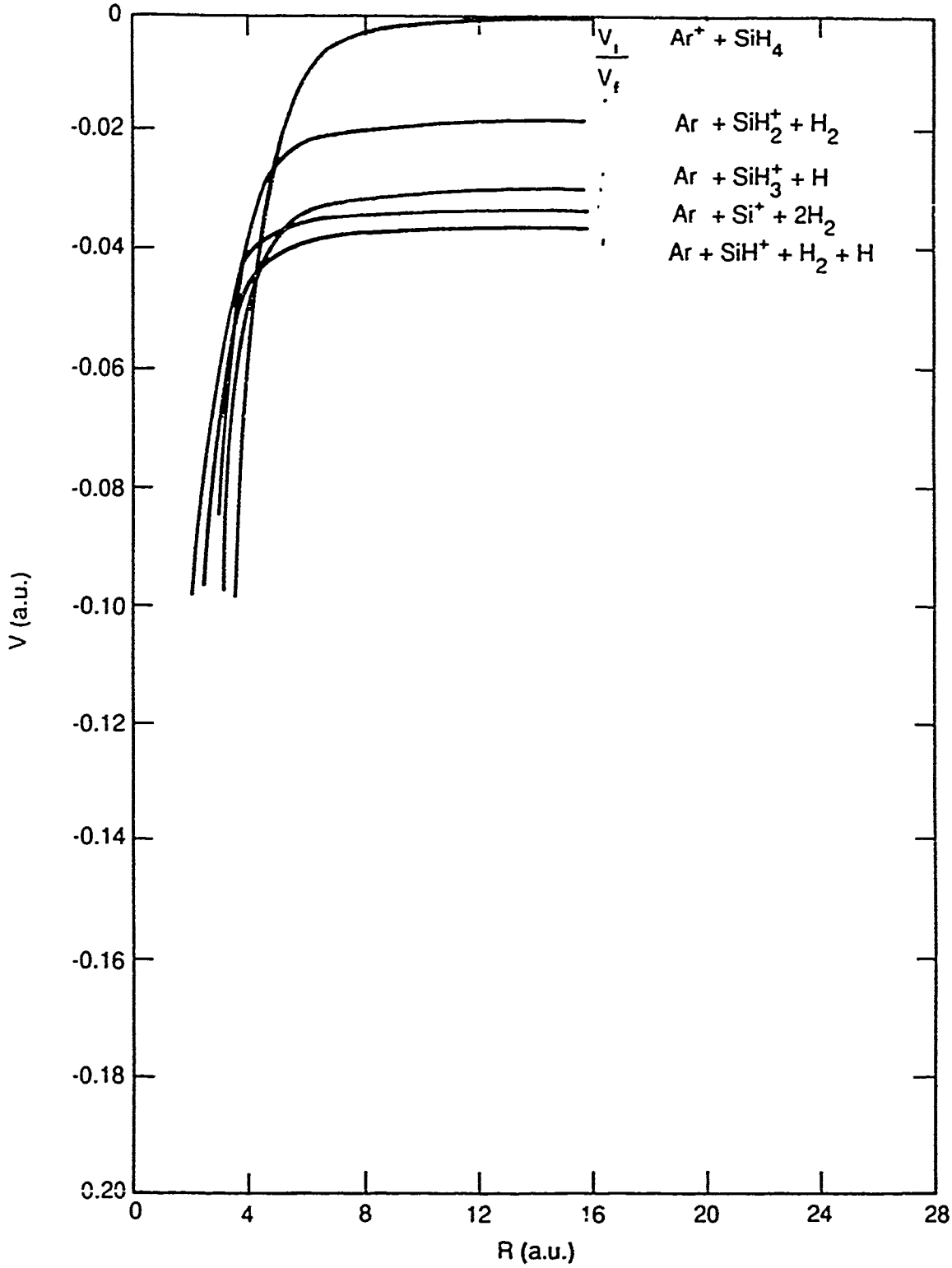

Figure 14. $Ar^+ + SiH_4$ Long Range Potentials.

with experimental observations. However, this suggests that reaction (99) should proceed efficiently at higher collision energies. Clearly more work is required to understand these reaction systems. A model for the $Ar^+ + SiH_4$ reaction proceeding along the Ar–H–Si bond can be developed based on the energetics of the charge transfer processes.

$$Ar^+ + SiH_4 \rightarrow [Ar^+–H–SiH_3]^* \quad (103)$$

$$[Ar^+–H–SiH_3]^* \rightarrow [Ar–H^+–SiH_3]^{**} \quad (104)$$

$$[Ar–H^+–SiH_3]^{**} \rightarrow [Ar–H–SiH_3^+]^{**} \quad (105)$$

In (103), the $Ar^+–SiH_4$ complex is formed at very long range: $R(Ar^+–SiH_4) \sim 10Å$. Step (104) illustrates charge transfer from Ar^+ to H. Finally, step (105) illustrates charge transfer from H^+ to SiH_3. A key feature of this model is that the bond energy of ArH^+ (144.3 kcal/mol) is equal to the proton affinity of SiH_3. This resonant situation exists only for the $Ar^+ + SiH_4$ system. The model can be looked at as a sort of super-exchange of the electron from $Ar^+–SiH_3^+$ to $Ar + SiH_3^+$. This picture suggests that SiH_3^+ may be readily formed in collisions at this orientation but with such low kinetic energy that these ions may not be efficiently detected.

A different explanation is offered by Fisher and Armentrout (Reference 85) and by Haaland (Reference 10) who suggest that there is a poor match in the ionization potential of Ar with either ionization of the $2t_2$ or $3a_1$ orbital of neutral SiH_4. In contrast, they suggest that $Xe^+ + SiH_4$ and $Kr^+ + SiH_4$ reactions should proceed with high efficiency through ionization of the $2t_2$ level of SiH_4, leading to primarily SiH_3^+ and SiH_2^+ products. Further, the reactions of $Ne^+ + SiH_4$, and $He^+ + SiH_4$, which have a better energy match through ionization of the $3a_1$ orbital of SiH_4, are predicted to yield primarily SiH^+ and Si^+ as products. Although these arguments correlate somewhat with the observed product distributions, there is no real justification in using an orbital energy criteria to correlate energy resonance in a system. One conclusion of this orbital energy resonance model would be that SiH^+ and Si^+ ion should be formed with lower efficiency in all of the rare gases, as compared to Ar, since the energy defect between the $3a_1$ orbital of SiH_4 and the rare gas ionization potential is smallest with Ar. Based on the data of Fisher and Armentrout (Reference 85), this is clearly not the case, suggesting that a more complete picture of the actual potential energy surfaces is required to explain the observed anomalous behavior of the $Ar^+ + SiH_4$ system. In addition, the positive energy dependence for the observation of all SiH_n^+ product ions for collisional energies > ~ 2.0 eV has no explanation within the Fisher and Armentrout model.

For collisions along the H–Ar–H bisection, we find that the SiH_4 target is distorted to C_s symmetry with a large energy barrier, relative to its equilibrium geometry. The resonant model of charge transfer described above does not appear to be correct for this orientation and long range charge transfer does not occur. Clearly, a more detailed study of the several potential energy

reaction surfaces is required to understand the physics of the $Ar^+ + SiH_4$ system. At this point, there is no satisfactory explanation for the observed efficiency of this reaction. However, further experimental studies are suggested to test whether SiH_3^+ ions may be formed, but with very low kinetic energies.

The $He^+ + CH_4$ ion-molecule reaction (reaction 6) was examined in detail. Our analysis is based on studies of the $He^+ + CH_4$ reaction surface. Our initial studies of this surface, using a 6-311G** basis, indicated that the interaction potential is very flat up to a He-C bond distance of ~ 5.4 Å. At this point there is a sudden electron jump (harpooning) from CH_4 to the He^+ center leaving a CH_4^+ radical to relax from an initial CH_4 geometry. This first step in the reaction is illustrated in Figure 15 which shows the sudden change in the electric potential as the electron transfers from CH_4 to He^+. The subsequent reaction is the decomposition of CH_4^+ to form $CH_2^+ + H_2$. This occurs smoothly on the $^2A_2$ surface of CH_4^+, as illustrated in Figure 16. A hydrogen molecule is released directly from the initial geometry, leaving a methylene cation as the basic charged fragment. The electric potential at various geometries along this decomposition path are illustrated in Figure 16.

A second decomposition pathway for CH_4^+ exists via the $^2A_1$ surface. Initial studies indicate that an H_2^+ ion is first formed as the C-H bond length increases, followed by an electron jump to again form $CH_2^+ + H_2$. The electric potential at various geometries along this decomposition path for CH_4^+ is illustrated in Figure 17. We find that a methylene fragment appears to form with the simultaneous expulsion of a H_2^+ cation. At $R \sim 2R_e$ for CH_2, a back charge transfer occurs, again yielding the thermodynamically more stable $CH_2^+ + H_2$ products. The calculated reaction rate for $He^+ + CH_4$ is close to Langevin with predicted products of CH_2^+ (most abundant) and with CH^+ and H^+ resulting from back charge transfer to the decomposing methylene radical. This analysis is in complete agreement with the experimental data of Chatham, Hils, Robertson and Gallagher (Reference 87).

Finally, an analysis of the $H^+(H_3^+) + SiF_4$ reaction (reaction 102) was carried out. Calculations of the lowest potential energy surface for $H^+ + SiF_4$ clearly illustrate that reaction (102) proceeds as a fluoride anion abstraction reaction with either H^+ or H_3^+ as the reactant ion. This observation is similar to that for the $H^+ (H_3^+) + SiH_4$ system. Only two channels are open for the $H_3^+ + SiF_4$ reaction below 50 kcal/mol collision energy. There is no apparent barrier for HF formation and the reaction rate is predicted to be close to the Langevin rate. The dominant product channel is predicted to be $SiF_3^+ + HF$.

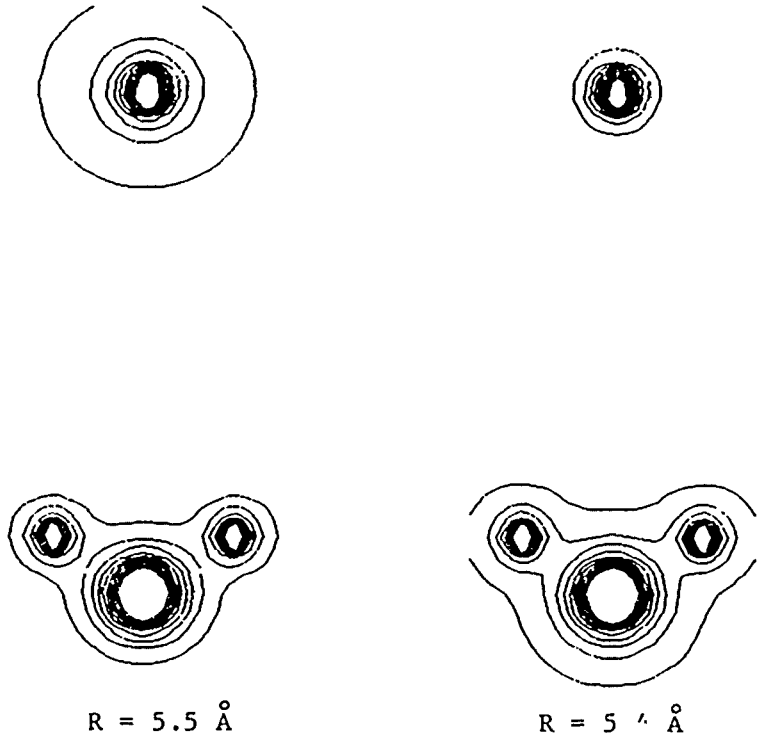

Figure 15. Electric Potential $CH_4 + He^+ \rightarrow CH_4^+ + He$.

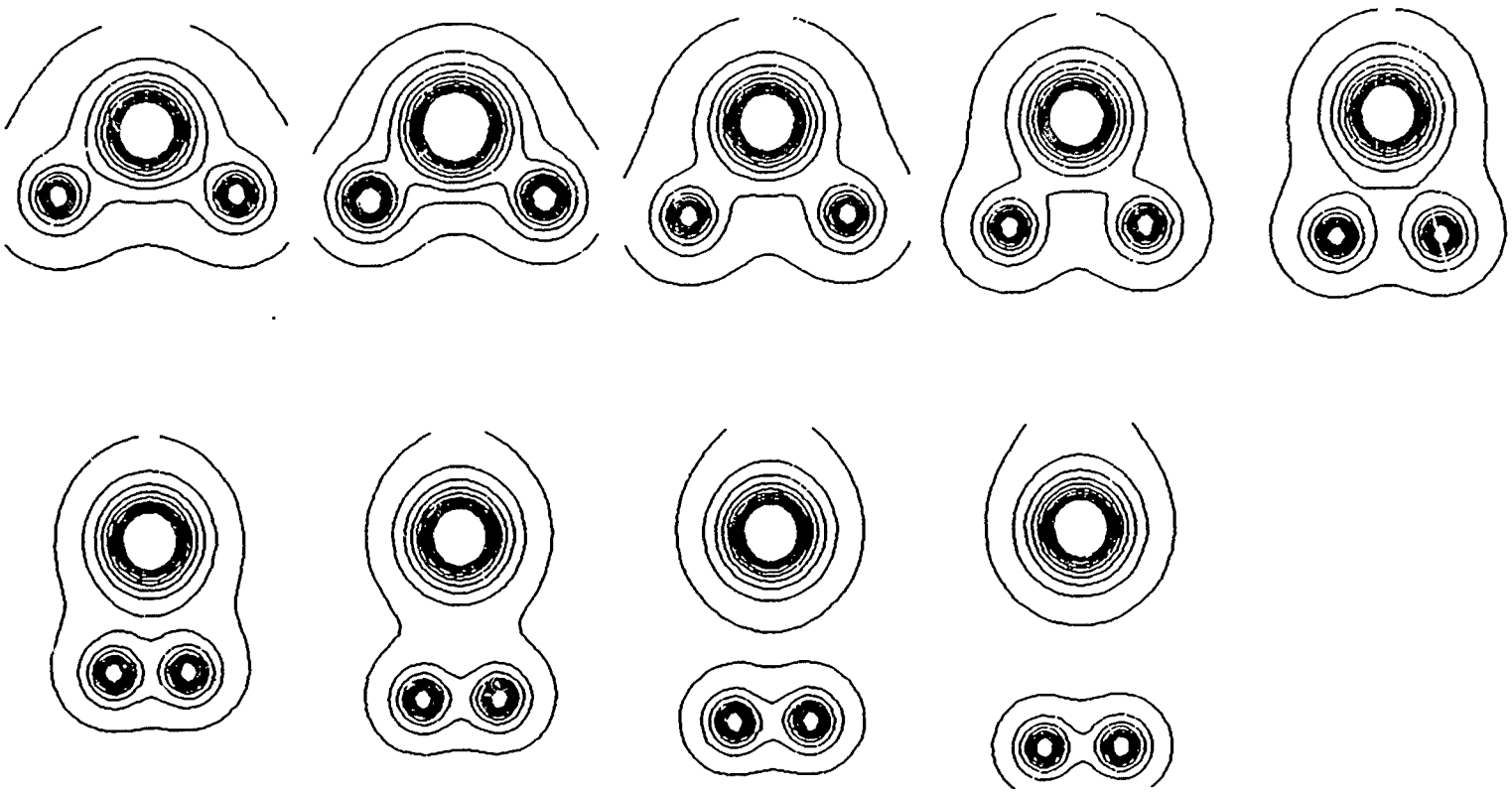

Figure 16. Electric Potential $CH_4^+ (^2A_2) \rightarrow CH_2^+ + H_2$.

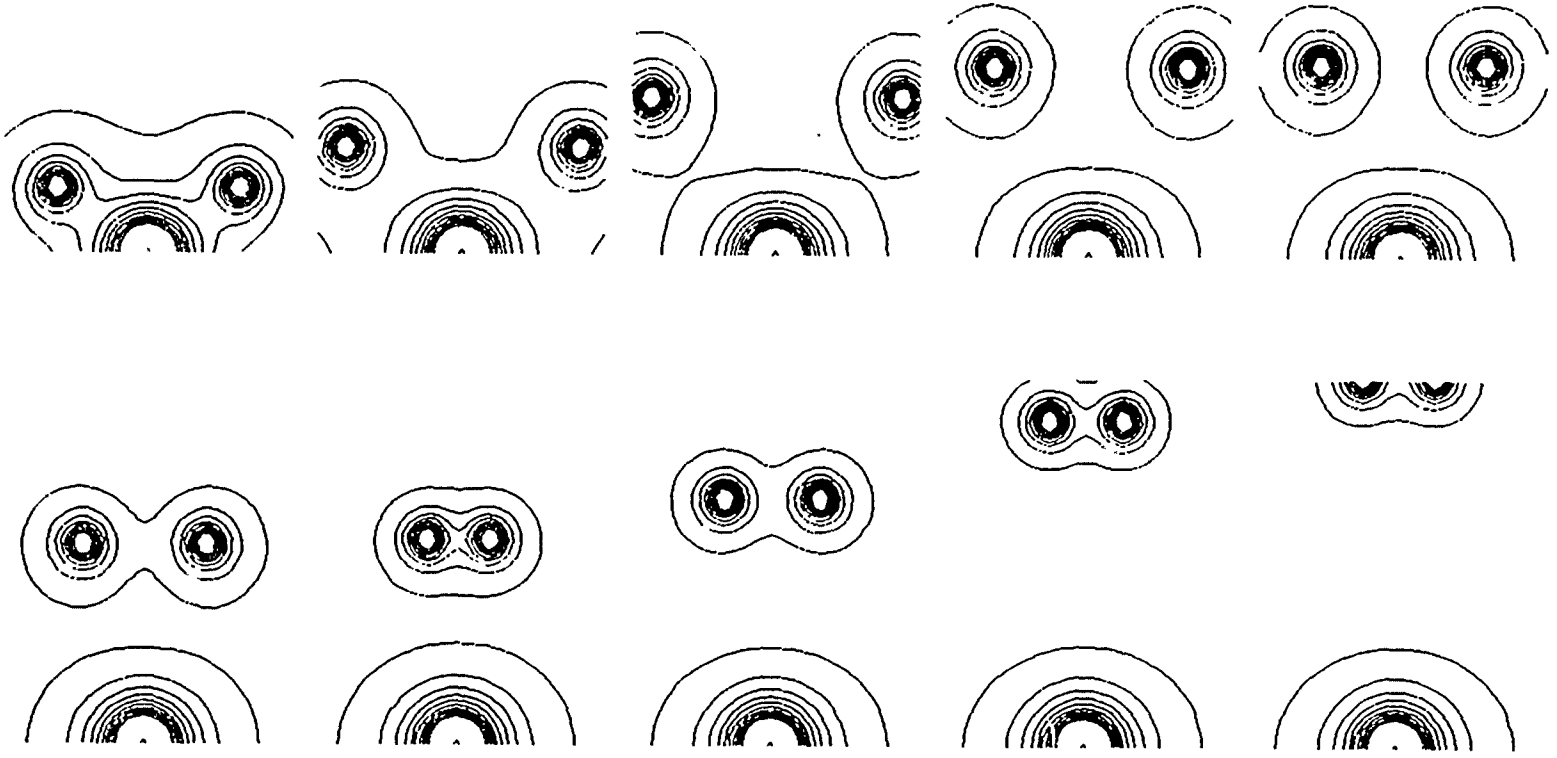

Figure 17. Electric Potential $CH_4^+ (^2A_1) \rightarrow CH_2 + H_2^+$

$\rightarrow CH_2^+ + H_2$.

3.2 $SiH_n^+ + SiH_4$ Clustering Reactions

In addition to our studies of silane dissociative charge transfer reactions, an analysis of the $Si^+ + SiH_4$ clustering reaction was initiated. Mandich, et al. (Reference 11) have experimentally studied the silicon cluster growth reactions starting with $Si^+ + SiH_4$. They find that the addition sequence stops at the $Si_5H_{10}^+$ structure. In a parallel theoretical study, Raghavachari (Reference 12) has reported *ab initio* calculations on these silicon growth reactions. The structures were optimized at the HF/6-31G* level of theory. The initial ion-molecule complex that is formed in the $Si^+ + SiH_4$ reaction is reported to be a near linear attack of Si^+ along an Si–H bond as shown in Figure 18. The bridge structure, also shown in Figure 18, is reported to be ~ 1.5 kcal/mol higher in energy. The barrier between these two structures has not been calculated but is estimated to be low owing to the extended Si^+–SiH_4 bond. Either of these structures is stabilized by the polarization forces of Si^+ on SiH_4. These result in a long-range $[-\alpha/R_4]$, attractive force balanced by exchange repulsion. The relative stability of the two structures shown in Figure 18 is therefore critically dependent on the value of the polarizability of SiH_4. Structure 2 should be favored for a larger value of the polarizability. It therefore becomes important to carefully examine the polarizability of SiH_4.

Haaland (Reference 10) has pointed out that the calculated polarizability of SiH_4 is too small (3.60 $Å^3$) even at the MP2/6-31++G** level of theory. The best experimental estimate for α is 4.62 $Å^3$, according to Haaland. We have computed the polarizability using several basis sets at the MP2 level of theory available in the CADPAC program. The results are summarized in Table 7 which illustrates that the use of diffuse basis functions on both Si and H is required for a quantitative estimate of the polarizability. Both the MP2/6-31G**(sp,d,s_n) and MP2/6-311G**(sp,d,s_n) calculations yield a calculated value for the polarizability within 90% of Haaland's estimate. The calculated value at the MP2/6-31G* level of theory ($\alpha = 3.21$ $Å^3$) is significantly smaller and therefore underestimated the long range attractive force in the $Si^+ + SiH_4$ reaction. This adversely affects the relative energetics of structures 1 and 2 shown in Figure 18.

To assess the role of the polarization potential in determining the relative stability of these loose charge transfer complexes, a series of calculations was undertaken. Using the 6-31G**(sp, d,s_n) basis, optimized UHF calculations were carried out for both the C_s Si–H bond structure and the C_{2v} bridge structure. The results are given in Table 8 which again indicate that the calculated energies are too close at the UHF level to choose between these two clustering mechanisms. However, all calculations at a correlated level indicate that the C_{2v} bridge structure is lower in energy. These new data shed doubt on the suggested $Si_2H_4^+$ equilibrium structure (Reference 12). Insertion of an Si atom into the long Si–H bond in the Cs ion-molecule structure yields the (C_s) equilibrium structure shown at the top of Figure 19. However, since the C_{2v} bridge structure shown at the bottom of Figure 19 is lower in energy at long Si–H_2 bond lengths, this may actually

Structure 1 (C_s)

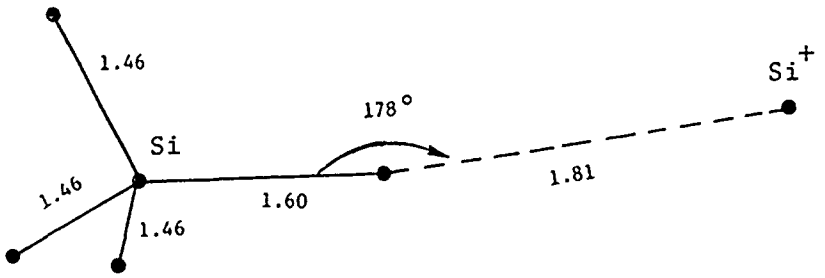

Structure 2 (C_{2v})

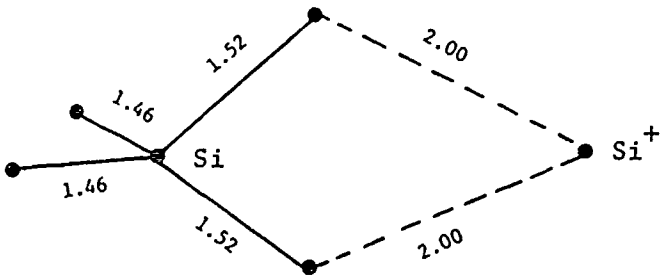

Figure 18. Si^+ - SiH_4 Ion-Molecule Clusters.

Table 7. Calculated MP2 Polarizabilities of SiH_4

Method	$R_{(Si-H)}$(Å)	E(hartrees)	α(Å^3)
MP2/6-31G*	1.4829	– 291.3168497	3.20
MP2/6-31G**	1.4726	–291.3498595	3.17
MP2/6-31++G**	1.4719	– 291.3531119	3.59
MP2/6-31G**(sp,d,s_n)	1.4730	– 291.3619018	4.12
MP2/6-311++G**	1.4737	– 291.4967731	3.74
MP2/6-311G**(sp,d,s_n)	1.4759	– 291.5030978	4.21
EXP.			4.62

$\alpha_{sp} = 0.025795$; $\alpha_d = 0.15$; $\alpha_{s_n} = 0.036$

Table 8. Energetics of the $Si^+ + SiH_4$ Clustering Reaction

Method	Geometry				Energy
	R_1	R_2	R_3	θ	
C_s Structure					
UHF/6-31G**	1.460	1.601	1.802	180.	– 579.80980
UHF/6-31G**(sp,d,s_n)	1.461	1.600	1.784	180.	– 579.81459
MP2/6-31G**	1.460	1.588	1.753	180.	– 579.98130
MP4/6-31G**//UHF					– 580.02340
C_{2v} Structure					
UHF/6-31G**	1.457	1.530	1.971		– 579.80650
UHF/6-31G**(sp,d,s_n)	1.457	1.534	1.975		– 579.81249
MP2/6-31G**	1.458	1.537	2.148		– 579.98620
MP4/6-31G**//UHF					– 580.02720

Bond lengths in Å, bond angles in degrees, energy in hartrees.

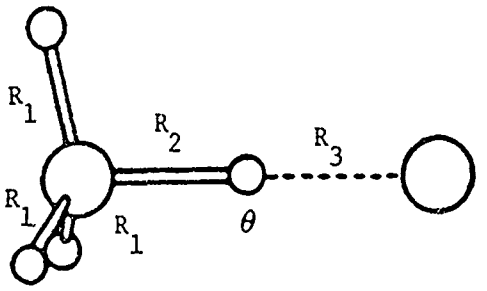

S1 (C_s)

Bond Structure

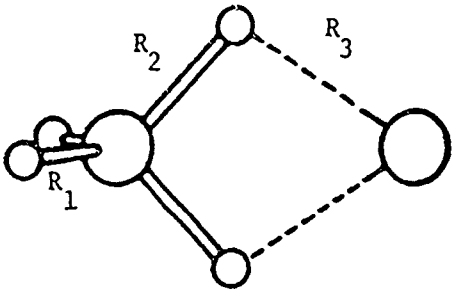

S2 (C_{2v})

Bridge Structure

Figure 19. Si^+ - SiH_4 Ion-Molecule Complexes.

represent the more stable equilibrium conformation. The bonding in higher order clusters should now be reexamined in light of this finding.

3.3 e + SiH_4 Collisional Dissociative Attachment

Ab initio calculations of the dissociative reaction surfaces for negative ion formation in silane were undertaken. In Table 9, we show the possible product branching for e + SiH_4. Two possible kinetic routes must be considered for conditions that exist in the cathode sheath region of a silane glow discharge. The first assumes that an unstable resonance state of SiH_4^- is formed by primary electron capture. Subsequently, this unstable negative ion can decay into the thermodynamically accessible product channels which correspond to dissociation products. Table 9 illustrates that reactions (2) - (6) fit this criteria but that (7) and (8) do not. Dissociation of SiH_4^- should exhibit thresholds of 1.27, 2.44, 2.78 and 3.09 eV for formation of SiH_2^-, SiH_3^-, Si^- and H^-, respectively, provided that there are no barriers for dissociation in the exit channels. Although taken with limited energy resolution, the data of Potzinger and Lampe (Reference 88) and Ebinghaus, Krauss, Müller-Duys: and Neuert (Reference 89) appear to be in agreement with these predictions for formation of SiH_2^- and SiH_3^-, although a unique reaction pathway cannot be determined from these experiments. Srivastava (Reference 90) has also observed resonances at ~ 2.5 eV which he attributes to SiH_2^- and SiH_3^- formation. The process of negative ion formation following decay of a resonance state of SiH_4^- was first described by Haaland (Reference 91).

In order to analyze the possible dissociation products for low energy collisions, the reaction surfaces governing the dissociative attachment (DA) of electrons to SiH_4 were analyzed using the intrinsic reaction coordinate procedure of Schmidt, Gordon and Dupuis (Reference 92). In Figure 20, we show the energetics of the reaction coordinate leading to dissociation of SiH_4 to SiH_3 + H. At the HF/6-31++G** level of theory, we find a bond dissociation energy of 3.27 eV. At the MP2/6-31++G** level, a bond energy of 3.85 eV, very close to the experimental value, is predicted. Shown on Figure 20 are data for the SiH_3^- + H and SiH_3 + H^- reaction surfaces. We find an avoided crossing of these two surfaces, very close to the internuclear separation where the ion curves cross the neutral SiH_3 + H + e surface, but probably in the region where the ion potentials are complex. Thus, the excited state ion channel, leading to SiH_3 + H^- may depopulate through this avoided crossing leaving SiH_3^- + H as the only significant products of the DA reaction. Experimental data by Haaland (Reference 91) and by Potzinger and Lampe (Reference 88) indicate that H^- is probably not formed by direct DA of e + SiH_4.

To facilitate analysis of the asymptotic behavior, we have calculated the polarizability of SiH_3 at the HF/6-31++G** level and find α = 3.95 Å^3. The corresponding value of the polarizability of SiH_4 at this level of theory is 3.25 Å^3. The leading term of the long-range potential of SiH_3 + H^-

Table 9. Thermodynamics of Negative Ion Formation in Silane

Reaction	ΔH (eV)	
$e + SiH_4[^1A_1] \rightarrow SiH_4^-[^2T_2]$	(+3.98)	(1)
$\rightarrow SiH_2^-[^2B_1] + H_2[^1\Sigma_g^+]$	+1.266	(2)
$\rightarrow SiH_3^-[^1A_1] + H[^2S]$	+2.442	(3)
$\rightarrow Si^-[^4S] + 2H_2[^1\Sigma_g^+]$	+2.783	(4)
$\rightarrow SiH_3[^2A_1] + H^-[^1S]$	+3.094	(5)
$\rightarrow Si[^3P] + H_2[^1\Sigma_g^+] + H[^2S] + H^-[^1S]$	+3.269	(6)
$\rightarrow SiH^-[^3\Sigma^-] + H_2[^1\Sigma_g^+] + H[^2S]$	+4.392	(7)
$\rightarrow SiH[^2\Pi] + H_2[^1\Sigma_g^+] + H^-[^1S]$	+4.915	(8)

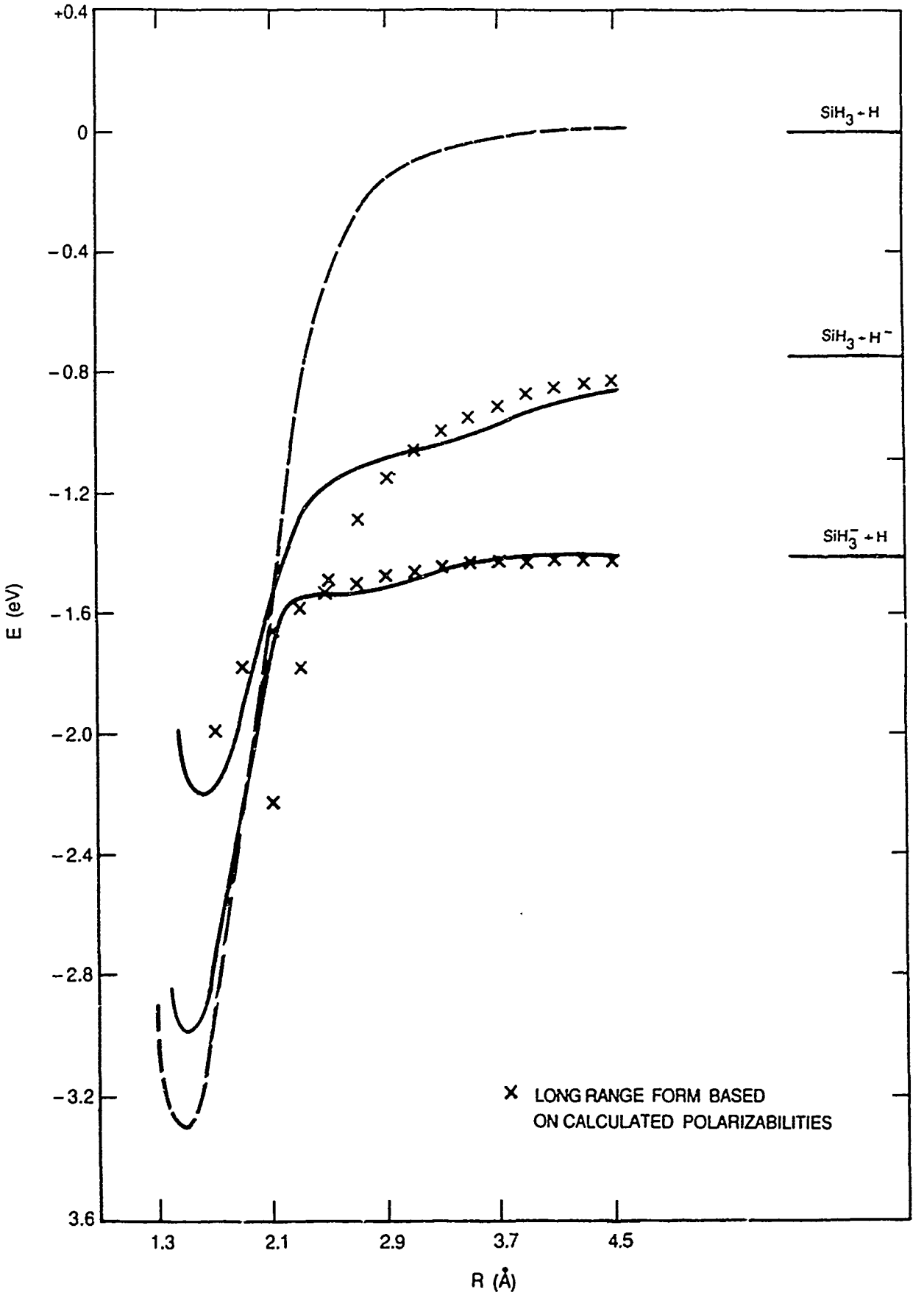

Figure 20. Intrinsic Reaction Pathway for Dissociation of SiH_4 and SiH_4^-.

and SiH_3^- + H can be calculated according to the form: $V(R\rightarrow\infty) = -\alpha/2R^4$. These asymptotic curves are shown on Figure 20 which clearly indicate that an avoided crossing between these two channels must occur.

Preliminary studies of dissociative attachment (DA) of electrons to silane were undertaken through analysis of the possible product channels and quantum coupling with the reactants. The lowest adiabatic attachment channel correlates to $SiH_2^-[^2B_1] + H_2[X^1\Sigma_g^+]$ at 1.266 eV. The SiH_4^- resonance state corresponding to this channel appears to be of the Feshbach type with a small capture width from reactants. In addition, as studies described below will indicate, there is a large barrier on the reaction surface leading to $SiH_2^- + H_2$ products. The second DA channel corresponds to the formation of $SiH_3^-[^1A_1] + H[^2S]$ at 2.442 eV. This channel corresponds to a shape resonance but also would appear to have a small DA cross section for vibrationally cold SiH_4. Srivastava (Reference 90) finds a resonance in the SiH_3^- + H channel at ~ 2.7 eV but this experimental energy appears to be the same for formation of Si^-, SiH^-, SiH_2^- and SiH_3^-, which should exhibit quite different threshold behavior. Recently, Wan, Moore and Tossell (Reference 93) have reported electron scattering cross sections for silane in the range 0.2→12.0 eV. They observe a broad maximum in the total electron scattering cross section at ~ 2.9 eV which they attribute to a virtual transition to the lowest unoccupied $\sigma^*(t_2)$ level in SiH_4. This feature has a large cross section (~ 50 Å^2) and may be related to the features seen by Srivastava in dissociative attachment (DA) at ~ 2.5 eV. Based on these known low-energy quantum processes, our conclusion is that low-energy direct electron dissociative attachment processes should have low probability.

The second kinetic route for DA of e + SiH_4 was examined by looking at the excited state surfaces of SiH_4^-. The DA mechanism for this route may be the initial capture of an electron into a high lying SiH_4^- state with subsequent statistical branching into the allowed product channels. For a mechanism of this type, the product distribution is uncorrelated with the initial dynamics of the reaction channel and standard DA cross section codes are not useful. However, the data of Srivastava suggests that a stochastic formation of product states, all formed from the same state(s) of SiH_4^- lying at 8-9 eV is occurring.

In order to identify the excitation channels for e + SiH_4, extensive configuration interaction (CI) studies of SiH_4^- were next carried out to identify the excited state reaction surfaces that play a role in dissociative attachment of electrons. In Table 10, we show the excitation spectrum for SiH_4^- calculated at the equilibrium geometry of SiH_4 (R = 1.477 Å). The basis employed in these calculations is that due to Handy (basically 6-31G** augmented by a diffuse sp shell (α = 0.025795) and a diffuse d function on Si (α = 0.15). This basis is known, from our previous studies, to give an accurate representation of the polarizability of SiH_4.

At the equilibrium geometry of SiH_4, the low-lying excited state surfaces are triply

Table 10. Vertical Excitation Spectrum for SiH_4^-

Eigenstate	Symmetry [C_{3v}]	ΔE (eV)
ψ_o	$^2A_1$	0.0
ψ_1 (3)	$^2A_1$	0.59
ψ_2 (3)	$^2A_1$	2.15
ψ_3 (3)	$^2A_2$	9.10

(3) triply degenerate in T_d symmetry

degenerate since the full point group with this symmetry is T_d. In the C_{3v} subgroup, the low-lying states of SiH_4^- are all of $^2A_1$ symmetry, which is representative of a loosely bound electron, symmetrically distributed about SiH_4. These are pseudoeigenstates of the system, strongly dependent on the chosen basis set, and are not physically meaningful. However, the third excitation (at 9.20 eV) is characterized by a compact charge distribution resulting from s→p promotion on the Si atom. We identify this state as $^2A_2$ in C_{3v} symmetry ($^2A''$ in C_s) and believe that it represents the first identification of the resonant excited states in this system. Our location of this state at 9.1 eV is in good agreement with previous experimental data placing the important dissociative attachment states in the 7-10 eV range.

To give some feel for the magnitude of these calculations, our configuration interaction (CI) expansion is composed of all single, double, triple and quartic excitations in an active orbital space of the lowest 16 natural orbitals. This results in a CI comprising some 28000 configurations. The identification of the 9.1 eV state as $^2A_2$ suggests that dissociative attachment should not be strong owing to symmetry restrictions which weakly couple this state to the $^2A_1$ channel corresponding to e + SiH_4. Based on this initial study, a more thorough examination of excited state surfaces of SiH_4^- is indicated.

Alternate kinetic routes for the production of negative ions of silane can be derived from the assumption of LTE (or at least quasi-steady state) in the cathode sheath region. In this situation, electron attachment can occur not only to SiH_4, but also possibly directly to the neutral silane fragments which are in the plasma. In Table 11, we illustrate electron attachment to SiH_3, SiH_2 and SiH. It can be seen that a wide spectrum of threshold energies is spanned by these molecules (0.39 - 2.53 eV) and that all possible negative ion species, including H^-, should be possible. The relative importance of these several processes is, of course, dependent on the reactant species concentration, so that knowledge of the neutral composition of the plasma in the sheath region becomes a requirement.

3.4 Negative Ion-Molecule Silane Reactions

3.4.1 Thermochemistry of SiH_n/SiH_n^- Species

Analysis of the negative ion-molecule silane reactions required development of a thermodynamic data base for these anions. Data on the SiH_n^- anions have been reported by Potzinger and Lampe (Reference 88), Drzaic, Marks and Brauman (Reference 94), Mead, Stevens and Lineberger (Reference 95) and Nimlos and Ellison (Reference 96). Using these data as a source for comparisons, a study of the electronic structure, predicted equilibrium geometry and resultant calculated thermochemistry for neutral and anion SiH_n species was undertaken. To establish a consistent thermodynamic base, an expanded basis was employed at the MP2 level of

Table 11. Thermodynamics of Negative Ion Formation in $SiH/SiH_2/SiH_3$

Reaction	ΔH (eV)
$e + SiH_3[^2A_1] \rightarrow SiH_3^-[^1A_1]$	-1.406
$\rightarrow SiH^-[^3\Sigma^-] + H_2[^1\Sigma_g^+]$	+0.544
$\rightarrow SiH_2^-[^2B_1] + H[^2S]$	+1.896
$\rightarrow SiH_2[^1A_1] + H^-[^1S]$	+2.266
$\rightarrow SiH[^2\Pi] + H[^2S] + H^-[^1S]$	+5.545
$e + SiH_2[^1A_1] \rightarrow SiH_2^-[^2B_1]$	-1.124
$\rightarrow Si^-[^4S] + H_2[^1\Sigma_g^+]$	+0.393
$\rightarrow SiH^-[^3\Sigma^-] + H[^2S]$	+2.002
$\rightarrow SiH[^2\Pi] + H^-[^1S]$	+2.525
$\rightarrow Si[^3P] + H[^2S] + H^-[^1S]$	+5.502
$e + SiH[^2\Pi] \rightarrow SiH^-[^3\Sigma^-]$	-1.277
$\rightarrow Si^-[^4S] + H[^2S]$	+1.592
$\rightarrow Si[^3P] + H^-[^1S]$	+2.223

theory. The silicon basis was the standard 6-31G* approximation, augmented by a diffuse (α = 0.025795) sp-shell and a second diffuse (α = 0.15) d-shell. The hydrogen atoms were represented using the standard 6-31G* basis, augmented by a diffuse (α = 0.036) s-shell. This basis yields a good approximation for the polarizability of silane (α = 4.11 Å^3) and should provide a reasonable compromise for calculating the thermodynamics for the formation of SiH_3^-, SiH_2^- and SiH^-.

In Table 12, we give the calculated geometry, electronic energy and predicted electron affinity for species of the SiH_n/SiH_n^- system at the MP2/6-31 (2d,sp,s_n) level of theory. With the exception of SiH_3^-, our calculated electron affinities are in reasonable agreement with the known experimental data. Additional diffuse functions on the H atoms are required to improve the agreement for SiH_3^-.

3.4.2 Thermochemistry of SiF_n/SiF_n^- Species

A study of the electronic structure of SiF_n and SiF_n^-, similar to that carried out for the SiH_n/SiH_n^- system, was also undertaken. Owing to the greater complexity of this system, a more restricted basis set was examined. The silicon basis was the standard 6-31G split-valence shell basis augmented by d polarization functions (α = 0.45) and a diffuse (α = 0.0331) sp shell. The fluorine atoms were also represented with the standard 6-31G* basis augmented by d polarization functions (α = 0.8) and a diffuse (α = 0.1076) shell. The calculated geometries and electron affinities are given in Table 13. Although F^- is well represented by this basis, it can be seen that the electron affinity of both Si and SiF_3 are underestimated. Experimental data on the electron affinity of SiF_3 have been reported by Richardson, Stephenson and Brauman (Reference 97). The use of the Handy/Amos basis for Si, which was chosen for our studies of the SiH_n/SiH_n^- system, would yield improved agreement but with a severe computational penalty owing to the extended size of the basis. The calculated electron affinities in Table 13 for SiF_n species, should therefore be interpreted as uniformly low, perhaps by 20 - 25%. It is interesting, however, that all SiF_n^- species, with the exception of the SiF_4^- resonant state, are predicted to be thermodynamically stable.

3.4.3 Silane Decomposition Mechanisms

The generation of the potential energy surface for the H^- + SiH_4 ion-molecule reaction was approached in two steps. Since the overall symmetry of this reaction correlates with that of H + SiH_4, our initial studies dealt with analysis of the thermal decomposition of SiH_4.

Hydrogen atom abstraction from SiH_4 occurs with no decomposition barrier as is illustrated in Figure 20. Our calculated bond dissociation energy at the MP2/6-31++G** level of theory is

Table 12. Calculated Energies and Geometries of Neutral and Negative-Ion SiH_n Species

MP2 Level of Theory

Basis: 6-31G**; Si: sp = 0.025795; d = 0.15

H: s = 0.036

Species	State	R(Å)	θ(deg)	E (hartrees) MP2	E_a (eV) Calc.	E_a (eV) Exp.
H	^2S			− 0.4988011		
H^-	^1S			− 0.5036267	+ 0.131	+ 0.754 [a]
Si	^3P			− 288.8964559 (P)		
Si^-	^4S			−288.9425435 (P)	+1.254	+1.385 [a]
H_2	$^1\Sigma_g^+$	0.7343		− 1.1577722		
H_2^-	$^2\Sigma_u^+$	0.7634		− 1.0849932		
SiH	$^2\Pi$	1.5166		− 289.4967536 (P)		
SiH^-	$^1\Delta$	1.5385		− 289.4980076	+0.034	+0.109 [b]
SiH^-	$^3\Sigma^-$	1.5443		− 289.5371537 (P)	+1.099	+1.277 [b]
SiH_2	$^1A_1$	1.5107	92.108	− 290.1083537		
SiH_2^-	$^2B_1$	1.5357	92.905	− 290.1426034 (P)	+0.932	+1.124 [b]
SiH_3	$^2A_1$	1.4739	111.109	−290.7213217 (P)		
SiH_3^-	$^1A_1$	1.5296	95.401	− 290.7571167	+0.974	+1.406 [c]
SiH_4	$^1A_1$	1.4730	109.471	− 291.3619018		
SiH_4^-	$^2A_1$	1.4702	109.471	− 291.3286672 (P)	− 0.903	

[a] ref. 95

[b] ref. 94

[c] ref. 96

Table 13. Calculated Energies and Geometries of Neutral and Negative Ion SiF_n Species

MP2 Level of Theory; Basis: 6-31+G*

Species	State	R(Å)	θ(deg)	E (hartrees) MP2	E_a (eV) Calc.	E_a (eV) Exp.
F	^2P			− 99.5009122		
F^-	^1S			− 99.6260705	+ 3.406	+ 3.399 [a]
Si	^3P			− 288.8847310 (P)		
Si^-	^4S			− 288.9233943 (P)	+ 1.052	+ 1.385 [a]
SiF	$^2\Pi$	1.6496		− 388.6061626 (P)		
SiF^-	$^1\Delta$	1.7177		− 388.5897919	− 0.445	
SiF^-	$^3\Sigma^-$	1.7392		− 388.6293228 (P)	+0.630	
SiF_2	$^1A_1$	1.6351	100.391	− 488.3506203		
SiF_2^-	$^2B_1$	1.7184	96.717	− 488.3573325 (P)	+ 0.183	
SiF_3	$^2A_1$	1.6101	108.041	− 588.0224293 (P)		
SiF_3^-	$^1A_1$	1.7037	96.739	− 588.1057925	+ 2.268	+ 2.9 [b]
SiF_4	$^1A_1$	1.5892	109.471	− 687.7795548		
SiF_4^-	$^2A_1$	1.6140	109.471	− 687.7424847 (P)	− 1.009	

(P) Projected UMP2 energy

[a] ref. 95

[b] ref. 97

3.85 eV, in good agreement with the experimental value of 3.90 eV. Figure 20 illustrates bond dissociation at the HF/6-31++G** level where a somewhat smaller (3.27 eV) bond strength is predicted. Correlated wavefunction calculations were next carried out for the concerted C_{2v} decomposition of $SiH_4 \rightarrow SiH_2 + H_2$. Since the SCF representation of this reaction surface is inadequate for description of the bond breaking in SiH_4 and formation of the H_2 bond, a correlated analysis is required. In Figure 21, we illustrate the decomposition of SiH_4 in C_{2v} symmetry. The parameter x represents the Si distance from the center of mass of the H_2 molecule. Clearly, there are two separate SCF descriptions at extreme values for x. At short distances, the system approaches the T_d symmetry of SiH_4. As x increases, we find a repulsive barrier of ~ 5 eV before the surface takes on $SiH_2 + H_2$ character. Starting from $SiH_2 + H_2$, we find long-range repulsion in C_{2v} symmetry. The smooth curve, shown in Figure 21, connecting $SiH_4 \rightarrow SiH_2 + H_2$ represents a two configuration treatment of Si-H bond breaking. For this concerted decomposition of SiH_4, we find that the initial ground state and final ground state correspond to different electronic configurations that cross with an energy barrier of ~ 5 eV. Thus, decomposition in C_{2v} symmetry is not a viable possibility.

The decomposition of $SiH_4 \rightarrow SiH_2 + H_2$ was next studied in symmetry lower than C_{2v}. Gordon, Geno, Binkley and Frisch (Reference 98) has reported the transition state for the decomposition of SiH_4 in C_s symmetry at several levels of theory. The highest level of theory used was MP2/6-311G (2d,2p) which predicts the transition state shown in Figure 22. Starting from this transition state, the path of steepest descent leading to the reactant, SiH_4, or the products, $SiH_2 + H_2$, can be followed analytically along the intrinsic reaction coordinate of the potential surface. This is illustrated in Figure 23 which shows the potential energy along the reaction coordinate. Points A, B, C and D correspond to : [A]: reactants ($SiH_2 + H_2$), [B]: a local van der Waals well, [C]. the transition state and [D]: the equilibrium structure of SiH_4. The transition state is predicted to lie 2.8 kcal.mol above the dissociation products, $SiH_2 + H_2$. Thus, the minimum energy required for this decomposition process is 2.8 + 65.6 = 68.4 kcal/mol. These results are in good agreement with the study reported by Gordon, et al (Reference 98). The initial $SiH_2^- + H_2$ pathway is also shown on Figure 23. This curve is drawn based on the calculated electron affinity of SiH_2^-. This negative curve must cross over the $SiH_2 + H_2$ surface at some intermediate geometry since SiH_4^- is not a stable negative ion.

3.4.4 Negative Ion-Molecule Reactions: $H^- + SiH_4$

Several studies have been reported which examine the mechanisms of the $H^- + SiH_4$ reaction. This is believed to be a classical second order nucleophilic substitution reaction (S_N2), similar to the $H^- + CH_4$ and $F^- + CH_3F$ systems which involve substitution at the carbon center with inversion of the MO configuration. Sheldon, Hayes and Bowie (Reference 99) explored the fully relaxed motion of $H^- + SiH_4$ leading to three possible kinds of products. a) deprotonation to form $H_2 + SiH_3^-$, b) equatorial addition to form SiH_5^- and c) apical addition to form SiH_5^-. They

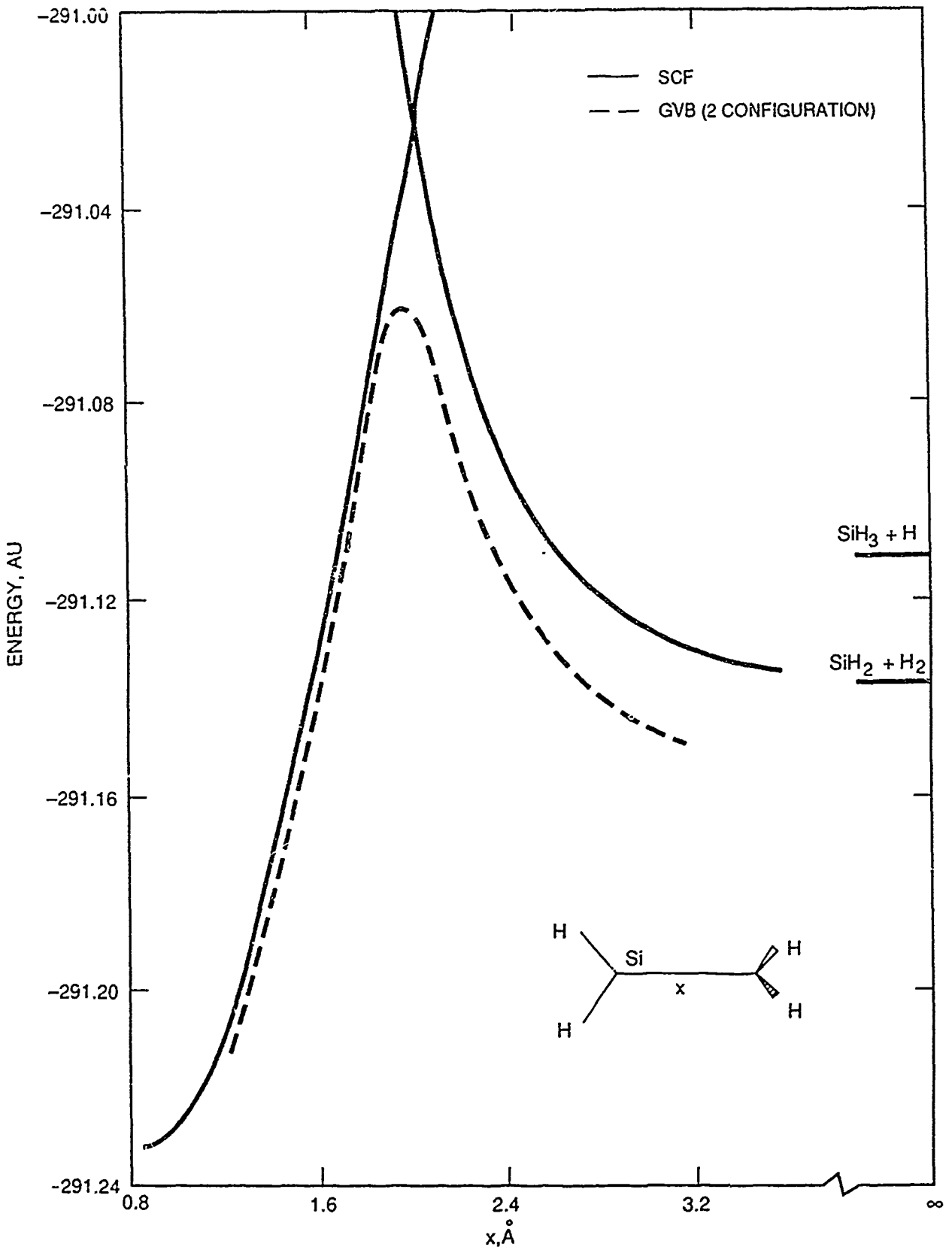

Figure 21. Potential Energy Surface for $SiH_4 \rightarrow SiH_2 + H_2$ (C_{2v} Symmetry).

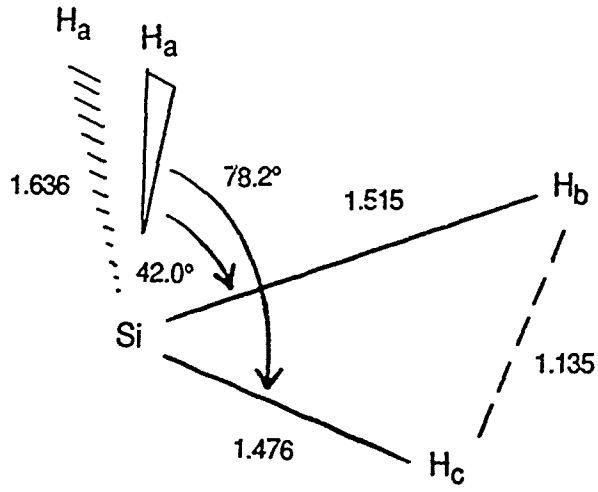

Figure 22. Transition State for $SiH_4 \rightarrow SiH_2 + H_2$ Decomposition.

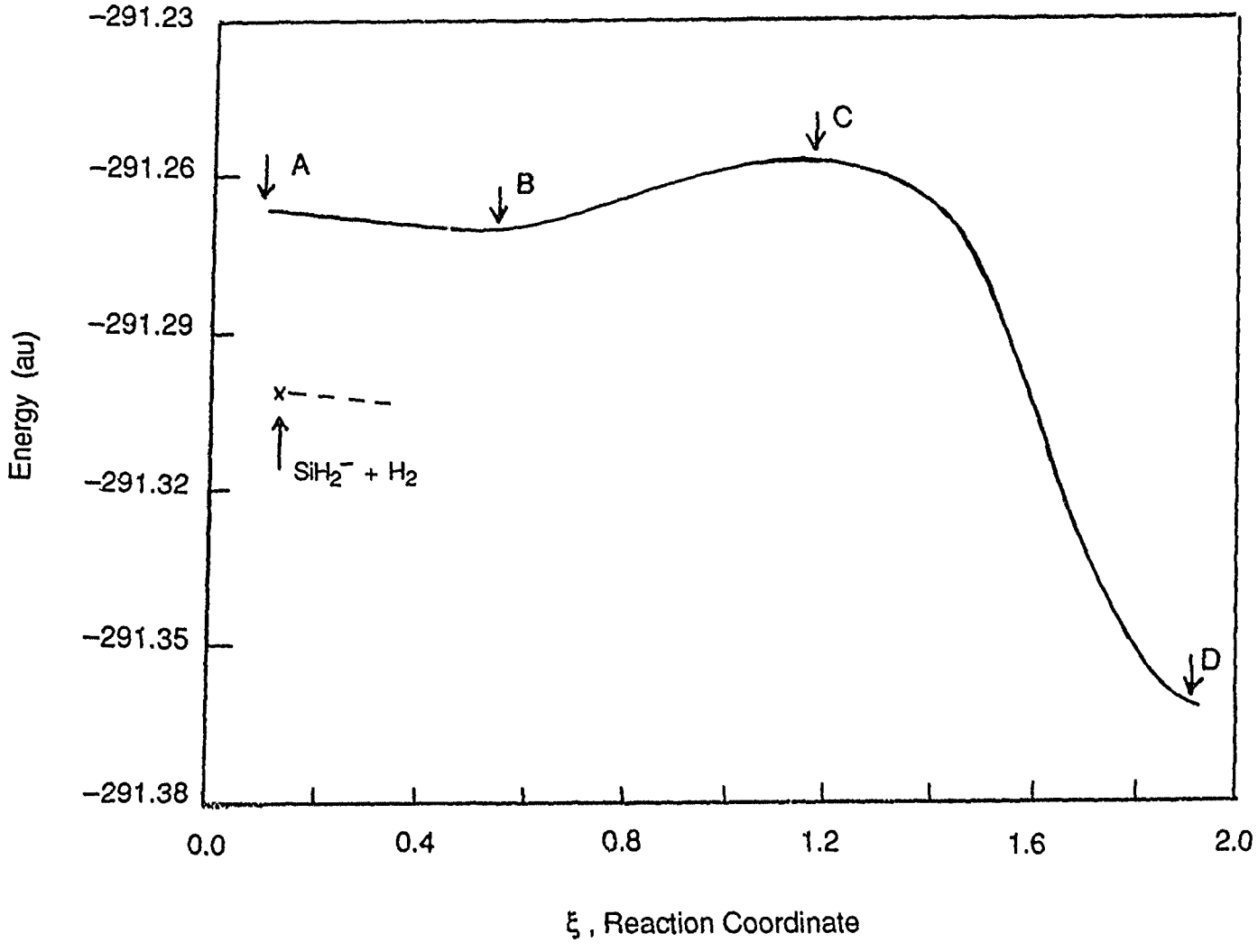

Figure 23. Potential Energy Along the Intrinsic Reaction Coordinate for the Reaction $SiH_4 \rightarrow SiH_2 + H_2$.

find no barriers for direct attachment of H^- to silane. Once formed, however, SiH_5^- was found to exhibit a barrier of ~ 70 kcal.mol relative to $SiH_3^- + H_2$ decomposition. These authors fail to report their calculated stability of SiH_5^- relative to $SiH_4 + H^-$ reactants. Earlier studies of this reaction have been reported by Wilhite and Spialter (Reference 100), Keil and Ahlrichs (Reference 101) and Baybutt (Reference 102). It has been assumed that, the S_N2-reaction of $H^- + SiH_4$ proceeds in C_{3v} symmetry, finally forming SiH_5^- as a D_{3h} (trigonal bypyramid) structure. There has been uncertainty about the stability of SiH_5^- relative to $H^- + SiH_4$ and some evidence of a barrier along this reaction path. Keil and Ahlrichs (Reference 101) and Baybutt (Reference 102) predict no barrier for this reaction whereas Wilhite and Spialter (Reference 100) predict a large (8.6 kcal/mol) barrier along the S_N2 reaction path, similar to that found for the $H^- + CH_4$ reaction.

A careful study of the $H^- + SiH_4$ reaction shows that the calculated interaction energy is very sensitive to the chosen basis set. In the conformational change from $H^- + SiH_4$ to SiH_5^- to $SiH_3^- + H_2$, the diffuse character moves from the hydrogen center onto the silicon center. Thus a balanced description of this reaction requires diffuse polarization functions located on all centers. In addition, a diffuse polarization function is needed on the hydrogen centers to smoothly permit charge transfer to silicon. In Table 14 we give a summary of the energetics of this reaction with several basis sets and approximations. We find that SiH_5^- is stable by ~ 20 kcal/mol relative to $SiH_4 + H^-$, in good agreement with the most accurate studies reported in Table 14. However, it is clear that the presence of a large (+39.4 kcal/mol) reaction barrier for formation of $SiH_3^- + H_2$ rules out the S_N2 pathway. The energetics of the $H^- + SiH_4$ reaction are illustrated in Figure 24.

Brandemark and Siegbahn (Reference 103) and Sheldon, et al (Reference 99) have made the interesting suggestion that the direct proton abstraction reaction may be the preferred pathway.

$$H^- + SiH_4 \rightarrow [H^- - H^+ - SiH_3^-] \rightarrow H_2 + SiH_3^- \qquad (106)$$

They find a much lower barrier (+17.0 kcal/mol) for this direct abstraction reaction, apparently ruling out the formation of SiH_5^- as an intermediate. An alternate possible route is to abstract H_2 from the C_{4v} pseudorotation transition state geometry which lies only ~ 2 kcal/mol above the SiH_5^- minimum energy structure (Reference 104). At the suggestion of Mark Gordon (Reference 105), we have examined dissociation pathways starting from the C_{4v} transition state of SiH_5^- which represents the intermediate state in the $D_{3h} \rightarrow C_{4v} \rightarrow D_{3h}$ pseudorotation process. As mentioned, the energy barrier to form the C_{4v} transition state structure is only ~ 2 kcal/mol, indicating that dissociation from this geometry may be energetically possible. Calculations to date, however, do not indicate a low barrier reaction pathway from the C_{4v} transition state. Both a concerted (C_{2v}) and relaxed (C_s) dissociation lead to high energy barriers for the removal of H_2. We conclude that the experimentally observed formation of SiH_3^- must arise from a proton transfer reaction along

Table 14. Energetics of the $H^- + SiH_4 \rightarrow SiH_5^- \rightarrow SiH_3^- + H_2$ Reaction

	ΔE (kcal/mol)					
	a	b	c	d	e	f
$H^- + SiH_4$	0.	0.	0.	0.	0.	0.
$[SiH_5^-]^*_{reactants}$	0.	8.6	0.	0.	0.	0.
SiH_5^-	---	– 13.8	– 18.6	– 20.3	– 20.7	– 10.2
$[SiH_5^-]^*_{products}$	+ 71.7	---	---	---	+ 39.4	---
$SiH_3^- + H_2$	– 3.1	---	---	---	– 9.5	– 4.1

a) Ref. 99 HF/6-21G

b) Ref. 100 CNDO/2; Basis: Si:[12s9p2d/6s4p2d], H:[6s/3s]

c) Ref. 102 HF/STO-3G and several larger basis sets developed from Si(10s6p) and H(5s) primitive sets.

d) Ref. 101 CEPA/large sp basis plus 2 sets of d-functions

e) Ref. 103 CI/large sp basis plus 2 sets of d-functions

f) Ref. 10 MP4/6-31++G**//MP2/6-31++G**

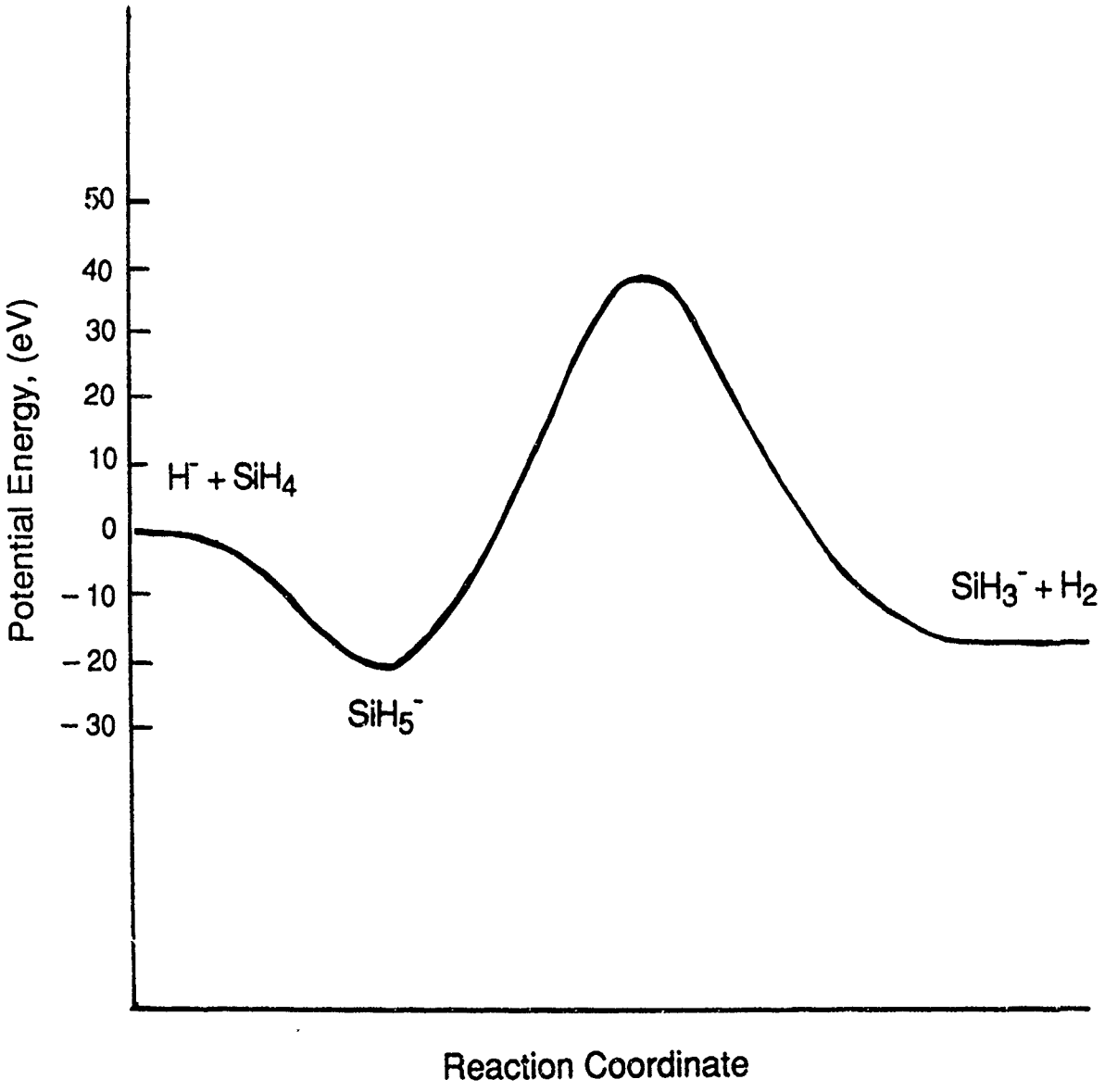

Figure 24. Reaction Path for H^- + SiH_4.

the Si-H bond to form $H_2 + SiH_3^-$, rather than abstraction of H_2 from SiH_5^- along the S_N2 reaction pathway.

3.4.5 Negative Ion-Molecule Reactions : $H^- + SiF_4$

The S_N2-reaction of $H^- + SiF_4$ has been studied in C_{3v} symmetry. The corresponding reaction of $H^- + SiH_4$ is described above. For that system, we did not find any barrier along the reaction path in the entrance channel. This result contrasts with the $H^- + CH_4$ system which experimentally exhibits a large (~ 8.6 kcal/mol) barrier toward reaction. In Table 15 we give the enthalpies for the silane/fluorine system, including the negative ion results calculated at the MP2/6-31+G* level of theory. It can be seen that all SiF_n (n=1-3) species support a stable negative ion and that SiF_3^- is particularly stable with an electron affinity of nearly 3 eV. The reaction:

$$H^- + SiF_4 \rightarrow HF + SiF_3^- \qquad (107)$$

is exothermic by 19.3 kcal/mol. At the MP2/6-31+G* level of theory, we find an exothermicity of 15.0 kcal/mol, in fair agreement with experiment, considering the limitations of the basis set.

Calculations of the $H^- + SiF_4$ reaction surface were carried out in C_{3v} symmetry. Figure 25 clearly shows that the reactants and products are represented by two different molecular orbital descriptions, characteristic of a S_N2-reaction pathway. The repulsive character along the entrance channel is similar to that found for the $H^- + CH_4$ reaction. The barrier shown in Figure 25 is clearly too high since a two-configuration MCSCF or GVB description of this system is required to carry the description smoothly from the $H^- + SiF_4$ reactant channel to $HF + SiF_3^-$ products. We estimate that a multi-configuration treatment will lower this barrier by approximately a factor of 2, yielding a somewhat larger barrier, than found for the $H^- + CH_4$ system. A more detailed investigation of this system is indicated, particularly in light of the great stability of the SiF_3^- ion. Based on the results of this initial study, we predict that the $H^- + SiF_4$ reaction would not proceed for collision energies below ~ 0.8 eV. At higher collision energies, the rate should approach Langevin ($k \sim 5 \times 10^{-9}$ cm^3/sec) with $HF + SiF_3^-$ as the dominant products.

Table 15. Enthalpies for Silane/Fluorine Gas Species

Species	ΔH_f^o (kcal/mol)	ΔH_f^o (eV)	I_p(eV)
SiF_4 $[^1A_1]$	– 384.9	– 16.68	[15.7]
SiF_3 $[^2A_1]$	– 239.	–10.4	[9.3]
SiF_3 $[^1A_1]$	– 139.	_ 6.0	7.54
SiF $[^3\Pi]$	106.6	4.623	8.15
SiF_4^+ $[^2A']$	[– 24.]	[– 1.0]	
SiF_3^+ $[^1A']$	[– 26.3]	[– 1.1]	
SiF_2^+ $[^2A_1]$	109.0	4.73	
SiF^+ $[^1\Sigma^+]$	170.4	7.39	
Si^+ $[^2P]$	294.5	12.771	
F_2 $[^1\Sigma_g^+]$	0.0	0.0	15.686
F_2^+ $[^2\Sigma_u^+]$	361.72	15.686	
F $[^2P]$	18.47	0.801	17.423
F^+ $[^3P]$	420.25	18.224	
F^- $[^1S]$	– 59.91	– 2.598	
SiF^- $[^3\Sigma^-]$	[– 25.]	[–1.1]	
SiF_2^- $[^2B_1]$	[– 143.]	[–6.2]	
SiF_3^- $[^1A_1]$	– 306.7	– 13.3	
H^- $[^1S]$	32.34		

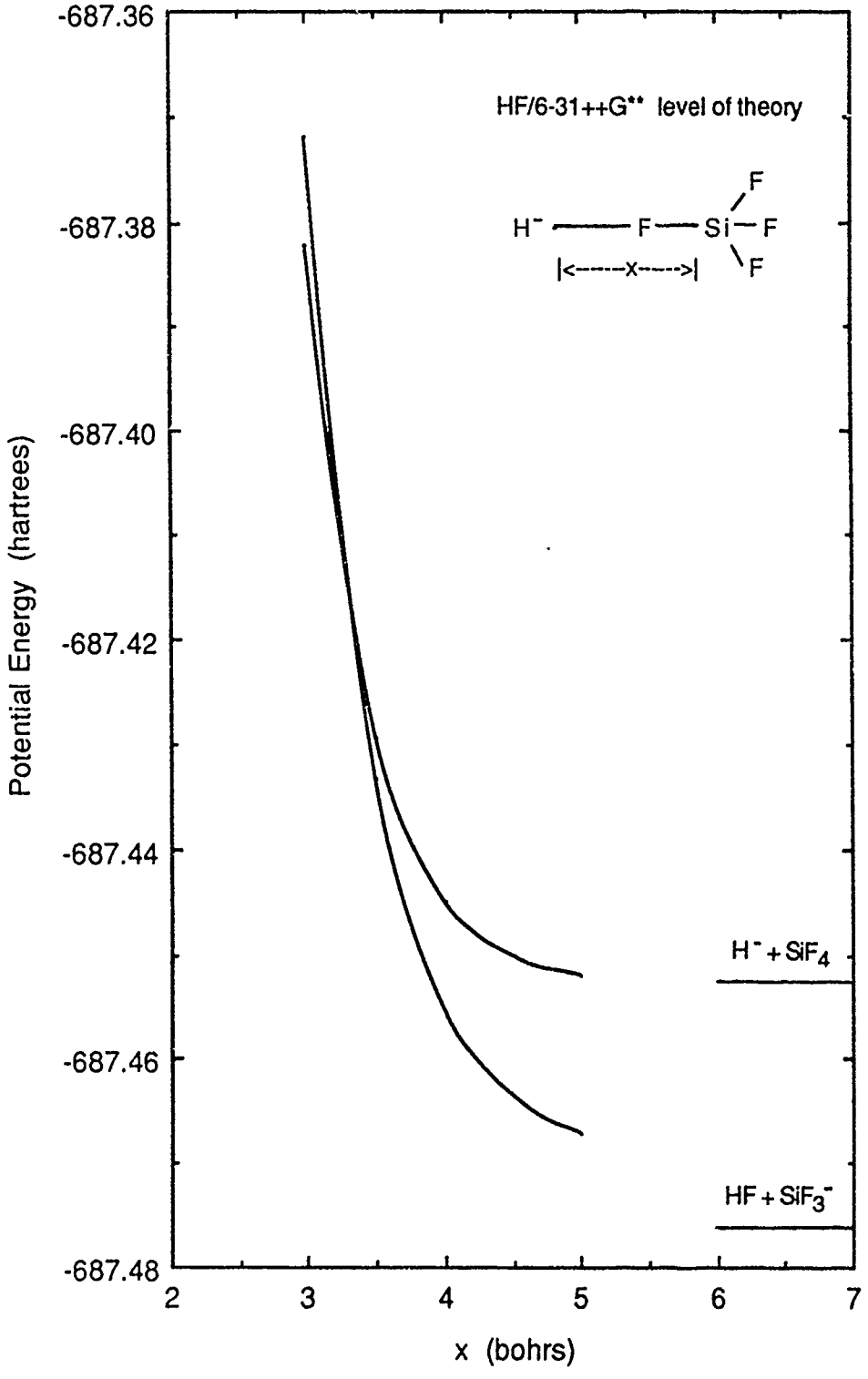

Figure 25. Reaction Path for H^- + SiF_4.

SECTION 4

CONCLUSIONS AND RECOMMENDATIONS

As discussed above, several qualitative pictures of both ion and neutral fragment production in silane discharges have been developed. Secondary ion-silane reactions to form disilane ions were proposed to explain the observed ion currents. A separate model was proposed by Turban, et al (Reference 7) in which primary silane ions are formed by low-energy electron impact dissociation, followed by secondary ion-molecule reactions. Chapman and Gallagher (Reference 5), however, have criticized the applicability of this model to cathode sheath conditions where it is believed that high energy electron processes (10-100 eV) govern the overall reaction kinetics. Their interpretation of the discharge ion chemistry is that electron impact dissociation of silane occurs as a primary process forming SiH_n^+ (n=0,3), with n=2 or 3 heavily favored over more highly stripped silane. Neutral SiH_n radical production as a primary process must also be considered. Based on the known rate of H atom abstraction from silane and the direct electron impact dissociation reaction, SiH_3 radicals are believed to predominate in the discharge region. SiH_2^+, and more highly stripped silane cations, are probably driven to SiH_3 by fast reactions of the type $SiH_n^+ + SiH_4 \rightarrow SiH_{n+1} + SiH_3^+$. The intent of this technical program was to address these uncertainties in the chemistry of silane ion-molecule reactions through a theoretical analysis of the governing reaction rates. Since dissociative reactions, with or without accompanying charge transfer, may occur, our approach was based on detailed quantum mechanical studies of the reaction surfaces to yield all possible reaction product channels. Subsequent to this analysis of the reaction energies, cross sections for the various ion-molecule processes were calculated within a quantum framework.

The research effort carried out under this program has clearly identified several areas where further theoretical studies should be carried out. These areas include a more detailed analysis of ion-molecule clustering reactions and an in-depth study of the role that negative ions play in silane plasmas. The premise that positive ion-molecule reactions in silane plasmas follow the characteristic growth pattern, forming large cluster ions which eventually form observable dust, has been questioned by both experimental (Reference 11) and theoretical work (Reference 12). A further argument against such a mechanism is that positive ions have short residence times in the discharge since they are swept to boundaries of the reactor by the ambipolar sheath fields (Reference 106). Garscadden (Reference 9), Haaland (Reference 107), and others have observed that such fields act to constrain negative ions in the homogeneous reactor region, thereby amplifying the importance of their gas phase chemistry.

As an extension of the research problems addressed under this technical program, we suggest that additional research be carried out to gain a better understanding of the role that negative silane

ions play in semiconductor deposition discharges. This research should include: 1) an examination of the thermodynamics of SiH_n^-, $Si_2H_n^-$, SiF_n^- and $Si_2F_mH_n^-$ anions, 2) studies of sequential clustering reactions of silane anions, 3) the role of dissociative attachment of electrons to silane species forming radical neutral and anion products, 4) studies of the formation and decomposition pathways for negative ion-molecule reactions such as $H^- + SiH_n$ and $H^- + SiF_n$, and analysis of the energy dependence of the kinetic rate of such processes. An outline of our recommendations in each of these areas is given below:

1. The thermochemistry of neutral SiH_n and SiF_n species, and their corresponding cations has been the subject of several experimental (References 108-113) and theoretical studies (References 114-119). In contrast, little is known about the corresponding anions, particularly the thermochemistry of SiF_n^- species. Under our current research program, an initial estimate of the anion thermochemistry was made at the MP2 level of theory. Although this gives a consistent picture of the relative stability of these species, higher order theory, such as the MP4 or QCISD, is required for predictions which are accurate to $\pm$ 1 kcal/mol.

2. A second recommended research task deals with the analysis of sequential clustering reactions among negative silane ions. As discussed above, Mandich (Reference 11) and Raghavachari (Reference 12) have examined the $Si^+ + SiH_4$ clustering sequence, leading to successive formation of $Si_2H_2^+$, $Si_3H_4^+$, $Si_4H_6^+$ and $Si_5H_{10}^+$. They find that $Si_5H_{10}^+$ does not undergo H_2 elimination and thereby becomes a bottleneck against growth of larger size clusters. The basic chemistry of these clustering reactions involved addition of the SiH_4 group across the Si-Si bond which leads to branched chain products rather than linear species. It is unclear whether a similar reaction pattern would be found for negative ion clustering where the relative bond strengths are weaker. It is also unclear whether Si^- and $Si_mH_n^-$ clusters would attack SiH_4 along a Si–H bond or bridge across two hydrogens in a perpendicular arrangement. The pattern of growth of negative ion clusters will be critically dependent on this mechanism of SiH_4 attachment.

3. A third recommended task is to examine dissociative attachment of $e + SiH_4$ in greater detail. Our preliminary studies of dissociative attachment (DA) of electrons to silane were concerned with an analysis of the possible product channels and quantum coupling with the reactants. The lowest adiabatic attachment channel correlates to $SiH_2^-[^2B_1] + H_2[X^1\Sigma_g^+]$. The SiH_4^- resonance state corresponding to this channel appears to be of the Feshbach type with a small capture width from reactants. In addition, there is a large barrier on the reaction surface leading to $SiH_2^- + H_2$ products. The second DA channel corresponds to the formation of $SiH_3^-[^1A_1] + H[^2S]$. This channel corresponds to a shape resonance but also would appear to have a small DA cross section for vibrationally cold SiH_4. Based on these known low-energy quantum processes, our conclusion under the present program was that low-energy direct electron dissociative attachment processes should have low probability.

The problem of DA of e + SiH_4 at higher (> 4 eV) collisional energies should be examined by looking at excited state surfaces of SiH_4^-. In this case, where the resonance state has a long lifetime, a two-step mechanism may best describe the attachment process. Step one involves the capture of an electron into a resonance state of the negative ion with lifetime such that this resonance state has forgotten its mode of formation before it decays. Step two governs the rate of dissociation of the resonance state into the possible product channels. This dissociation can occur along a number of exit channels, subject to the usual conservation laws of total energy and angular momentum. The competition among the various possible modes of dissociation, however, does not depend on the manner in which the resonance state was initially formed. We suggest an examination of this model in detail for DA of e + SiH_4, based on an analysis of the location and symmetries of the excited states of SiH_4^- lying in the 7-10 eV region above the ground state of e + SiH_4.

4. Finally, we suggest a study of the formation of negative silane ions through ion-molecule reactions, such as H^- + SiH_4 and H^- + SiF_4. Our initial studies of the H^- + SiH_4 reaction indicated that the most probable reaction pathway was abstraction of H^+ from SiH_4 to form H_2 + SiH_3^-. The reaction sequence : $H^- + SiH_4 \rightarrow SiH_5^- \rightarrow SiH_3^- + H_2$ in contrast to the H^- + CH_4 system, does not exhibit a barrier to the formation of SiH_5^-. However, the abstraction of H_2 occurs with a 57 kcal/mol barrier, making the overall reaction improbable. In the H^- + SiF_4 reaction, we find a large barrier in the entrance channel leading to $SiHF_4^-$, similar to the corresponding hydrocarbon system. The topology of this reaction surface is more complicated than the SiH_5^- system and further studies of the potential energy surfaces are required.

In summary, a quantitative description of all of the major reactions that occur in the discharge region, including electron impact dissociation and ionization, and the chemical role of both cations and anions (formed by dissociative attachment) is required to permit reliable modeling of rf discharge sheaths. A goal of this research program was to identify the positive ion chemistry occurring in silane discharges, and to predict both kinetic reaction rates and product distributions. Emphasis was placed on the development of sound theoretical methods to predict the collisional energy dependence of the reaction rates and on examination of the role of dissociative charge transfer in silane ion-molecule reactions. We suggest additional studies to examine the role of anion reactions in both charge transfer and reactive rearrangement collisions. An overall goal would be to build a data base, consisting of both thermochemical and reactive cross section calculations, which will help establish the role that negative silane and fluorinated silane ions play in discharge reactors.

REFERENCES

1. Spear, W. E. and P. G. Le Comber: Solid State Communications, 17, p. 1196, 1975.

2. Polycrystalline and Amorphous Thin Films and Devices, edited by L. L. Kazmerski, Academic Press, NY, 1980.

3. Long, Jr., W., W.F. Bailey and A. Garscadden: Electron Drift Velocities in Molecular-Gas-Rare-Gas Mixtures. Physical Review A. 13, p. 471, 1976.

4. Joseph, Jr., C. A., P. D. Haaland and A. Garscadden: On the Decomposition of Silane in Plasma Deposition Reactors. IEEE Transactions on Plasma Sciences, PS-14, p. 155, 1986.

5. Chatham, H. and A. Gallagher: Ion Chemistry in Silane DC Discharges. Journal of Applied Physics 58, p. 159, 1985.

6. Haller, I.: Ionic Species in a Silane Plasma. Applied Physics Letters, 37, p. 282, 1980; Importance of Chain Reactions in the Plasma Deposition of Hydrogenated Amorphous Silicon. Journal of Vacuum Science and Technology, A1, p.1376, 1983.

7. Turban, G., Y. Catherine and B. Grolleau: Plasma Chemistry Plasma Processing, 2, p. 61. 1982.

8. Hess, G. G. and F. W. Lampe: Ionic Reactions in Gaseous Monosilane. Journal of Chemical Physics, 44, p. 2257, 1968.

9. Garscadden, A.: Effects Due to Negative Ions and Particles in Plasmas. Presented at the NATO Conference, Aquafredden-Maraten, Italy, August 1989.

10. Haaland, P.: Ion Kinetics in Silane Plasmas, AFWAL Interim Report AFWAL-TR-88-2043, April, 1988.

11. Mandich, M. L., W. D. Reents, Jr. and M. F. Jarrold: Sequential Clustering Reactions of Si^+ with SiD_4: Identification of a Bottleneck Preventing Rapid Growth of Hydrogenated Silicon Particles. Journal of Chemical Physics, 88, p.1703, 1988.

12. Raghavachari, K.: Sequential Clustering Reactions of Si^+ with Silane. A Theoretical Study of the Reaction Mechanisms. Journal of Chemical Physics, 88, p. 1688, 1988.

13. Schaefer, F. E. and F. E. Harris: *Ab Initio* Calculations of 62 Low-Lying States of the O_2 Molecule. Journal of Chemical Physics, 48, p.4946, 1968.

14. Michels, H. H. and F. E. Harris: Predissociation Effects in the $A^2\Sigma^+$ State of the OH Radical. Chemical Physics Letters, 3, p. 441, 1969.

15. Harris, F. E.: Open-Shell Orthogonal Molecular Orbital Theory. Journal of Chemical Physics, 46, p. 2769, 1967.

16. Roothan, C. C. J. and P. S. Bagus: Atomic Self-Consistent Field Calculations by the Expansion Method. Methods in Computational Physics. Edited by B. Alder, 2, p.47, 1963.

17. Harris, F. E. and H. H. Michels: Open-Shell Valence Configuration-Interaction Studies of Diatomic and Polyatomic Molecules. International Journal of Quantum Chemistry, IS, p.329, 1967.

18. Givens, W.: Eigenvalue-Eigenvector Techniques. Oak Ridge Report Number ORNL 1574 (Physics).

19. Shavitt, I., C. F Bender, A. Pipano and R. P. Hosteny: The Iterative Calculation of Several of the Lowest or Highest Eigenvalues and Corresponding Eigenvectors of Very Large Symmetry Matrices. Journal of Computational Physics, 11, p. 90, 1973.

20. Raffenetti, R. C.: A Simultaneous Coordinate Relaxation Algorithm for Large, Sparse Matrix Eigenvalue Problems. Journal of Computational Physics, 32, p.403, 1979.

21. Harris, F. E. and H. H. Michels: The Evaluation of Molecular Integrals for Slater-Type Orbitals. Advances in Chemical Physics, 13, p.205, 1967.

22. Hehre, W. J., L. Radom, P. von R. Schleyer and J. A. Pople: *Ab Initio* Molecular Orbital Theory, Wiley-Interscience, New York, 1986.

23. Dupuis, M., D. Spangler and J. J. Wendoloski: GAMESS User's Guide, NRCC Software Catalog, Vol. 1, Program QG01, Lawrence Berkeley Laboratory, 1980.

24. Davidson, E. R.: Natural Expansion of Exact Wavefunctions, III. The Helium Atom Ground State. Journal of Chemical Physics, 39, p.875, 1963.

25. Wahl, A. C., P. J. Bertoncini, G. Das and T. L. Gilbert: Recent Progress Beyond the

Hartree-Fock Method for Diatomic Molecules, The Method of Optimized Valence Configurations. International Journal of Quantum Chemistry, IS, p. 123, 1967.

26. Ruedenberg, K., L. M. Cheung and S. T. Elbert: MCSCF Optimization Through Combined Use of Natural Orbitals and the Brillouin-Levy-Berthier Theorem. International Journal of Quantum Chemistry, 16, p.1069, 1979.

27. Dupuis, M., H. F. King, J. Rys and T. Takada: HONDO Documentation. QCPE Software Catalog, 17, Indiana University, Department of Chemistry, 1985.

28. Amos, R. D. and J. E. Rice: The Cambridge Analytic Derivatives Package Documentation, Issue 4.0. University Chemical Laboratory, Cambridge, England, 1988.

29. Dupuis, M., J. D. Watts, H. O. Villar and G. J. B. Hurst: HONDO: Version 7.0 (1987) Documentation. IBM, Kingston, New York, 1988.

30. Lischka, H., R. Shepard, F. B. Brown and I. Shavitt: New Implementation of the Graphical Unitary Group Approach for Multireference Direct Configuration Interaction Calculations. International Journal of Quantum Chemisty, Symposium 15, p. 91, 1981.

31. Ahlrichs, R., H. J. Böhm, C. Ehrhardt, P. Scharf, H. Schiffer, H. Lischka and M. Schindler: Implementation of an Electronic Structure Program System on the Cyber 205. Journal of Computational Chemistry, 6, p. 200, 1985.

32. Shavitt, I.: Unitary Group Approach to Configuration Interaction Calculations of the Electronic Structure of Atoms and Molecules. Mathematical Frontiers in Computational Chemical Physics, Editor - D. G. Truhlar, Springer-Verlag, Berlin, 1988.

33. Pople, J. A. and R. K. Nesbet: Self-Consistent Orbitals for Radicals. Journal of Chemical Physics, 22, p. 571, 1954.

34. Nesbet, R. K.: Approximate Methods in the Quantum Theory of Many-Fermion Systems. Reviews of Modern Physics, 33, p. 28, 1961.

35 Roothan, C. C. J. and P. S. Bagus: Atomic Self-Consistent Field Calculations by the Expansion Method. Methods in Computational Physics, Edited by B. Alder, 2, p. 47, 1963.

36 Roothan, C. C. J. : New Development in Molecular Orbital Theory. Reviews of Modern Physics, 23, p 69, 1951.

37. Bates, D. R.: Dissociative Recombination. Physical Review, 78, p. 492, 1959.

38. Bardsley, J. N. : The Theory of Dissociative Recombination. Proceedings of Physical Society, B1, p. 365, 1968.

39. Berry, R. S. and S. E. Nielson: Dynamic Coupling Phenomena in Molecular Excited States. I: Formulation and Vibronic Coupling in H_2. Physical Review, A1, p. 383, 1970.

40. Berry, R. S. and S. E. Nielson: Dynamic Coupling Phenomena in Molecular Excited States. II: Autoionization and Predissociation in H_2, HD and D_2. Physical Review, A1, p. 395, 1970.

41. Cook, G. R. and P. H. Metzger: Photoionization and Absorption Cross Sections of O_2 and N_2 in the 600- to 1000-Å Region. Journal of Chemical Physics, 41, p. 321, 1964.

42. Nielson, S. E. and J. S. Dahler: Theory of the Dissociation Recombination and Associative Ionization of Hydrogen. Journal of Chemical Physics, 45, p. 4060, 1964.

43. Russek, A., M. R. Patterson and R. L. Becker: Auto-Ionization in Molecular Systems. Physical Review, 167, p. 17, 1968.

44. Bardsley, J. N.: The Ionization of Molecules Near Threhold. Chemical Physics Letters, 1, p. 229, 1967.

45. Nielson, S. E. and R. S. Berry: Vinronic Autoionization and Predissociation in Hydrogen. Chemical Physics Letters, 2, p. 503, 1968.

46. Bardsley, J. N.: Configuration Interaction in the Continuum States of Molecules. Journal of Physics B, 1, p. 349, 1968.

47. Aaron, R., R. Amado and B. Lee: Divergence of the Green's Function Series for Rearrangement Collisions. Physical Review, 121, p. 319, 1961.

48. Bates, D. R. and R. McCarroll: Charge Transfer. Suppl. Phil. (Advances in Physics), 11, p. 39, 1962.

49. Bates, D. R. and R. McCarroll: Electron Capture in Slow Collisions. Proc. Roy. Soc. (London), A245, p. 175, 1958.

50. Bates, D. R. and D. A. Williams: Low-Energy Collisions Between Hydrogen Atoms and Protons. Proc. Phy. Soc., A83, p.425, 1964.

51. Fulton, M. J. and M. H. Mittlemen: Scattering of H^+ by H. Annals of Physics, 33, p. 65, 1965.

52. Quong, J.: Approximations in the Theory of Rearrangement Collisions and Applications to a Tractable Model of Charge-Exchange Scattering. Lawrence Radiation Laboratory Report UCRL-17034, August, 1966.

53. Riley, M. E.: Strong-Coupling Semiclassical Methods. The Average Approximation for Atom-Atom Collisions. Physical Review A8, p. 742, 1973.

54. Choi, B. H. and K. T. Tang: Theory of Distorted-Wave Born Approximation for Reactive Scattering of an Atom and a Diatomic Molecule. Journal of Chemical Physics, 61, p. 5147, 1974.

55. Shan, Y., B. H. Choi, R. T. Poe and K. T. Tang: Three-Dimensional Quantum Mechanical Study of the $F + H_2$ Reactive Scattering. Chemical Physics Letters, 57, p. 379, 1978.

56. Baer, M. and J. A. Beswick: Electronic Transitions in the Ion-Molecule Reaction $(Ar^+ + H_2 \leftrightarrow Ar + H_2^+) \rightarrow ArH^+ + H$. Physical Review A19, p. 1559, 1979.

57. Top, Z. H. and M. Baer: Incorporation of Electronically Nonadiabatic Effects into Bimolecular Reactive Systems. II. The Collinear ($H_2 + H^+$, $H_2^+ + H$) System. Chemical Physics, 25, p. 1, 1977.

58. Halavee, V. and M. Shapiro: A Collinear Analytic Model for Atom-Diatom Chemical Reactions. Journal of Chemical Physics, 64, p. 2826, 1976.

59. Schatz, G. C. and J. Ross: Franck-Condon Factors in Studies of Dynamics of Chemical Reactions I. General Theory Application to Collinear Atom-Diatom Reactions. Journal of Chemical Physics, 66, p. 1021, 1977; Franck-Condon Factors in Studies of Dynamics of Chemical Reactions. II. Vibration-Rotation Distributions in Atom-Diatom Reactions, 66, p.1037, 1977; Franck-Condon Factors in Studies of the Dynamics of Chemical Reactions. III. Analysis of Information Theor for Vibration-Rotation Distributions and Isotopic Branching Ratios, 66, p. 2943, 1977.

60 Henglein, A., K. Lacmann and G. Jacobs: Collision Mechanism in Bimolecular Reactions. I.

Theory and Experimental Determination Methods of the Velocity Spectrum of the Products Resulting from the Simple H-transfer Reactions of $X^+ + H_2 \rightarrow XH^+ + H$ Type. Ber. Bunsenges. Physik. Chem., 69, p. 279, 1965.

61. Bates, D. R., C. J. Cook and F. J. Smith: Classical Theory of Ion-Molecule Rearrangement Collisions At High Impact Energies. Proceedings of the Physical Society, 83, p. 49, 1964.

62. Marcus, R. A.: Analytical Mechanics of Chemical Reactions. III. Natural Collision Coordinates. Journal of Chemical Physics, 49, p. 2610, 1968; On the Analytical Mechanics of Chemical Reactions. Quantum Mechanics of Linear Collisions, 45, p. 4493, 1966.

63. Stechel, E. B., T. G. Schmalz and J. C. Light: Quantum Theory of Exchane Reactions: Use of Nonorthogonal Bases and Coordiantes. Journal of Chemical Physics, 70, p. 5640, 1979.

64. Diestler, D. J.: Close-Coupling Techniques for Chemical Exchange Reaction of the type $A + BC \rightarrow AB + C$, $H + H_2 \rightarrow H_2 + H^*$. Journal of Chemical Physics, 54, p. 4547, 1971.

65. Michels, H. H. : Theoretical Research Investigation Upon Reaction Rates to the Nitric Oxide (Positive) Ion. AFGL-TR-80-0072, Final Report for AFGL Contract F19628-77-C-0248, 1980.

66. Michels, H. H. : Theoretical Studies of the $O^+ + N_2$ Ion-Molecule Reaction, AFGL-TR-81-0151, Final Report for AFGL Contract F19628-80-C-0209, 1981.

67. Stückelberg, E. C. G.: Helv. Phys. Acta, 5, p. 369, 1932.

68. Russek, A.: Rotationally Induced Transition in Atomic Collisions. Physical Review A, 4, p. 1918, 1971.

69. Magee, J. L.: The Mechanism of Reactions Involving Excited Electronic States: The Gaseous Reactions of the Alkali Metals and Halogens. Journal of Chemical Physics, 8, p. 687, 1940.

70. Herschbach, D. R.: Reactive Scattering in Molecular Beams. Advances in Chemical Physics, 10, p. 319, 1966.

71. Bauer, E., E. R. Fischer and F. R. Gilmore: De-excitation of Electronically Excited Sodium by Nitrogen. Journal of Chemical Physics, 51, p. 4173, 1969.

72. McDaniel, E. W., V. Cermak, A. Dalgarno, E. E. Ferguson and L. Friedman: Ion-Molecule Reactions. Wiley-Interscience, New York, 1970.

73. Geise, C. F.: The Reaction $C^+ + N_2 \rightarrow NO^+ + N$. Ion-Molecule Reaction in Gas Phase, Advances in Chemistry Series, 58, p. 20, 1966.

74. Ferguson, E. E., D. K. Bohme, F. C. Fehsenfeld and D. B. Dunkin: Temperature Dependence of Slow Ion-Atom Interchange Reactions. Journal of Chemical Physics, 50, p. 5039, 1969.

75. Gioumousis, G. and D. P. Stevenson: Reactions of Gaseous Molecule Ions with Gaseous Molecules. V. Theory. Journal of Chemical Physics, 29, p. 294, 1958.

76. Stevenson, D. P. and D. O. Schissler: Reactions of Gaseous Molecule Ions with Gaseous Molecules. IV. Experimental Method and Results. Journal of Chemical Physics, 29, p. 282, 1958.

77. Frisch, M. J., M. Head-Gordon, G. W. Trucks, J. B. Foresman, H. B. Schlegel, K. Raghavachari, M. A. Robb, J. S. Binkley, C. Gonzalez, D. J. Defees, D. J. Fox, R. A. Whiteside, R. Seeger, C. F. Melius, J. Baker, R. L. Martin, L. R. Kahn, J. J. P. Stewart, S. Topiol and J. A. Pople: Gaussian 90, Gaussian Inc., Pittsburgh PA, 1990.

78. Curtiss, L. A. and J. A. Pople: Theoretical Thermochemistry 4. Ionization Energies and Proton Affinities of AH_n Species (A=Li to B and Na to Al); Geometries and Enthalpies of Formation of Their Cations. Journal of Physical Chemistry, 92, p. 894,1988.

79. Haaland,P. and A. Rahbee: The Molecular Silane Cation. Chemcial Physics Letters, 114, p. 571, 1985.

80. Pople, J. A. and L. A. Curtiss: Theoretical Thermochemistry. 2. Ionization Energies and Proton Affinities of AH_n Species (A=C to F and Si to Cl); Heats of Formation of Their Cations. Journal of Physical Chemistry, 91, p. 155, 1987.

81. Berkowitz, J., J. P. Greene and H. Cho: Photoionization Mass Spectrometric Studies of SiH_n (n=1-4). Journal of Chemical Physics, 86, p.1235, 1987.

82. Börlin, K., T. Heins and M. Jungen: Photoionization Mass Spectrometry of Silane. Chemical Physics, 103, p. 93, 1986.

83. Weber, M. E. and P. B. Armentrout. Energetics and Dynamics in the Reaction of Si^+ with

SiF_4. Thermochemistry of SiF_x and SiF_x^+ (x=1,2,3). Journal of Chemical Physics, 88, p.6898, 1988.

84. Chase, Jr, M. W., C. A. Davies, J. R. Downey, Jr., D. J. Frurip, R. A. McDonald and A. N. Syverud: JANAF Thermochemical Tables, 3rd Ed., Journal of Physical and Chemistry Reference Data, 14, Suppl. 1, 1985.

85. Fisher, E. R. and P. B. Armentrout: Kinetic Energy Dependence of Dissociative Charge Transfer Reactions of He^+, Ne^+, Ar^+, Kr^+ and Xe^+ with Silane. Journal of Chemical Physics, 93, p.4858, 1990.

86. Bowers, M. T. and D. D. Elleman: Thermal Energy Charge Transfer Reactions of Rare-Gas Ions to Methane, Ethane, Propane and Silane. The Importance of Franck-Condon Factors. Chemical Physics Letters, 16, p.486, 1972.

87. Chatham, H., D. Hils, R. Robertson and A. C. Gallagher: Reactions of He^+, Ne^+ and Ar^+ with CH_4, C_2H_6, SiH_4 and Si_2H_6. Journal of Chemical Physics, 79, p. 1301, 1983.

88. Potzinger, P. and F. W. Lampe: An Electron Impact Study of Ionization and Dissociation of Monosilane and Disilane. Journal of Physical Chemistry, 73, p. 3912, 1969.

89. Ebinghaus, Von H., K. Kraus, W. Müller-Duysing and H. Neuert: Negative Ions durch Elektronenresonanzeinfang in PH_3, AsH_3 und SiH_4. Z. Naturforschg. 19a, p. 732, 1964.

90. Srivastava, S. K.: personal communication.

91. Haaland, P.: Dissociative Attachment in Silane. Journal of Chemical Physics, 93, p. 4066, 1990.

92. Schmidt, M. W., M. S. Gordon and M. Dupuis: The Intrinsic Reaction Coordinate and the Rotational Barrier in Silaethylene. Journal of the American Chemical Society, 107, p. 2585, 1985.

93. Wan, H., J. H. Moore, and J. A. Tossell: Electron Scattering Cross Section and Negative Ion States of Silane and Halide Derivatives of Silane. Journal of Chemical Physics, 91, p. 7340, 1989.

94. Drzaic, P. S., J. Marks and J. I. Brauman in Gas Phase Ion Chemistry, Vol. 3, M. T. Bowers, Ed., Academic Press, Orlando, p. 167, 1984.

95. Mead, R. D., A. E. Stevens and W. C. Lineberger in Gas Phase Ion Chemistry, Vol. 3, M. T. Bowers, Ed., Academic Press, Orlando, p. 123, 1984.

96. Nimlos, M. R. and G. B. Ellison: Photoelectron Spectroscopy of SiH_3^- and SiD_3^-. Journal of the American Chemical Society, 108, p. 6522, 1986.

97. Richardson, L. M., L. M. Stephenson and J. I. Brauman: Photodetachment of Electrons from Trifluoromethyl and Trifluorosilyl Ions; the Electron Affinities of CF_3 and SiF_3. Chemical Physics Letters, 30, p. 17, 1975.

98. Gordon, M. S., D. R. Gano, J. S. Binkley and M. J. Frisch: Thermal Decomposition of Silane. Journal of the American Chemical Society, 108, p. 2191, 1986.

99. Sheldon, J. C., R. N. Hayes and J. H. Bowie: Do Barriers Exist for Nucleophilic Substitution at Tetravalent Silicon in the Gas Phase? An *ab Initio* and Ion Cyclotron Resonance Study. Journal of the American Physical Society, 106, p. 7711, 1984.

100. Wilhite, D. L. and L. Spialter: Electronic Structure of SiH_5^- and Model Studies of Inter-and Intra-Molecular Exchange in Pentacoordinate Silicon Species. An *ab Initio* Investigation. Journal of the American Chemical Society, 95, p. 2100, 1973.

101. Keil, F. and R. Ahlrichs: Theoretical Study of the Molecular Silicon Hydride Ions SiH_5^- and SiH_3^-. Chemical Physics, 8, p. 384, 1975.

102. Baybutt, P.: The Molecular Orbital Description of S_N2 Reactions at Silicon Centres. Molecular Physics, 29, p. 389, 1975.

103. Brandemark, U. and Per E. M. Siegbahn: The Reactions Between Negative Hydrogen Ions and Silane. Theoret. Chim. Acta, 66, p. 233, 1984.

104. Gordon, M. S., T. L. Windus, L. W. Burggraf and L. P. Davis: Theoretical Study of Pseudorotation of Pentacoordinated Silicon Anions: The Prototypical SiH_5^-. Journal of the American Chemical Society, in press, 1990.

105. Gordon, M. S.: personal communication.

106. Drevillon, B., J. Huc, A. Lloret, J. Perrin, G. De Rosny and J. P. M. Schmitt: Positive and

Negative Ions in Silane Plasmas. Proceedings of the 5th International Symposium in Plasma Chemistry, eds. B. Waldie and G. A. Farnell, p. 634, 1981.

107. Haaland, P.: Negative Ions in Silane Plasmas, to be published.

108. Berkowitz, J. J. P. Greene, H. Cho and B. Ruscic: Photoionization Mass Spectrometric Studies of SiH_n (n=1-4). Journal of Chemical Physics, 86, p. 1235, 1987.

109. Walsh, R.: Thermochemistry of Silicon-Containing Compounds, Part 1 - Silicon-Halogen Compounds, An Evaluation. Journal of the Chemical Society, Faraday Trans. 1, 79, p. 2233, 1983.

110. Farber, M. and R. D. Srivastava: Mass Spectrometric Determination of the Heats of Formation of the Silicon Subchlorides SiCl(g), $SiCl_2$(g) and $SiCl_3$(g). Journal of the Chemical Society, Faraday Trans. 1, 73, p. 1672, 1977.

111. Doncaster, A. M. and R. Walsh: Kinetics of the Gas-Phase Reaction Between Iodine and Monosilane and the Bond Dissociation Energy D(H_3Si-H). International Journal of Chemical Kinetics, 13, p. 503, 1981.

112. Doncaster, A. M. and R. Walsh: Kinetics of the Gas-Phase Reaction Between Iodine and Trifluorosilane and the Bond Dissociation Energy D(F_3Si-H). International Journal of Chemical Kinetics, 10, p. 101, 1978.

113. Farber, M. and R. D. Srivastava: Mass Spectrometric Determination of the Heats of Formation of the Silicon Fluorides SiF(g), SiF_2(g) and SiF_3 (g). Journal of the Chemical Society, Faraday Trans. 1, 74, p. 1089, 1978.

114. Curtiss, L. A. and J. A. Pople: Theoretical Enthalpies of Formation of SiH_n and SiH_n^+ (n=1-4). Chemical Physics Letters, 144, p.38, 1988.

115. Ho, P., P. M. E. Cotrin, J. S. Binkley and C. F. Melius: Theoretical Study of the Heats of Formation of SiH_n, $SiCl_n$, and SiH_nCl_m Compounds. Journal of Physical Chemistry, 89, p. 4647, 1985.

116. Garrison, B. J. and W. A. Goddard III: Dissociation Energies of SiF Systems of Relevance to Etching Reactions. Journal of Chemical Physics, 87, p.1307, 1987.

117. Schlegel, H. B.: Heats of Formation of Fluorine-Substituted Silylenes, Silyl Radicals and Silanes. Journal of Physical Chemistry, 88, p. 6254, 1984.

118. Dixon, D. A.: Calculated Geometries, Vibrational Spectra, Energetics and Electronic Properties of Fluorinated Methanes and Silanes. Journal of Physical Chemistry, 92, p. 86, 1988.

119. Ignacio, E. W. and H. B. Schlegel: Heats of Formation of SiH_mF_n Calculated by *ab initio* Molecular Orbital Methods. Journal of Chemical Physics, 92, p. 5404, 1990.

APPENDIX A

PUBLICATIONS AND PRESENTATIONS

The significant results obtained under this contract have been prepared for publication in technical journals or presented at technical meetings. These papers and meetings are listed below. Abstracts of the talks presented at meetings are included in Appendix B. Appendix C contains the latest paper to be submitted for publication on SiH_4.

A. Technical Papers in Journals

1. "Dissociative Electron Attachment of e + SiH_4." H. H. Michels, R. H. Hobbs and J. M. Wadehra, to be submitted to Chemical Physics Letters, 1991.

B. Presentations

1. "Potential Energy Surfaces for Silane Ion-Molecule Reactions." H. H. Michels and R. H. Hobbs, presented at the Gordon Research Conference on Plasma Chemistry, Tilton, New Hampshire, August 15-19, 1988.

2. "Dissociative Charge Transfer in $H^+(H_3^+)$ + SiH_4 Reactions." H. H. Michels and R. H. Hobbs, presented at the 1988 41st Gaseous Electronics Conference, Minneapolis, Minnesota, October 18-21, 1988.

3. "Electronic Structure and Thermochemistry of Silicon Hydride and Silane Fluoride Anions." H. H. Michels and R. H. Hobbs, to be presented at the 1991 Annual American Chemical Society meeting, Atlanta, Georgia, April 14-19, 1991.

APPENDIX B
ABSTRACTS

APPENDIX B-1

POTENTIAL ENERGY SURFACES FOR SILANE ION-MOLECULE REACTIONS

H. H. Michels and R. H. Hobbs
United Technologies Research Center
East Hartford, CT 06108

ABSTRACT

Commercial silane discharge reactors usually operate with a mixture of silane and a noble gas. A reaction set involving collisions between hydrogen ions, noble gas ions and silane (or disilane) must therefore be considered for a complete description of the ion-molecule chemistry in such devices. Existing experimental data suggest that no simple reaction model for collisional dissociative charge transfer can be inferred for this system. A theoretical quantum mechanical study has therefore been initiated to define the pertinent potential energy reaction surfaces. The definition of these multidimensional reaction surfaces, through electronic structure calculations, should yield information on the energetics and branching probabilities for the various product channels.

We have completed a study of the reaction surfaces for the dissociative charge transfer reaction:

$$H^+ + SiH_4 \rightarrow SiH_n^+ + m\,H_2 + \ell\,H$$
$$(n=0,3;\ n+\ell+2m=5)$$

The dominant product ion is found to be SiH_3^+, formed from a hydride abstraction mechanism. Dissociation channels connecting to SiH_2^+ and Si^+ exhibit, surprisingly, significant reaction barriers relative to the SiH_3^+ product channel. A complete set of the potential surfaces for this reaction and a preliminary analysis of the kinetic rates and product distribution are described.

Supported in part by WL under Contract F33615-87-C-2718.
Presented at the Gordon Research Conference on Plasma Chemistry, Tilton, NH, 1988.

APPENDIX B-2

DISSOCIATIVE CHARGE TRANSFER IN $H^+(H_3^+)$ + SiH_4 REACTIONS

H. H. Michels and R. H. Hobbs
United Technologies Research Center
East Hartford, CT 06108

ABSTRACT

An *ab initio* study of the potential energy reaction surfaces for the dissociative charge transfer reaction: $H^+ + SiH_4 \rightarrow SiH_n^+ + mH_2 + \ell H_2$, (n=0,3; $n+\ell+2m=5$) has been undertaken. The basis set employed was the standard 6-31G* representation, augmented with diffuse functions (Si:3d, H:2p) for an accurate description of the polarizability of SiH_4. Dissociative channels connecting to SiH_2^+ and SiH^+ exhibit, surprisingly, significant reaction barriers relative to the SiH_3^+ product channel. The dissociative channel leading to Si^+ from either SiH_2^+ or SiH^+, however, exhibits no reaction barrier. The dominant product ion is found to be SiH_3^+, formed from a hydride abstraction mechanism. A preliminary calculation of the rate for SiH_3^+ formation, using a modified R-matrix propagator technique, yields results close to the Langevin prediction, $K_L = 5.2 \times 10^{-9}$ cm^3/sec. The chemistry of the $H_3^+ + SiH_4$ reaction is qualitatively similar with $SiH_3^+ + 2H_2$ formed as primary products.

Supported in part by WL under Contract F33615-87-C-2718.
Presented at the 41st Gaseous Electronics Conference, Minneapolis, Minnesota, 1988.

APPENDIX B-3

ELECTRONIC STRUCTURE AND THERMOCHEMISTRY OF SILICON HYDRIDE AND SILICON FLUORIDE ANIONS

H. H. Michels and R. H. Hobbs
United Technologies Research Center
East Hartford, CT 06108

ABSTRACT

An *ab initio* study of the electronic structure of the SiH_n^- and SiF_n^- anions has been carried out using Møller-Plesset perturbation theory. Optimized geometries were calculated at the SCF and MP2 levels of theory using several basis sets. Correlation energy treatments included both MP4 and QCISD methods. The anion thermochemistry was calculated through several isogyric processes for internal consistency. Excellent agreement with experimental electron affinities is found for the SiH_n^- anions. We find that all SiF_n^- anions are stable with the exception of SiF_4^- which exhibits two low-lying resonance states. Corresponding resonance states are also found for the SiH_4^- anion. These states adiabatically correlate to SiH_3^- + H and SiH_3 + H^- products but exhibit a potential energy curve crossing at ~ 2.1 Å. The role of these anions in plasma chemical vapor deposition of silane and fluorosilane is examined.

Supported in part by WL under Contract F33615-87-C-2718.
Presented at the Annual American Chemical Society Meeting, Atlanta, Georgia, 1991.

APPENDIX C

DISSOCIATIVE ELECTRON ATTACHMENT OF e + SiH_4

H.H. Michels and R. H. Hobbs
United Technologies Research Center
East Hartford, CT 06108

J. M. Wadehra
Department of Physics and Astronomy
Wayne State University
Detroit, Michigan 48202

ABSTRACT

Dissociative electron attachment of e + SiH_4 has been studied as a mechanism for forming the negative fragment ions: SiH_3^-, SiH_2^-, SiH^- and Si^- in silane discharge plasmas. Detailed calculations of the low-lying dissociative reaction surfaces for SiH_4^- indicate that low-energy direct attachment processes should have low probability. At higher electron collision energies (7-10 eV), a long-lived resonance state of SiH_4^-, which statistically decomposes into the accessible negative fragment ions, appears to be the dominant attachment process.

Supported in part by WL under Contract F33615-87-C-2718 and by AFOSR under Contract F49620-89-C-0019 and Grant AFOSR-87-0342.
To be submitted to Chemical Physics Letters, 1991.

1. Introduction

Dissociative electron attachment (DA) of e + SiH_4 is being studied as a mechanism for forming the negative fragment ions: SiH_3^-, SiH_2^-, SiH^- and Si^- in silane discharge plasmas. Owing to the constraining effects of the sheath fields of typical plasma reactors, it is believed that clustering of negative ions may occur in such devices. In contrast, positive ions typically have a short residence time in the discharge region, leaving some question to their importance as nucleation centers.

The first measurements of DA in silane are those of Ebinghausen, et al [1] who report the formation of SiH_3^-, SiH_2^-, SiH^- and Si^- as products, all with appearance potentials between 7 and 8 eV. Similar results were found by Potzinger and Lampe [2] who first suggested that the observed negative ion products, SiH_3^- and SiH_2^-, may correspond to decay channels from a single resonant structure of SiH_4^- lying at 7-8 eV. More recently, Srivastava [3] has reported DA cross sections for the formation of SiH_3^-, SiH_2^-, SiH^- and Si^-, all peaking in the 8-9 eV region. Potzinger and Lampe [2] and Srivastava [3] also report the appearance of a much weaker attachment process at 2-3 eV for the formation of SiH_3^- and SiH_2^-. In the present study, the low-lying dissociative reaction surfaces for SiH_4^- have been examined in an effort to identify the dissociative attachment mechanism.

2. Theoretical Considerations

The traditional DA process occurs by the following mechanism:

$$e + AB \rightarrow [AB^{**}]^- \rightarrow A^{-(*,\dagger)} + B^{(*,\dagger)} \qquad (1)$$

where AB is any diatomic or polyatomic molecule, [AB**] is a resonant state of the corresponding negative ion and $A^{-(*,\dagger)}$ and $B^{(*,\dagger)}$ represent the possible set of dissociation products, possibly with internal electronic$^{(*)}$ or rovibrational$^{(\dagger)}$ excitation. The cross section for such an attachment process is governed by the characteristics of the resonant state [AB**]. In resonant scattering theory [4], assuming a local width approximation, the scattering wavefunction, $\xi(R)$, satisfies:

$$\left[-\frac{1}{2\mu}\nabla^2 + \frac{J(J+1)}{2\mu R^2} + V^-(R) - \frac{i}{2}\Gamma(R) - E \right] \xi(R) = -V(R)\,\zeta_{VJ}(R) \qquad (2)$$

where $\zeta_{VJ}(R)$ is the nuclear motion wavefunction of the neutral target molecule, E is the total (conserved) energy of the system, and $V^-(R) - i/2\,\Gamma(R)$ is the complex interaction potential. The envelope of $|\xi(R)|^2$ decreases with R(t), owing to the possibility of autodetachment, and the probability for dissociative attachment is thus governed by the asymptotic limit of $|\xi(R)|^2$:

$$\sigma_{DA} = \frac{4\pi^2}{\mu}\left(\frac{K}{k}\right) \lim_{R\rightarrow\infty} |\xi(R)|^2 \qquad (3)$$

where $k^2/2$ is the energy of the incident electron and $K^2/2$ is the relative kinetic energy of the ion-atom or ion-molecule product state. Eq. (2) is developed on the basis that the outgoing wavepacket is directly coupled to the incident channel comprised of a free electron and the neutral target molecule. In such a case, DA occurs as a sequence of dissociation reactions, each process occurring with maximum cross section at the energy threshold corresponding to the opening of a particular product channel.

In the case where the resonant state has a long lifetime, a two-step mechanism may best describe the attachment process:

$$e + AB \Leftrightarrow [AB^{**}]^- \; : \; \langle \psi_{AB}{}^0 f(\varepsilon) | \mathcal{H}_C | \psi_{AB^{**}} \rangle \tag{4}$$

$$[AB^{**}]^- \rightarrow A^{-(*,\dagger)} + B^{(*,\dagger)} \; : \; \langle \psi_{AB^{**}} | \mathcal{H}_D | \psi_{A^-}{}^{(*,\dagger)} \psi_B{}^{(*,\dagger)} \rangle \tag{5}$$

Eq (4) governs the rate of capture into the resonant state of the negative ion and the corresponding rate of autoionization. Eq. (5) governs the rate of dissociation of the resonant state into the possible product channels. This dissociation can occur along a number of exit channels, subject to the usual conservation laws of total energy and angular momentum. The competition among the various possible modes of dissociation, however, does not depend on the manner in which the resonant state was initially formed. It follows that the overall attachment probability can be written as a product of two terms:

$$w[\psi_i(\varepsilon_R), \psi_\alpha] = w_{cap}[\psi_i(\varepsilon_R)] \, w_{decay}[\psi_\alpha] \tag{6}$$

$$w_{cap}[\psi_i(\varepsilon_R)] = 2\pi \, \Gamma_{cap} |\psi_i(\varepsilon_R)|^2 \tag{7}$$

$$w_{decay}[\psi_{\alpha'}] = \Gamma_\alpha / \Gamma_{tot} \, , \tag{8}$$

where ε_R is the energy corresponding to a particular resonant state in the incident scattering channel, Γ_{cap} is the energy width for coupling the incident channel into the resonant state, and Γ_α is the partial width corresponding to the probability that the resonant state will dissociate into products α. Obviously, the total decay width, $\Gamma_{tot} = \sum_\alpha \Gamma_\alpha$, is the sum of the partial widths for all open dissociation channels. This mechanism is often described in the literature of nuclear physics, where the resonant state is referred to as a "compound nucleus" [5,6]. The independent probabilities for the formation and subsequent decay of the resonant state are thus interpreted as a model whereby the resonant state has "forgotten" its mode of formation before it decays.

This model for DA can also be understood in terms of a semiclassical analysis of scattering theory [7,8]. In such a description, the cross section for DA can be written as a product of two factors:

$$\sigma_{DA}(\varepsilon) = \sigma_{cap}(\varepsilon)S \qquad (9)$$

where $\sigma_{cap}(\varepsilon)$ is the cross section for the capture of an electron to form the resonant negative ion state. S is the survival probability, which is classically related to the decay width of the resonant state:

$$S = \exp\left(-\int_{R_c}^{R_s} \frac{\Gamma(R)}{v}\, dR\right) \qquad (10)$$

where the region of interaction extends from the classical capture radius, R_c, to the effective radius of stabilization of the ion-atom or ion-molecule products, for which $V^-(R_s) = V^o(R_s)$. Thus the resonant state decays exponetially with mean life $1/\Gamma$.

3. Results and Discussion

Calculations of the dissociative reaction surfaces for negative ion formation in silane were undertaken. In Table 1, we show the possible product branching for e + SiH_4. Two possible kinetic routes must be considered for conditions that exist in the cathode sheath region of a silane glow discharge. The first assumes that a Jahn-Teller unstable [$^2T_2$] resonance state of SiH_4^- is formed by primary electron capture. Subsequently, this unstable negative ion can decay into the thermodynamically accessible product channels which correspond to dissociation products. Table 1 illustrates that reactions (2) - (6) fit this criteria but that (7) and (8) do not. Dissociation of $SiH_4^-[^2T_2]$ should exhibit thresholds of 1.27, 2.44, 2.78 and 3.09 eV for formation of SiH_2^-, SiH_3^-, Si^- and H^- respectively. Although taken with limited energy resolution, the data of Potzinger and Lampe [2] appears to be in agreement with these predictions for formation of SiH_2^- and SiH_3^-. Srivastava [3] has also observed resonances at ~2.5 eV which he attributes to SiH_2^- and SiH_3^- formation. This process of negative ion formation following decay of the $^2T_2$ resonance state of SiH_4^- was first described by Haaland [9].

The reaction surfaces governing the low-energy dissociative attachment (DA) of electrons to SiH_4 have been analyzed using the intrinsic reaction coordinate procedure. In Fig. 1, we show the energetics of the reaction coordinate leading to dissociation of SiH_4 to SiH_3 + H. At the HF/6-31++G** level of theory, we find a bond dissociation energy of 3.27 eV. At the MP2/6-31++G** level, a bond energy of 3.85 eV, very close to the experimental value, is predicted. Also shown on Fig.1 are preliminary data on the SiH_3^- + H and SiH_3 + H^- reaction surfaces. We find an avoided crossing of these two surfaces, very close to the internuclear separation where the ion curves cross the neutral SiH_3 + H + e surface, but probably in the region where the ion potentials are complex. Thus, the excited state ion channel, leading to SiH_3 + H^- may depopulate through this avoided crossing leaving SiH_3^- + H as the only significant products of the DA reaction. Experimental data by Haaland [9] and by Potzinger and Lampe [2] indicate that H^- is probably not formed by direct

DA of e + SiH_4. These dissociative attachment studies, including the work reported by Ebinghaus, et al [1], all indicate that low energy (< 3 eV) DA to SiH_4 must occur with a small cross section ($\sigma < 10^{-20}$ cm^2). Our calculations of the low-energy structure of the $SiH_4^-[^2T_2]$ resonance suggest that autoionization is strongly formed over DA since the resonance state geometry is very close to that of neutral SiH_4. Quantum calculations of the cross sections for low energy DA of e + SiH_4 are currently in progress [10].

In contrast, if the resonance state is long-lived, a statistical breakup may occur with nearly equal probabilities (a priori) for all accessible product channels. This alternate kinetic route can be derived from the assumption of LTE (or at least quasi-steady state). In this case, electron attachment can occur not only to SiH_4, but also directly to the neutral silane fragments which result from the decompositions of the negative ion resonance state. The product reaction channels are most likely those correlating to repulsive Rydberg or high lying valence states of SiH_4. In Table 2, we illustrate electron attachment to SiH_3, SiH_2 and SiH. It can be seen that a wide spectrum of threshold energies is spanned by these molecules (0.39 - 2.53 eV) and that all possible negative ion species, including H^-, should be possible. The relative importance of these several processes is, of course, dependent on the branching probabilities for decomposition of the resonance state and direct attachment process to the various neutral silane fragments. Knowledge of the neutral composition of the plasma in the sheath region now becomes a requirement for analyzing the relative importance of direct versus statistical breakup electron attachment.

References

[1] V. H. Ebinghaus, K. Kraus, W. Müller-Duysing and H. Neuert, Z. Naturforschg. 19a (1964) 732.

[2] P. Potzinger and F. W. Lampe, J. Phys. Chem. 73 (1969) 3912.

[3] S. K. Srivastava, private communication.

[4] J. N. Bardsley, A. Herzenberg and F. Mandel, Proc. Phys. Soc. (London) 89 (1966) 305.

[5] N. Bohr, Natur 137 (1936) 344.

[6] G. Breit and E. Wigner, Phys. Rev. 49 (1936) 519.

[7] J. N. Bardsley and F. Nandl, Rep. Prog. Phys. 31 (1968) 471.

[8] I. S. Elets and A. K. Kazanskii, Sov. J. Chem. Phys. 2 (1985) 1439.

[9] P. Haaland, Ion Kinetics in Silane Plasmas, AFWAL-TR-88-2043, AFWAL, Kirtland AFB, NM April, 1988.

[10] J. M. Wadehra and H. H. Michels, in preparation.

Table 1. Thermodynamics of Negative Ion Formation in Silane.

Reaction	ΔH (eV)	
$e + SiH_4[^1A_1] \rightarrow SiH_4^-[^2T_2]$	≤ 4.0	(1)
$\rightarrow SiH_2^-[^2B_1] + H_2[^1\Sigma_g^+]$	+1.266	(2)
$\rightarrow SiH_3^-[^1A_1] + H[^2S]$	+2.442	(3)
$\rightarrow Si^-[^4S] + 2H_2[^1\Sigma_g^+]$	+2.783	(4)
$\rightarrow SiH_3[^2A_1] + H^-[^1S]$	+3.094	(5)
$\rightarrow Si[^3P] + H_2[^1\Sigma_g^+] + H[^2S] + H^-[^1S]$	+3.269	(6)
$\rightarrow SiH^-[^3\Sigma^-] + H_2[^1\Sigma_g^+] + H[^2S]$	+4.392	(7)
$\rightarrow SiH[^2\Pi] + H_2[^1\Sigma_g^+] + H^-[^1S]$	+4.915	(8)

afwal22-1.5/89

Table 2. Thermodynamics of Negative Ion Formation in $SiH/SiH_2/SiH_3$

Reaction	ΔH (eV)
$e + SiH_3[^2A_1] \rightarrow SiH_3^-[^1A_1]$	-1.406
$\rightarrow SiH^-[^3\Sigma^-] + H_2[^1\Sigma_g^+]$	+0.544
$\rightarrow SiH_2^-[^2B_1] + H[^2S]$	+1.896
$\rightarrow SiH_2[^1A_1] + H^-[^1S]$	+2.266
$\rightarrow SiH[^2\Pi] + H[^2S] + H^-[^1S]$	+5.545
$e + SiH_2[^1A_1] \rightarrow SiH_2^-[^2B_1]$	-1.124
$\rightarrow Si^-[^4S] + H_2[^1\Sigma_g^+]$	+0.393
$\rightarrow SiH^-[^3\Sigma^-] + H[^2S]$	+2.002
$\rightarrow SiH[^2\Pi] + H^-[^1S]$	+2.525
$\rightarrow Si[^3P] + H[^2S] + H^-[^1S]$	+5.502
$e + SiH[^2\Pi] \rightarrow SiH^-[^3\Sigma^-]$	-1.277
$\rightarrow Si^-[^4S] + H[^2S]$	+1.592
$\rightarrow Si[^3P] + H^-[^1S]$	+2.223

afwal22-2.5/89

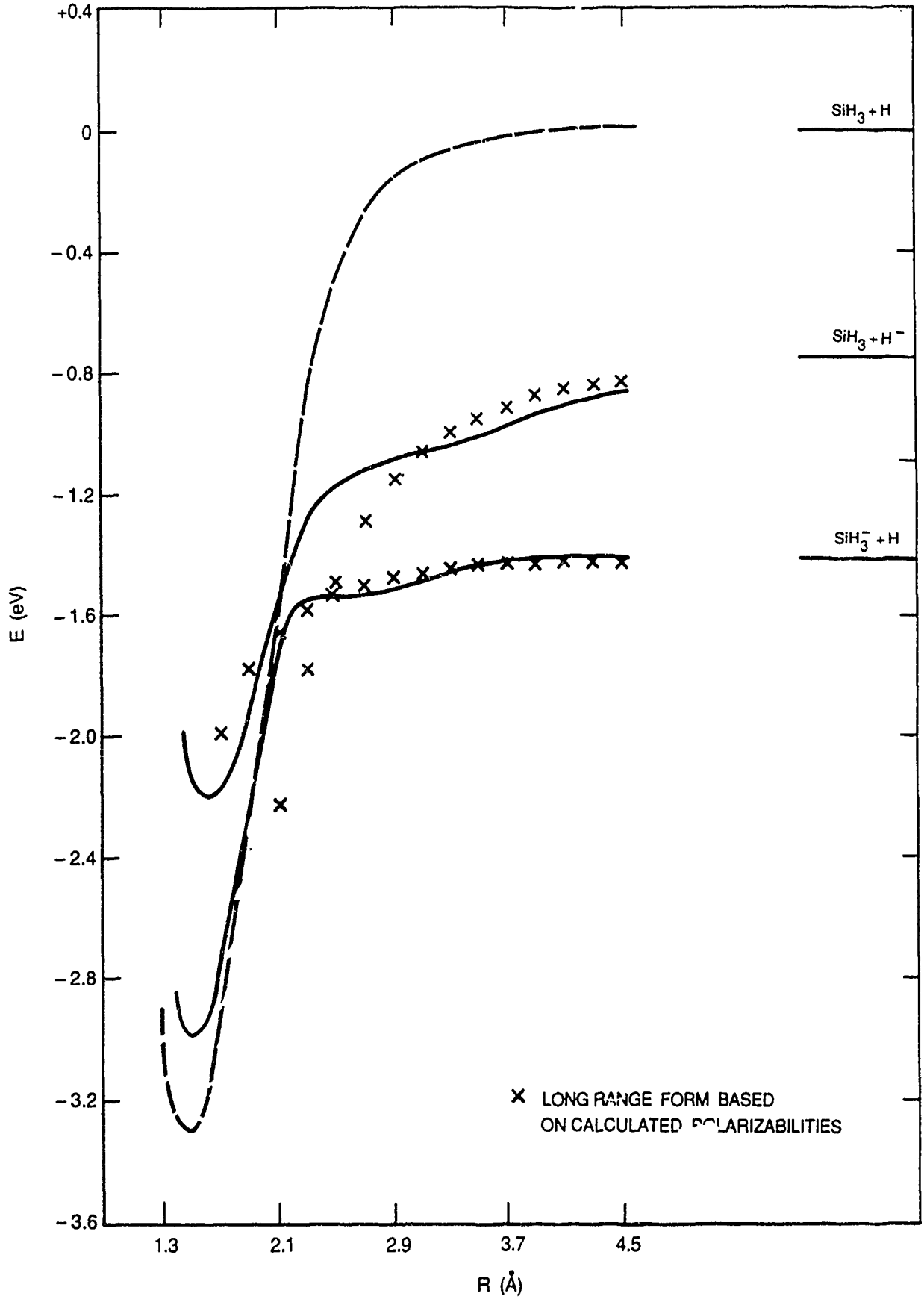

Figure 1. Intrinsic Reaction Pathway for Dissociation of SiH_4 and SiH_4^-.

☆U.S. Government Printing Office:1991—648-127/62021